SIMULTANEOUS EFFICIENCY, NOx, AND SMOKE IMPROVEMENTS THROUGH DIESEL/GASOLINE DUAL-FUEL OPERATION IN A DIESEL ENGINE

A Dissertation

by

JIAFENG SUN

Submitted to the Office of Graduate and Professional Studies of
Texas A&M University
in partial fulfillment of the requirements for the degree of

DOCTOR OF PHILOSOPHY

Chair of Committee,	Timothy J. Jacobs
Committee Members,	Jerald A. Caton
	Reza Tafreshi
	Mark T. Holtzapple
Head of Department,	Andreas A. Polycarpou

August 2014

Major Subject: Mechanical Engineering

ABSTRACT

Diesel/gasoline dual-fuel combustion uses both gasoline and diesel fuel in diesel engines to exploit their different reactivities. This operation combines the advantages of diesel fuel and gasoline while avoiding their disadvantages, attains spatially stratified low temperature combustion (LTC), and yields very low NOx and PM emissions while maintaining good efficiency. It is promising in solving the problems of conventional LTC through better control of ignition and combustion.

The benefits of dual-fuel operation and the potential of using gasoline fumigation to realize these benefits provide the major motivation to this research. This research is aimed at using gasoline fumigation in a medium-duty diesel engine to identify and quantify the influencing factors of diesel/gasoline dual-fuel LTC on engine efficiency and emissions. The factors include gasoline fraction, injection settings, rail pressure, intake pressure, and EGR level. This objective was realized through a series of experimental tests done at 1400 rpm and three loads, including both diesel baseline tests and dual-fuel tests.

First, design of experiments and relevant statistical techniques were applied to tests. Twenty-three best models between 6 factors (intake pressure, rail pressure, SOI for diesel baseline tests, SOI for dual-fuel tests, EGR level, and gasoline fraction) and 5 targets (efficiency, NOx, smoke number, HC, and CO) were obtained through regression of test data. Confirmation tests were done based on best models. Generally, the observations are improved NOx and smoke emissions, but unimproved or deteriorated efficiency, HC and CO emissions. The optimization effort makes some achievements, but needs further improvement. The influence of each factor is analyzed. The measures to get better models are explained.

Second, parametric studies of gasoline fraction and injection timing were done to find their influence on efficiency and emissions. Efficiency generally decreases slightly as gasoline fraction increases or injection timing is retarded. Generally, increasing gasoline

fraction is beneficial for NOx and smoke emissions, but HC and CO emissions deteriorate. An advance in injection timing, however, has the opposite influence.

Finally, individual cycle data were analyzed to study cyclic variability (CV) and its influence on dual-fuel efficiency and emissions. Factors causing or influencing CV were identified. The CV in dual-fuel operation is more serious than that in diesel operation, in terms of magnitude. Most of the test data studied do not have strong determinism, and the influence of gasoline addition is small.

ACKNOWLEDGEMENTS

First and foremost, I would like to express my deep appreciation to my advisor, Dr. Timothy Jacobs, for his long-time patience and enthusiastic support and guidance during the entire period of my schooling in TAMU. He has motivated me a lot during my research presented here. He helps me gain insight into different aspects of the engine field through several projects and conferences. He helps me a lot in finding internship and job opportunities. He serves as a role model to me, in terms of his compassion for his students, teachings, manner, and friendship. I am honored that he is able to serve as my chair of advisory committee.

My committee members – Dr. Jerald Caton, Dr. Reza Tafreshi, and Dr. Mark Holtzapple – are thanked for their involvement in the successful completion and scientific validity of this dissertation. Each committee member has provided helpful comments and suggestions which I greatly appreciate. Each committee member also helps me in other aspects than dissertation: courses, research, overseas experience, and knowledge in chemical engineering. I also owe many thanks to them for such help. Dr. Sergio Capareda is also thanked for his help in my research.

I want to express my gratitude to my lab mates for their camaraderie, friendship, and help: Josh Bittle, Jue Li, Brandon Thompkins, Aaron Griffin, Mike Penny, Junnian Zheng, Xingyu Xue, Jacob Hedrick, and Hoseok Song. Especially I want to thank Josh, Jue and Aaron for helping acquire valuable lab skills and solve the problems of test facilities, providing inspiring ideas on my research, and joining my engine tests.

I would like to thank all my friends for their motivation and support.

Finally, I wish to thank my family for their love. They have always encouraged and supported me along the way. They have influenced me a lot in my life. This big step in my life would not be forwarded and happy without them.

NOMENCLATURE

AKI	anti-knock index
ASME	American Society of Mechanical Engineers
ASTM	American Society for Testing and Materials
ATDC	after top dead center
BMEP	brake mean effective pressure
BSCO	brake specific CO emission
BSEC	brake specific energy consumption
BSFC	brake specific fuel consumption
BSHC	brake specific HC emission
BSNOx	brake specific NOx emission
CA	crank angle
CA10	the crank angle at which MFB equals 10%
CA50	the crank angle at which MFB equals 50%
CA90	the crank angle at which MFB equals 90%
CO	carbon monoxide
CO_2	carbon dioxide
COV	coefficient of variation
CV	cyclic variability
DI	direct injection
DOE	design of experiment
EGR	exhaust gas recirculation
EVO	exhaust valve open
FID	flame ionization detection
GDI	gasoline direct injection
H_2	hydrogen
HC	hydrocarbon
HCCI	homogeneous charge compression ignition

IMEP	indicated mean effective pressure
IMEPg	gross indicated mean effective pressure
IMEPn	net indicated mean effective pressure
IVC	intake valve closing
LHV	lower heating value
LMPRR	location of max pressure rise rate
LPP	location of peak pressure
LTC	low temperature combustion
MFB	mass fraction burned
MHRR	max heat release rate
MPRR	max pressure rise rate
N_2	nitrogen
NDIR	nondispersive infrared
NOx	oxides of nitrogen
O_2	oxygen
PCCI	premixed charge compression ignition
PDF	probability density function
PFI	port fuel injection
PM	particulate matter
PP	peak pressure
ppm	parts per million
RCCI	reactivity-controlled compression ignition
rpm	revolution per minute
SAE	society of automotive engineers
SOC	start of combustion
SOI	start of injection
TDC	top dead center
UHC	unburned hydrocarbon

TABLE OF CONTENTS

LIST OF FIGURES

LIST OF TABLES

1. INTRODUCTION

1.1 Background

Energy saving and environment protection have long been the main thrust to the development of internal combustion engines. Countless engines are providing economically viable and reliable power for both stationary and mobile applications. Most engines are operated with non-renewable petroleum-based fuel. The depletion of fuel stocks and rising fuel price motivate researchers to improve the efficiency of engines. Moreover, cleaner engines are being developed because harmful emissions from engines raise more concern with more widespread use of engines, and government mandated emission regulations become more and more stringent.

In recent years, advanced combustion modes including low temperature combustion (LTC) have been widely investigated to improve the performance and reduce the emissions of compression ignition engines. Various forms of LTC such as homogeneous charge compression ignition (HCCI) and premixed charge compression ignition (PCCI) require creating a homogenous mixture prior to ignition. Therefore, lean fuel/air mixture and high exhaust gas recirculation (EGR) level are used to increase ignition delay, high-pressure and multiple injections are used to decrease mixing time, and port injection or early direct injection are used to allow more time for mixing. In such cases, the ignition and combustion are not controlled directly; instead, chemical kinetics solely direct the rate of reaction.

These combustion modes face some problems, including difficulty to control combustion (e.g., timing and rate), misfire, high hydrocarbon (HC) and carbon monoxide (CO) emissions at light loads, knock, low efficiency at some operational points, and narrow operation range [1, 2, 3]. The problems are partly attributed to the fact that only one kind of fuel is used. As stated in [4], either gasoline or diesel in their neat forms has specific advantages and shortcomings for advanced combustion operation. The evaporation of gasoline is rapid and a premixed charge can be obtained using port fuel injection. But because its autoignition qualities are poor, it becomes difficult to

achieve combustion at low-load conditions. Conversely, diesel fuel has superior autoignition qualities, but this can result in difficulty controlling the combustion phasing as engine load is increased. Moreover, its poor volatility limits its use as a premixed fuel.

Since in these combustion modes the combustion is controlled by chemical kinetics, fuel physical-chemical properties play an important role, including boiling point and distillation, latent heat of evaporation, cetane number, octane number, molecular structure, and oxygen content. Therefore to solve the above problems, dual-fuel operations have been done in engines, namely simultaneous use of different fuels or addition of additives. The fuels include diesel fuel, gasoline, primary reference fuels (PRF, namely isooctane and n-heptane), alternative fuels (DME or dimethyl ether, LPG or liquefied petroleum gas, natural gas, biogas, hydrogen, and alcohols such as methanol, ethanol, iso-propanol, and n-butanol), and fuel additives (MTBE or methyl tertiary-butyl ether, H_2O_2 or hydrogen peroxide, 2-EHN or ethylhexyl nitrate and DTBP or di-tert-butyl peroxide) [5, 6, 7, 8, 9, 10].

As a kind of fuel design and management, the study of diesel/gasoline dual-fuel operation is becoming popular in recent years, and much of the research is about reactivity-controlled compression ignition (RCCI) [11, 12, 13, 14]. RCCI combustion is a novel combustion mode that uses two fuels or addition of additives to exploit the different reactivities for attaining operations with high efficiency, high power, and low emissions.

Diesel/gasoline RCCI is characterized by very early injection of diesel fuel in either single or double pulse and premixing gasoline, and the fueling method is gasoline PFI (port fuel injection) + diesel DI (direct injection). This operation combines the advantages of diesel fuel and gasoline while avoiding their disadvantages, and is promising in solving the problems of conventional LTC through better control of ignition and combustion. With an overall lean gasoline/air mixture, autoignition is avoided prior to the diesel fuel injection. The early diesel injection then provides a timed and distributed ignition source. Effectively, the resulting LTC process is spatially stratified according to the mixture reactivity in each sub volume of the combustion

chamber. This yields very low oxides of nitrogen (NOx) and particulate matter (PM) emissions while maintaining good efficiency.

In addition to the dominant gasoline PFI + diesel DI fueling method, another fueling method for using gasoline in diesel engine is gasoline fumigation (in intake pipe or manifold) + diesel DI. Because only one gasoline injector is used, one obvious advantage is that gasoline fumigation lessens the demand for fuel supply hardware when applied in multi-cylinder engines. The two methods are not substantially different, and the former is studied extensively in realizing RCCI. Much fewer, however, studies are published with gasoline fumigation.

1.2 Objective

The benefits of diesel/gasoline dual-fuel operation, and the potential of using gasoline fumigation to realize these benefits provide the major motivation to this research. This research is aimed at using gasoline fumigation in a medium-duty diesel engine to identify and quantify the influencing factors of diesel/gasoline dual-fuel low temperature combustion on engine efficiency and emissions. The factors include gasoline fraction, injection settings, rail pressure, intake pressure, and EGR level. This objective will be realized through a series of experimental tests described in Section 4, 5, and 6.

2. LITERATURE REVIEW

Till recently, 54 papers on diesel/gasoline dual-fuel research have been reviewed, most of which are about experimental study. Dual-fuel research has gained considerable attention recently, and most of its study is carried out in a few institutions. The general conclusions about combustion, efficiency, and emissions in diesel/gasoline operation are summarized in Sections 2.1 - 2.3, with emphasis on the influence of variable parameters. The comparison presented is generally between diesel/gasoline operation and conventional diesel operation at the same load and speed unless otherwise stated. The main characteristics of diesel/gasoline operation as compared to conventional diesel operation are: in-cylinder stratification of fuel reactivity and equivalence ratio, longer ignition delay, staged combustion, longer combustion duration, good efficiency at medium and high loads, simultaneous significant decrease of NOx and smoke emissions, and increase of HC and CO emissions. The variable parameters such as gasoline fraction, diesel injection settings, and EGR level, need to be applied and adjusted carefully to get favorable combustion, efficiency and emissions.

2.1 Combustion

The conventional diesel and gasoline combustion process (summarized from [15, 16]) are introduced in the next 4 paragraphs, forming a basis for comparison with diesel/gasoline operation.

In a diesel engine, diesel fuel is injected into the cylinder toward the end of the compression stroke. The fuel then atomizes into small drops, penetrates through the combustion chamber, and mixes with the charge (mixture of air, residual gas, and/or recirculated exhaust gas) in the cylinder. Because the charge's high temperature and pressure are above the fuel's ignition point, spontaneous ignition of portions of the charge occurs after an ignition delay of a few crank angles. The combustion causes pressure and temperature to increase significantly, reducing the evaporation time of the remaining liquid fuel and improving the mixing of air and fuel vapor. Therefore the

fuel/air mixture within combustible limits then burns rapidly. Essentially all the fuel has to pass through the atomization, vaporization, fuel-air mixing, and combustion processes. Moreover, mixing of the air with burning and burned gases continues throughout the combustion and expansion processes.

The combustion process can be divided into four stages: ignition delay, premixed combustion, mixing-controlled combustion, and late combustion. Ignition delay is the period between start of fuel injection (SOI) and start of combustion (SOC). In premixed combustion stage, the mixture within flammability limits prepared in the ignition delay stage burns rapidly in a few crank angle degrees, featuring high heat release rate. In mixing-controlled combustion stage, the burning is controlled primarily by the air/fuel mixing process. The heat release rate may or may not reach a second (usually lower) peak. The late combustion stage continues well into the expansion stroke with lower heat release rate because of incomplete combustion and low pressure and temperature caused by expansion.

In a conventional gasoline engine the fuel and air are mixed in the intake system, enter the cylinder, mix with residual gas, and then are compressed. Combustion is initiated by an electric discharge from the spark plug towards the end of the compression stroke. Then a turbulent flame develops and propagates through the premixed mixture until it reaches the combustion chamber walls and extinguishes.

The combustion process can be divided into three stages: early flame development, flame propagation, and flame termination. After spark discharge, the flame development stage is influenced primarily by the mixture state, composition, and motion near the spark plug. In the flame propagation stage featuring rapid burning, most of the charge burns as the flame propagates to the chamber walls. This stage is influenced by conditions throughout the combustion chamber. In the flame termination stage the remainder of the charge burns to completion.

The compression ignition and mixing-controlled combustion of diesel fuel, and the spark ignition and propagation-controlled combustion of gasoline, stem from the fuels' different autoignition qualities. Diesel fuel constituents have longer saturated aliphatic

chains than gasoline constituents. As a result, diesel fuel exhibits higher low-temperature reactivity and consequently higher overall oxidative reactivity than gasoline in engine applications. It tends to have earlier temperature and pressure increases in an engine cycle through low temperature heat release and therefore earlier onset of hot ignition [17]. In diesel/gasoline operation, because part of diesel is replaced with gasoline, the mixture ignition delay becomes longer [18, 19, 20], and the combustion is different from conventional diesel and gasoline combustion.

The addition of reactivity stratification results in a staged consumption of diesel fuel to gasoline, which is shown in experiments [20, 21, 22] and modeling images [4]. Tests were done by Duffour, et al [21] on a single-cylinder diesel engine at 2000 rpm and indicated mean effective pressure (IMEP) of 17 bar, with 85% gasoline and 35% EGR. Three steps are observed in the combustion process, represented by three peaks of heat release rate curves. The diesel premixed flame and the propagation flame are represented by the first two peaks. The third peak is much higher and corresponds to the autoignition of the remaining mixture of air and gasoline. In [4], the modeling images show that the ignition location for all cases coincides with the location of the highest concentration of diesel fuel (n-heptane). Furthermore, gasoline fuel (isooctane) consumption did not occur until n-heptane transitions from thermal preparation to thermal ignition (i.e., formaldehyde consumption and hydroxyl accumulation). The staged combustion leads to longer combustion duration and less intense heat release, as shown in the RCCI timing sweep done by Pohlkamp and Reitz [23] on a Yanmar L70AE single-cylinder diesel engine at 25%, 50% and 75% loads.

The important variable parameters used in diesel/gasoline operation include gasoline fraction, diesel fuel injection parameters (in the following text “injection” refers to diesel fuel injection unless otherwise stated), and EGR level. The influence of each parameter on combustion is summarized in the following paragraphs.

Gasoline fraction

Here gasoline fraction refers to the mass fraction of gasoline in all the fuel including gasoline and diesel. The gasoline fraction ranges from 0 to 1. Different engine configurations and test settings have different favorable gasoline fractions, otherwise misfire, incomplete combustion, autoignition, knock or combustion instability can occur. For example, Yoshida et al. [24] fixed diesel fuel flow rate and then introduced gasoline gradually into a single-cylinder 0.211 L diesel engine. It is found that the gasoline/air mixture with equivalence ratio between 0.098 and 0.42 could be ignited and burned by diesel fuel. But the compression autoignition of this mixture occurred when the total fuel/air equivalence ratio was over 0.735 at any mass flow rate of diesel fuel, not controlled by diesel injection.

The combustion process changes with changing gasoline fraction, which is shown in [25]. Tests were done on a Yanmar L70AE single-cylinder diesel engine at 3600 rpm, 75% load and two intake port temperatures - 48 °C and 57 °C. Three groups of heat release rate curves could be distinguished, corresponding to certain ranges of gasoline fractions. Ignition delay, combustion phasing and heat release change with changing gasoline fraction.

RCCI operation features greatly advanced diesel injection timing, which consequently allows combustion phasing to be linearly dependent on gasoline fraction [26, 27]. As mentioned in [27], when gasoline and diesel fuel have enough time to mix, the local reactivity depends on the ratio of the two fuels. Increasing gasoline fraction causes delay in combustion phasing which is very predictable. This dependence has two implications for the practical application of RCCI. First, the quantity of each fuel must be accurately controlled. Second, the RCCI combustion process regains the coupling between the injection and combustion events that is lost with traditional HCCI or early injection PCCI combustion. Such dependence can be used to control combustion phasing. In a plot of CA50 (the crank angle at which mass fraction burned, or MFB, equals 50%) as function of gasoline fraction, if $\Delta CA50/\Delta GF$ (Δ means difference. GF is gasoline fraction) is large, then a relatively small change of gasoline fraction can result in a large

change of combustion phasing. When the injection timing of diesel/gasoline operation is not advanced greatly, namely in the range of conventional diesel injection timing, then combustion phasing does not depend so much on gasoline fraction, as shown in [24, 25, 28].

Injection timing

A wide range of injection timing has been studied. For single injection and double injections, the injection timings can be as early as IVC (intake valve closing. [4]) and -73º ATDC (after top dead center) [23] respectively, and both injection timings can be as late as near TDC (top dead center) [13, 29].

In general, early injection timings produce a more homogeneous mixture in terms of equivalence ratio and reactivity, or mitigate over-stratification and lead to a more reactive in-cylinder charge [29]. A similar statement is mentioned in [11]: increased mixing time allows the diesel fuel to spread more homogenously throughout the combustion chamber. Thus, the local fuel reactivity of the most reactive regions (i.e., with the highest concentration of diesel fuel) is reduced. On the other hand, late injection timings stratify both equivalence ratio and reactivity [30], and raise local fuel reactivity [20]. As a result, advanced injection often leads to retarded combustion phasing, while retarded injection often leads to advanced combustion phasing. With early injection, combustion phasing is largely governed by the reactivity of in-cylinder charge. In contrast, with an injection near TDC, combustion phasing is robustly controlled by injection [31]. The early and late injection timings are manifested differently in heat release rate. As mentioned in [30], at early timings the charge is well mixed with PCCI/HCCI-like Gaussian-shaped heat release. At late timings, the combustion event exhibits a sharp, more abrupt rise in heat release after the low temperature heat release, followed by a diesel-like tail. Similar phenomenon is also observed by Yang, et al [32].

As mentioned in [32], the close correlation between injection timing and CA50 is desirable for ignition and combustion phasing control. Similar to $\Delta CA50/\Delta GF$ mentioned in “gasoline fraction” section, $\Delta CA50/\Delta SOI$ is used to indicate the ability to

control combustion phasing with changing injection timing [13]. A suitable value means a suitable bandwidth of control, namely the combustion phasing can be easily changed by adjusting injection timing. This is the case in Leermakers's test [13] of "80-10-10-D2" (gasoline fraction is 80%; diesel fuel is equally delivered in double injections, and the timing of the second injection is varied) on one cylinder of a six-cylinder 12.6 L diesel engine. It is noted that the value needs to be chosen carefully, because a high value means a very sensitive CA50. This could make it difficult to control combustion timing, or at least hold combustion timing stable.

Double injections

The function of double injections is summarized in [4, 30]: the first injection sets the background fuel reactivity, and the second injection sets the reactivity gradient. To increase the quantity of diesel fuel in the first injection would increase the background fuel reactivity, and more diesel fuel is distributed in the squish and bowl regions. On the other hand, because the second injection occurs later, diesel fuel has less time to penetrate and vaporize, locally rich zones exist and have reactivity gradient with surrounding homogeneous mixture.

Because the total diesel fuel amount is split into two injections, small amount is injected in each injection. Moreover, the first injection or both injections are greatly advanced, so low injection pressure needs to be used to prevent fuel spray from wall impingement. Therefore, it is possible that insufficient spray penetration, and bad vaporization and mixing might hamper the ignition of the premixed gasoline/air mixture. This is hypothesized by Leermakers et al. [13] when very poor combustion efficiency was observed in three double injection strategies.

In general, double injections need careful application to achieve desired results.

Injection quantity distribution

This topic is about the distribution of diesel fuel amount between two injections in the case of double injections at a certain gasoline fraction. It seems that the fuel amount in

the second injection should be less to get desirable results. For example, Hanson et al. [20] did tests on a Caterpillar 3401E SCOTE (single-cylinder oil test engine) engine at 1300 rpm and 9 bar IMEPn (net indicated mean effective pressure) with gasoline fraction of 0.73. The fraction of the fuel amount in the second injection was varied at 0.38, 0.5 and 0.64. As this amount was increased, so was the mixture stratification. The increased local equivalence ratio and fuel reactivity then advanced combustion phasing creating undesirable results of increased combustion temperature, pressure rise rate, PM and NOx emissions. In the simulation done by Zhang et al. [31] with gasoline fraction of 0.85, 60% Qp (the fraction of the diesel fuel amount in the first injection) yielded higher NOx than 70% Qp. This is largely because 70% Qp led to better mixing between diesel and premixed charge, resulting in less locally hot and rich regions and consequently reducing NOx emissions.

EGR

From the conclusions of [17, 18, 32], the influence of EGR on combustion in diesel/gasoline operation is summarized below, as a result of heating and diluting effect of EGR gas: improving the atomization of gasoline; making the mixture more homogeneous; reducing air/fuel ratio; lowering mixture reactivity; retarding combustion phasing; preventing premature autoignition and stabilizing combustion.

EGR is often combined with other measures. For example, by varying both the percent of premixed gasoline and EGR level, stable combustion can be extended over more of the light-duty drive cycle load range [17].

2.2 Efficiency

As a result of the combustion process described in Section 2.1, most papers report good efficiency in diesel/gasoline operation. For example, Alperstein et al. [33] did tests on a single-cylinder CFR (Co-operative Fuels Research) cetane test engine at 900 rpm and 3.92 bar BMEP (brake mean effective pressure). Gasoline was introduced into the intake manifold in the form of fine mist. When gasoline amount was 17% of the total

fuel, the calculated brake fuel conversion efficiency achieves maximum increase of 4.4%. Hanson et al. [34] carried out piston bowl optimization for RCCI combustion on a light-duty 1.9 L 4-cylinder diesel engine. In their study, RCCI cases have higher brake thermal efficiency than the conventional combustion case. The efficiency increase is due to decreased heat transfer and exhausts via the decreased combustion temperature of RCCI [26].

Diesel/gasoline combustion sometimes suffers poor efficiencies at light loads [19, 23]. For example, Pohlkamp and Reitz [23] did RCCI timing sweep tests on a single-cylinder 0.296 L diesel engine. At 25% load of RCCI combustion, the combustion efficiency decreased, and the fuel conversion efficiency was about 33%, lower than diesel combustion by about 2.5%.

Energy balance was done by some researchers to analyze the factors influencing fuel conversion efficiency [12, 26, 34, 35, 36, 37, 38]. The fuel energy is distributed among brake power, incomplete combustion, friction loss, exhaust, and heat transfer. The relative magnitudes of the losses affect brake power, and thus brake fuel conversion efficiency. Except brake power, most fuel energy is spent on heat transfer, exhaust, and mechanical losses. At constant brake load, decreased heat transfer and exhaust due to low temperature combustion or shortened combustion duration are beneficial for fuel efficiency, while increased incomplete combustion is mainly responsible for decreasing efficiency.

The influences of some variable parameters on engine efficiency are summarized in the following paragraphs.

Gasoline fraction

The influence of gasoline fraction on efficiency is different depending on the basis of comparison and test conditions.

Sahin et al. [39] did test on a Ford XLD 418T turbocharged IDI (indirect injection) four-cylinder 1.75 L diesel engine. FDRs (fuel delivery rates, including diesel and gasoline, expressed as percentage of diesel fuel delivery rate at full load) were kept

constant at five values with varying gasoline fraction at each speed. When gasoline fraction changed from 0 to 0.24 at each speed and FDR, brake specific fuel consumption (BSFC) decreased and effective efficiency increased. Similarly, the BSFC reduction and effective efficiency increment percentages rates become higher at high gasoline fractions.

In the tests done by Yoshida et al. [24], diesel fuel flow rate was fixed and gasoline was gradually introduced into the intake manifold. On one hand, for the same amount of added gasoline, the case with smaller amount of diesel fuel has higher thermal efficiency. On the other hand, in the case of a small amount of diesel fuel, thermal efficiency increases with increasing gasoline. Therefore, brake thermal efficiency is improved when relatively rich pre-mixture is ignited by a small amount of diesel fuel.

In the tests done by Dunbeck and Reitz [25], when gasoline fraction increased from 0 to 0.5 at a certain load, combustion efficiency decreased from 0.99 to 0.95, thermal efficiency decreased from 0.405 to 0.38, and ISFC (indicated specific fuel consumption) increased from 210 to 235 g/kWh.

Injection timing

Generally, under diesel/gasoline operation, advance of diesel injection timing is an effective approach to reduce fuel consumption and improve combustion efficiency and thermal efficiency by enhancing reactivity homogeneity [29, 31], advancing combustion phasing and promoting more complete combustion [13, 21]. For example, Pohlkamp and Reitz [23] studied the influence of injection timing with double injections at three loads. The thermal efficiency, combustion efficiency and ISFC,d (diesel equivalent indicated specific fuel consumption) were improved with advancing injection timing at 25% and 50% loads, but deteriorated at 75% load (the extent was very small).

Double injections

Due to the complexity of double injection, no consistent conclusions are reached about its influence on efficiency. For example, Hanson et al. [20] did three sets of tests with double injections on a Caterpillar 3401E engine at 1300 rpm and 9 bar IMEPn. The

timings of first and second injection, and the fuel percentage of first injection were swept. In all the tests, net thermal efficiency of about 50% was achieved. In the simulation done by Zhang et al. [31], it is found that two diesel injections generally resulted in higher combustion efficiency and lower fuel consumption than single-diesel injection, due to enhanced mixing between diesel and gasoline. On the other hand, all double injection strategies have an indicated efficiency of about 10% lower than the single injection strategy in the investigation done by Leermakers et al [13] because of the low combustion efficiency.

EGR

Application of EGR is usually good for increasing RCCI efficiency. As shown in [22], with the increase of EGR level from 0.3 to 0.5, the indicated thermal efficiencies of all three modes (gasoline PFI + diesel fuel early DI, gasoline PFI + diesel fuel late DI, dieseline DI) increase slightly. This increase is attributed to the higher specific heat of the EGR gas which displaces the air, resulting in lower burned gas temperature and therefore, lower heat loss. It is thought the resulting gamma of the burned mixture (that which is expanding) could be higher if the EGR causes a lower mixture temperature, and also contribute to higher efficiency. Duffour et al. [21] carried out 2D variations of EGR level and SOI on a single-cylinder diesel engine at 2000 rpm and10 bar IMEP, with gasoline fraction of 0.7. Efficiency increases with advanced SOI and higher EGR level. The maximum efficiency is reached at SOI of around -20º ATDC and 30% EGR level.

2.3 Emissions

Most of the reviewed papers show consistent conclusions despite various test conditions and different basis of comparison: simultaneous significant decrease of NOx and smoke emissions, and increase of HC and CO emissions [4, 18, 19, 20, 23, 29, 32, 40, 41, 42, 43]. The conclusions are the same for individual test points and drive cycles [17, 23].

NOx mechanism

It is generally accepted that in internal combustion engines, NOx mainly comes from atmospheric nitrogen, and its formation is governed by the extended Zeldovich mechanism [44]. NOx formation is strongly related to high temperature [44]. When gasoline is used in a diesel engine, the reactivity of in-cylinder charge is reduced, combustion phasing is delayed, in-cylinder temperature is lowered, so NOx formation is reduced [29, 34, 41].

Smoke mechanism

Five reasons for decrease of smoke or soot emission are given in the literature. First, volatile gasoline improves the fuel mixture homogeneity leading to lower local equivalence ratios [4, 23, 25, 29]. Second, longer ignition delay allows adequate time for mixing prior to SOC; thus, rich regions are reduced and soot formation is inhibited [4, 23, 25, 29]. The third reason is the possible effects of gasoline on soot precursor formation. The interruption in the chemical path from fuel to soot means less soot for the same level of mixing [25]. The fourth reason is another benefit of better mixing: smoke is mainly produced in the diffusive combustion phase, while the addition of gasoline enhances the mixing of diesel fuel with air and gasoline combustion products homogenously and quickly, which leads to an improvement in diffusive combustion [39]. The fifth reason is given in [28]: preflame reactions of fumigated gasoline accelerate ignition of main diesel fuel, so combustion is more nearly completed in the vicinity of TDC. By the way, although the influences of local temperature and fuel components on smoke emission were not found in the literature on dual-fuel operation, they are mentioned in various sources. For example, the former influence in [44] and [45], and the latter influence in [45].

HC and CO mechanism

The cause of high HC and CO emissions is summarized below [13, 17, 22, 23, 27, 28, 29, 32]: highly premixed charge, long mixing time and globally lean mixture lead to

overleaning; gasoline vapor is trapped in cold regions such as cylinder wall and crevice volume, and then either is unoxidized or only goes through partial low temperature oxidation; advanced diesel injection causes spray wall impingement.

De Ojeda et al. studied exhaust hydrocarbon speciation from a single-cylinder compression ignition engine operating with in-cylinder blending of gasoline and diesel fuels [29]. [29] provides detailed descriptions of HC components and the cause of high HC emission. For example, under diesel/gasoline operation, unburned hydrocarbons (UHCs) are primarily present as mono-aromatics and C4-C7 alkanes, which are likely either unoxidized or lightly oxidized gasoline constituents, while light hydrocarbon species are the dominant exhaust hydrocarbon species from diesel-only operation.

Gasoline fraction

Increasing gasoline fraction generally decreases NOx and smoke emissions, and increases HC and CO emissions [23, 29, 32, 34]. As mentioned in [41] and [46], with the increase of gasoline fraction (0 - 80% by energy) at intake air temperature of 20°C or 80 °C, NOx emission decreases linearly from 400 ppm to slightly over 100 ppm. The exhaust soot concentration decreases at an overall load condition, and at a gasoline fraction of over 60%, soot emission becomes almost zero. In the test done by Himabindu and Mahalakshmi [47] on a single-cylinder 0.661 L diesel engine at 1500 rpm and 75% load, when gasoline fraction increases from 0 to 40%, NOx emission is reduced from 593 ppm to 290 ppm, and HC and CO emission increase by 54.46% and 0.18% respectively.

Injection timing

The influence of injection timing on emissions is more complex than that of gasoline fraction. De Ojeda et al. studied the effect of injection timing and reactivity on emissions [29]. Significant reduction in UHC emission (by up to 65%) and CO emission can be achieved while maintaining low soot and NOx emissions. The advance of SOI helps to enhance the reactivity-homogeneity of in-cylinder charge and minimize the low-

reactivity regions. There are optimal SOIs where UHC and CO emissions can be minimized [23]. In the injection timing sweep tests shown in [23], HC emission generally decreases with increasing load and advancing injection timing. The CO emission exhibits different trends for different engine loads. As injection timing is advanced, CO emission increases at 25% load, is nearly constant at 50% load, and decreases at 75% load. This is potentially due to over-mixing effects at light load. NOx emission is very low for all the data, but increases with increasing load as expected. Also, NOx emission shows local minima at injection timings near -46 - -44º ATDC for all load cases but is most pronounced at 50% load. Soot emission is also near zero with 25% load actually producing the most soot.

Double injections

Splitter et al. studied injection effects in low load RCCI combustion [30]. The fueling method is isooctane PFI + n-heptane DI. Single injection timing was swept from −145° ATDC to −15° ATDC with 10° interval. In the case of double injections, first injection timing was swept from −145° ATDC to −35° ATDC with 10° interval, and the second injection timing was later by 25º. It was found that at later injection timings that avoided liner impingement, double injections proved to be advantageous, with up to 50% reductions in CO and HC. This advantage is attributed to the more distributed mixture of the direct-injected fuel in the squish and bowl regions. On the other hand, HC and CO emissions for the double injection strategies might be poor, as shown in the test results from [13]. This might be due to the potential disadvantage of double injections mentioned in Section 2.1.

Injection quantity distribution

The influence of injection quantity distribution on emissions through both modeling and experiments is shown in [12]. The modeling results show that at high load of 23 bar IMEP by reducing the diesel fuel fraction in the first injection from 90% to 50%, the NOx emission and max pressure rise rate (MPRR) can be reduced without significant

increases in soot emission. The soot emission does not increase rapidly until significant diesel fuel is removed from the first injection and placed in the second, such that the second injection begins overlapping with the timing of high-temperature heat release. The fraction of diesel fuel in the first injection was swept experimentally and similar conclusions are reached. As the fraction reduced from 72% to 64%, the NOx emissions are reduced by 50% and the MPRR by 25%. The soot emissions, however, increase significantly which are likely over predicted.

EGR

Lee et al. did tests on a single-cylinder 0.673 L diesel engine [18]. At any gasoline fraction within the range of 0 to 0.6, NOx emissions decrease significantly with EGR level increasing from 0 to 0.3. Unburned hydrocarbon concentration increases with increasing gasoline fraction, but it was reduced when EGR was applied at high premixed ratio. This trend can be inferred from the temperature rise of the mixture heated by hot EGR gas, which improves atomization of premixed fuel and air–fuel mixture becomes more homogeneous than the case without EGR.

2.4 Summary

The literature review reveals the benefits of diesel/gasoline dual-fuel operation: very low NOx and PM emissions with good efficiency. These benefits and the potential of using gasoline fumigation to realize them provide the major motivation to this research, the objective of which is shown in Section 1.2.

Moreover, the literature review reveals gaps present in the current state-of-the-art of RCCI research, which will be filled by this study.

The first gap is most research done on multi-cylinder engines uses gasoline PFI, meaning one gasoline injector is used per cylinder. This complicates control strategy and increases hardware cost.

This gap will be filled by the proposed research with gasoline fumigation on a four-cylinder medium-duty diesel engine. Gasoline fumigation means only one gasoline

injector is installed on the intake manifold to provide gasoline for all cylinders. So if satisfactory dual-fuel operation can be realized through gasoline fumigation, the control strategy will be simpler and the hardware cost will be decreased.

The second gap is the limitation exhibited by the experimental studies on gasoline fumigation + diesel DI [24, 28, 33, 38, 39, 48,]. The engines are mainly single-cylinder or light-duty. The gasoline and diesel fuel supply systems are mainly mechanically controlled. Few research adopted the most commonly-used basis of comparison: constant brake load. Gasoline fractions are lower than 0.5. The injection timings are within the range of conventional diesel fuel injection timings.

These limitations offer great opportunity for the proposed research. Tests can be done on a multi-cylinder engine, and fuel distribution among cylinders can be studied. The injection settings can be adjusted flexibly with electronically-controlled gasoline and diesel fuel supply systems. Tests can be done on constant brake load. Gasoline fractions and injection timings can be adjusted within wide ranges.

The third gap is about test method. Many papers on dual-fuel use parametric study to investigate the influences of factors, but do not consider combining these factors to get optimal outcome such as engine efficiency and emissions [49, 50]. Other papers use single factor alternate method and get optimal outcome [51, 52]. Still other papers describe procedures to get optimal outcome, but lack sufficient information for other researchers to repeat [53, 54]. On the other hand, many papers and dissertations discuss engine research other than dual-fuel research, with DOE (design of experiment) and relevant statistical techniques applied [55, 56, 57, 58].

This gap will be filled by applying DOE and relevant statistical techniques to this study. Special sets of tests can be designed and done. Based on the results, regression models containing factors and targets can be obtained. The most appropriate models can be used for optimization. Finally the factor settings for better target(s) can be determined and used to guide future tests. This study could provide a guideline to direct DOE-oriented development of diesel/gasoline dual-fuel engine research.

The fourth gap is that few papers on dual-fuel research discuss the results on cycle-to-cycle basis or cyclic variability (CV). This research fills the gap by studying CV in dual-fuel operation and its influence on engine performance and efficiency. The details are given in Section 6.1.

3. EXPERIMENTAL SETUP AND METHODOLOGY

3.1 Experimental apparatus

Test bench

The test bench consists mainly of the engine, dynamometer, fuel supply systems, emission measuring system, and data acquisition system. It is shown in Figure 1, indicating major components, engine parts, gas and fuel flow, and where the important parameters are measured.

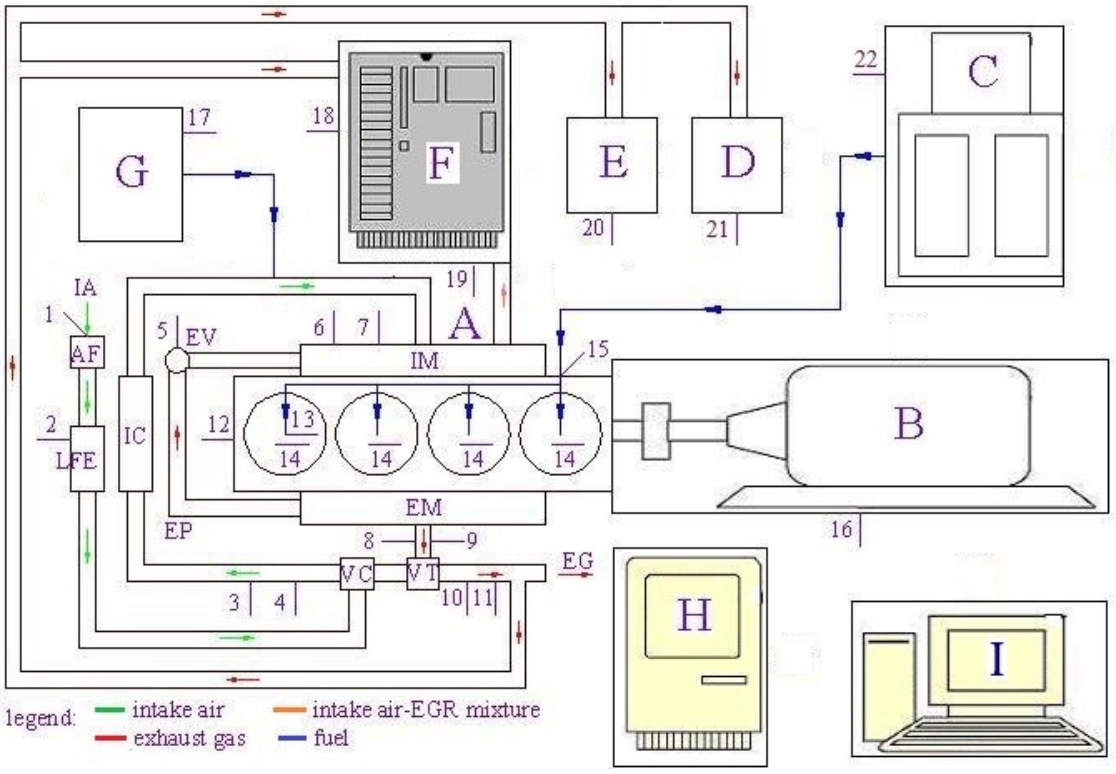

Note:

- Components:
  - A. John Deere engine
  - B. dyno
  - C. diesel supply system
  - D. smoker meter
  - E. mini dilution tunnel
  - F. emission bench
  - G. gasoline supply system
  - H. data acquisition system
  - I. dyno controller

Figure 1 *Test bench showing the engine apparatus and various measurement points*

- Engine parts and gas:

IA: intake air	AF: air filter	LFE: laminar flow element
VC: VGT compressor	VT: VGT turbine	IC: intercooler
EP: EGR pipe and cooler	EV: EGR Valve	IM: intake manifold
EM: exhaust manifold	EG: exhaust gas	

- Important parameters measured and the locations:

1. air temperature, humidity and barometric pressure	2. pressure difference upstream and downstream LFE (used to calculate air flow rate)	3. temperature at VGT compressor outlet
4. pressure at VGT compressor outlet	5. EGR valve position	6. temperature of gas inside intake manifold
7. pressure of gas inside intake manifold	8. temperature of gas at VGT turbine inlet	9. pressure of gas at VGT turbine inlet
10. temperature of gas at VGT turbine outlet	11. pressure of gas at VGT turbine outlet	12. engine speed and crank angle
13. injection current and needle lift	14. cylinder pressure	15. rail pressure
16. torque	17. gasoline flow rate	18. exhaust CO, HC, NOx, CO_2, O_2 concentrations
19. intake CO_2 concentration	20. particulate matter	21. smoke number
22. diesel flow rate		

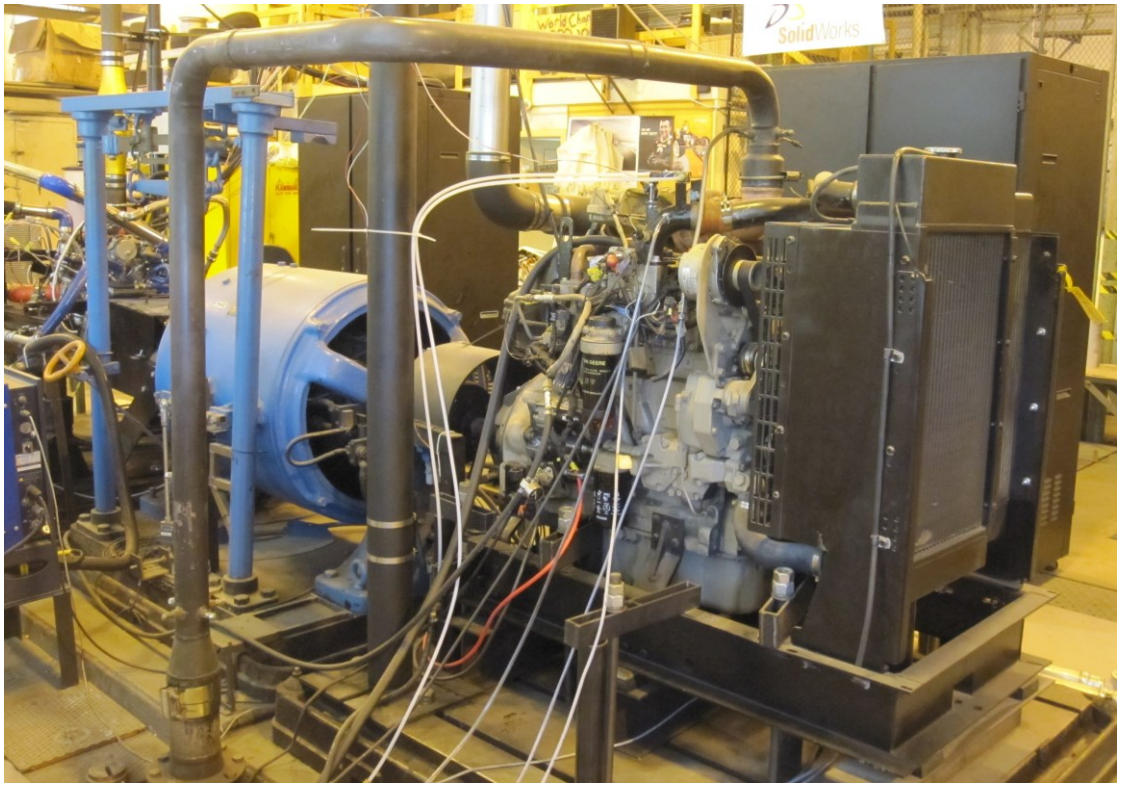

Figure 1 *continued*

Engine

A John Deere model 4045HF485 medium-duty diesel engine is used. Its main specifications are listed in Table 1. The advanced technologies enabling this study include a high pressure common rail fuel system, electronically-controlled fuel injectors, a variable geometry turbocharger (VGT), and a cooled EGR system. Full-authority control over engine parameters is made possible with the use of a third-party engine controller (Drivven, Inc., San Antonio, TX).

Table 1 *Main specifications of the John Deere model 4045HF485 diesel engine*

Parameter	unit	Value
cylinder number	-	4
displacement volume	L	4.5
bore	mm	106
stroke	mm	127
compression ratio	-	16.57:1 (measured. Nominally 17:1)
valves per cylinder	-	2 intake valves and 2 exhaust valves
rated power	hp (kW) @ rpm	154 (115) @ 2400
peak torque	lb-ft (N•m) @ rpm	424 (575) @ 1400
fuel system	-	Electronic common rail, direct injection
air system	-	VGT with EGR
intake valve timing	° ATDC (exhaust)	-27.4 - 218.6
exhaust valve opening	° ATDC (exhaust)	-245 - 28
emission certification	-	EPA Tier 3, EU STAGE III A and CARB

Dynamometer (dyno)

A DC electric dynamometer holds the engine speed constant and absorbs the brake load of the engine. The dyno loads the engine via automatic feedback control adjustment of the field current to maintain the desired engine speed. The dyno obtains torque measurements by applying a braking force or load on the engine shaft connected to the dyno. The dyno controller applies a current to the dyno, setting the applied braking force on the rotor by the housing or stator of the dyno. The magnitude of the current controls

the magnitude of braking force. The force is measured with a load cell connected to the dyno housing. The load cell force is then multiplied by the distance from the force to the center of the rotor giving the measured torque produced by the engine.

Emission measuring system

HORIBA MEXA-7000 automotive emission analyzer system is used to measure NOx, HC, CO, CO_2 and O_2 concentrations in the engine's exhaust and intake (intake CO_2 concentration is measured for calculation of EGR level) gases. The measuring techniques for the gaseous species are heated chemiluminescence for NOx, heated FID (flame ionization detection) for HC, NDIR (nondispersive infrared) for CO and CO_2, and magneto-pneumatic for O_2. Gas samples are delivered either through sample lines heated to 190°C (to NOx and HC analyzers, and smoke meter) or through sample lines cooled and dehumidified (CO, CO_2, and O_2 analyzers). Each analyzer is calibrated at the start of each test and checked routinely throughout the day's testing. Moreover, an AVL 415S smoke meter is used to measure smoke emission, and a mini dilution tunnel is used to get PM emission.

Fuel metering system

Figure 2 shows the system for measuring diesel fuel flow rate. The fuel is sucked out of the drum, follows the red arrows, and enters the vapor eliminator. Here, part of the fuel flows back to the drum following the pink arrows. The rest passes the flow meter and level controller, and finally flows to the engine, following the green arrows. Part of this fuel is injected into the cylinders and consumed, and the rest returns to the cabinet following the blue arrows. The ventilation follows the cyan arrows.

The core parts including vapor eliminator, flow meter, transmitter, and level controller are from Max Machinery, Inc. The vapor eliminator unit removes bubbles from the fuel which would otherwise cause measurement errors as they pass through the flow meter. The bubbles could come from air trapped or fuel vaporized in the fuel lines. The fuel meter has a volumetric flow rate range from 1 to 1800 CCM (cc per minute) and an

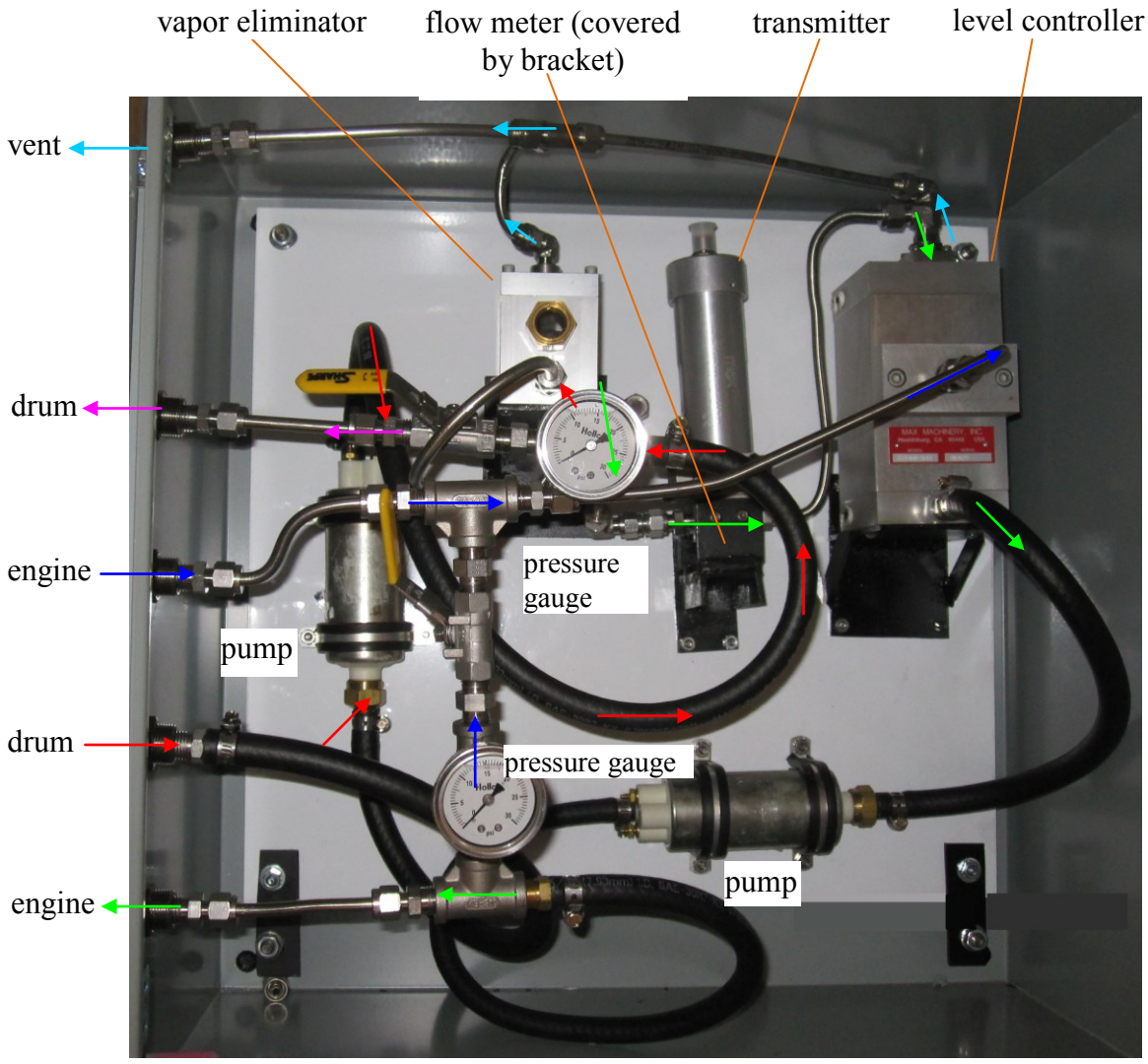

Figure 2 *Diesel fuel metering system*

accuracy of 0.2%. In the flow meter, four radial pistons drive a crankshaft. Each piston acts as a 3-way valve which controls the filling and discharge cycle for a neighboring piston and its cylinder. The transmitter senses the crankshaft rotation and produces a voltage. The linear correlation between the voltage (VDC) and flow rate (CCM) is given in the calibration certificate provided with the products. The DAQ system receives the voltage signal, calculates with the correlation, fuel density, and engine speed, and finally outputs fuel mass flow rate in g/s. The level controller serves as a vented, recirculation

tank to collect return fuel and route it back to the supply side of the engine, while maintaining its level through a float valve that controls the fuel flow through the flow meter.

The fuel metering system for gasoline is similar, but involves fewer parts, as shown in Figure 3.

Gasoline supply system

As shown in Figure 3, gasoline flows out of the tank, through the prefilter, pump 1 and fine filter, to the inlet of fuel metering cabinet. Here, part of the fuel flows through the fuel metering cabinet and out to pump 2, while the other fuel returns to the tank. The fuel supply pressure to the cabinet can be adjusted by the valve and shown by the pressure gauge. Pump 2 supplies fuel to the fuel rail and injector, which are mounted on the intake elbow, upstream of the intake manifold but downstream of the intercooler. Extra fuel leaves the fuel rail and flows back to the pressure regulator, and then to the fuel metering cabinet. The pressure regulator is connected to the intake pipe with an air hose to get pressure reference. It keeps the fuel pressure at 3 bar higher than the intake air into which the fuel is injected. The Drivven CompactRIO PFI driver module kit controls the injection timing and injection duration. The Drivven CompactRIO controller can remotely switch the two pumps on or off through the two relays, which is especially useful in case of emergency. Gasoline is injected 4 times per cycle with an interval of 180º, and in the same order as firing, namely 1-3-4-2. The injection occurs early in the intake stroke, just after the valve overlap period is over.

It is noted that this fuel supply system can also be used for possible future investigation of alternative fuels such as ethanol and biogasoline.

At first, a SIEMENS injector was installed vertically on the intake elbow, so the fuel spray was along the air flow. It was found during the initial dual-fuel tests with high gasoline fractions the cylinder variation was rather serious, even when the cylinders were balanced with only diesel injection before gasoline was added: the IMEP, cylinder pressure, and heat release rate profiles were very different among cylinders. The

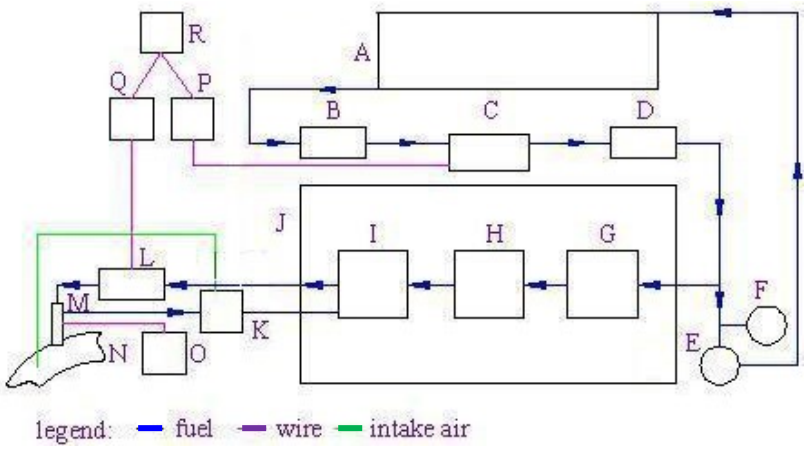

Note:

A. tank
B. prefilter
C. pump 1
D. fine filter
E. valve
F. pressure gauge
G. vapor eliminator
H. flow meter and transmitter
I. level controller
J. fuel metering cabinet
K. pressure regulator
L. pump 2
M. fuel rail and injector
N. intake pipe
O. Drivven CompactRIO PFI driver module kit
P. relay 1
Q. relay 2
R. Drivven CompactRIO controller

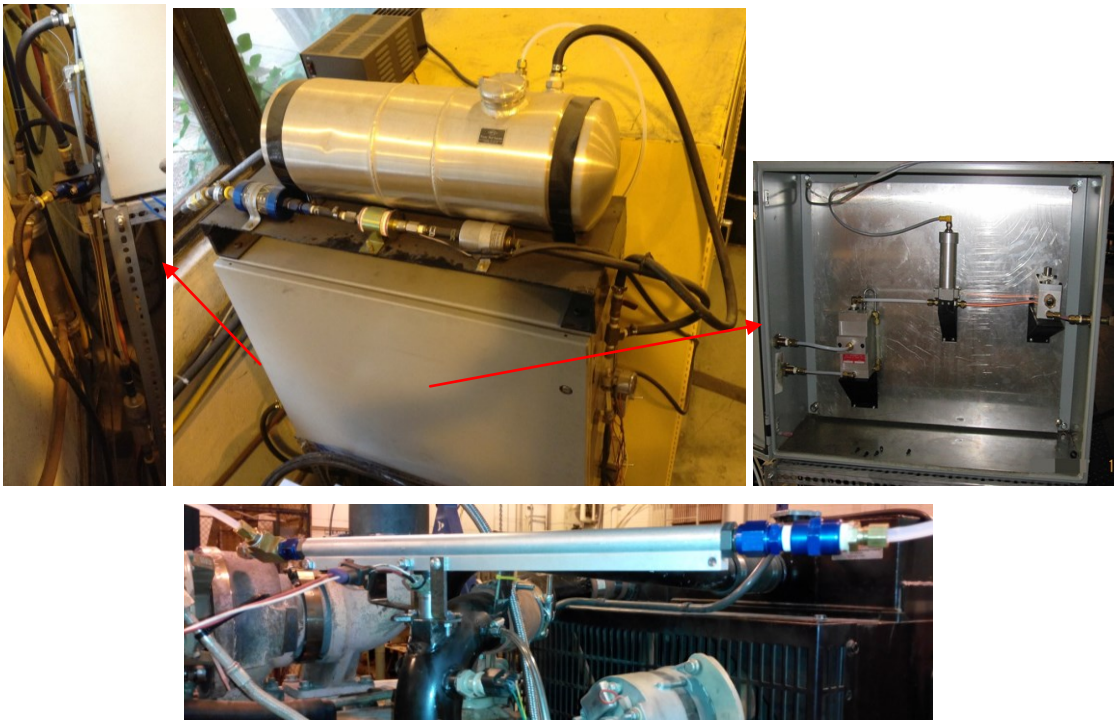

Figure 3 *Gasoline supply system*

injection was visually checked, and the fuel atomization was very poor. This explains why cylinder 3 almost always has the highest IMEP, and highest and much advanced cylinder pressure and heat release rate profiles. Probably fuel tended to accumulate at the interface of the intake manifold and cylinder head. Cylinder 3 is just downstream of the intake manifold, so it could inhale much of the accumulated fuel. The timings and durations of diesel injections in each cylinder and gasoline injections were adjusted separately or together to balance cylinders, to make IMEPn values and high-speed profiles among the cylinders as close as possible. But the effect is limited.

Then the gasoline supply system was modified to improve gasoline distribution among cylinders. A DENSO and a BOSCH injector were obtained, with better fuel atomization. A fuel rail was installed upstream of the injector to reduce the fluctuation caused by fuel injection. Engine tests were done with both injectors when they were installed vertically or horizontally (fuel spray was along and against the air flow, respectively), to check gasoline distribution. The BOSCH injector gave relatively better results when installed vertically, which was chosen as the final fueling method.

Figure 4 shows examples of high-speed profiles in two tests: 5.65-1124--9.4-0.5 with SIEMENS injector and 5.65-1124--11-0.4 with BOSCH injector. The test names are in the format of "BMEP (bar) - rail pressure (bar) - SOI (° ATDC) – desired gasoline fraction". It is obvious that the cylinder variation was greatly improved with the BOSCH injector because the corresponding profiles are much closer to each other respectively, compared to the profiles with the SIEMENS injector. This is also reflected by cylinder gasoline fractions and IMEPn among all the cylinders. The former's standard deviations are 0.268 and 0.084 for SIEMENS and BOSCH injector respectively. The latter's standard deviations are 1.715 bar and 0.367 bar respectively.

Other solutions to improve gasoline distribution were considered but not used, as explained in the following paragraphs.

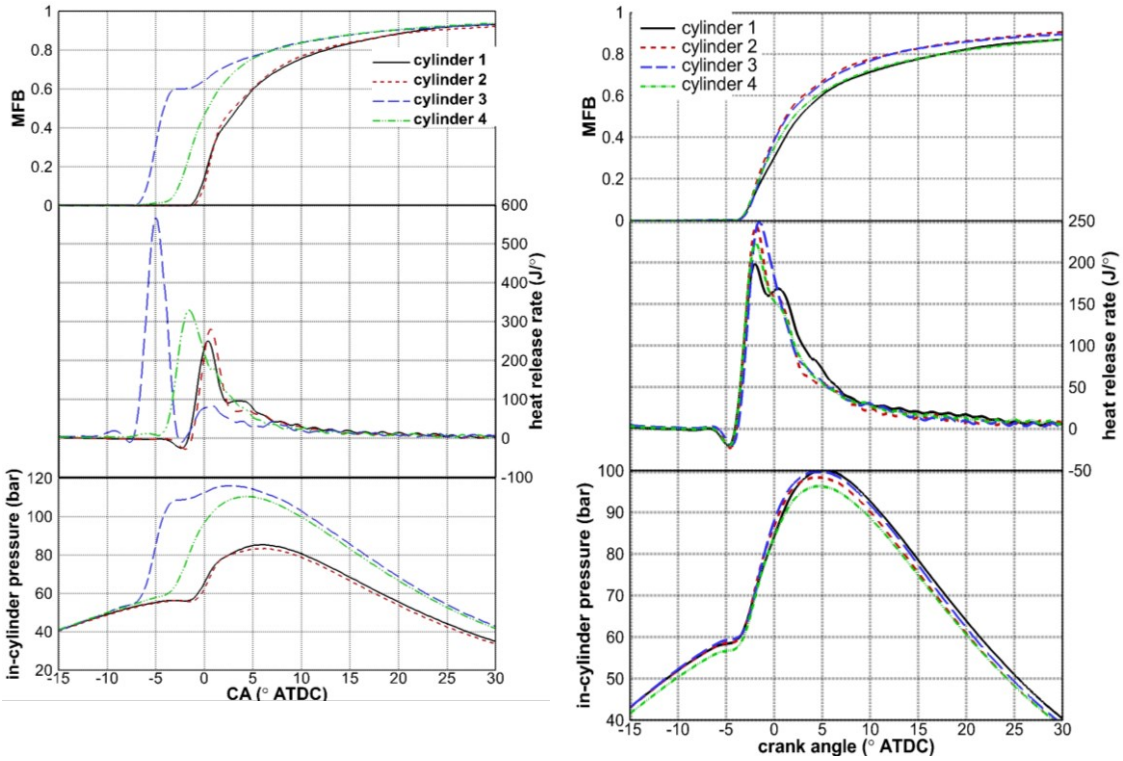

(with SIEMENS injector) (with BOSCH injector)

Figure 4 *Comparison of cylinder variation*

The best solution is to mount an injector on each intake port. This was considered in the beginning of the dual-fuel research but then abandoned because it involves significant modification to the cylinder head and cover.

A kind of gasoline distributor was designed, as inspired by [59] (a paper on the distribution of the fuel flow in a cold start system using an electronic fuel injector), but the design was abandoned because it was considered not effective.

The supply of gasoline to only one cylinder was considered but not established, because it would decrease the significance of this research which is based on multi-cylinder engine.

Better modeling of the intake flow/manifold and better injection timing control were proposed. In other words, if the distribution issues are understood, perhaps the gasoline fuel injection scheme can be tailored to dose the intake stream with appropriate

quantities to correspond to which cylinder is breathing. This was done with GT Power by a student, which did not get any results, partly because the detailed geometry information of intake manifold and ports were not available.

Increasing injection pressure was considered. The pressure of common port gasoline injectors is similar to the pressure of the BOSCH injector, with the max value of 6 bar shown in some papers [60]. GDI (gasoline direct injection) injector was considered because it can provide much higher pressure, but the drive and plumbing pose challenges. A GDI injector was used in [41], with injection pressure of 55 bar, but it is not mentioned how the pump was driven. In GDI engines the pumps are driven by engine shaft, which is impractical in diesel engines.

Installing a mixer or mini axial flow fan downstream the gasoline injector in the intake manifold, heating the gasoline in the fuel line, and heating the intake mixture were also considered but not established.

Finally, compared to PFI system, gasoline fumigation has two advantages: simplified control strategy and reduced hardware cost.

About simplified control strategy, although the injector driver module kit used in the research can accommodate up to four injectors, obviously controlling four injectors is more complex and make the controller more prone to malfunction.

For either gasoline fumigation or PFI system, the parts commonly needed to be added to a diesel engine include injector(s), rail, tank, pressure regulator, filters, pumps, valves, hoses, brackets, couplings, wires, pressure sensors, fuel metering system, and injector driver module kit. All these cost about $8300, and the last two cost $6770. For PFI system, extra injectors are needed, and will cost additional $220 if on a 4-cylinder engine.

Moreover, gasoline fumigation system requires less modification to intake system than PFI system. The two systems involve modification to intake manifold and intake ports respectively. The latter modification is more complex and costly, because compared to intake manifold, the intake port has smaller outer surface, the surrounding is more restricted, and causes more disturbance to the intake gas flow.

The additional gasoline supply system is more influential for a smaller engine because the engine cost less so the system is a bigger proportion in the engine's total cost. On the other hand, gasoline is cheaper than diesel in the USA. For example, regular gasoline price is about $3.34/gallon, while diesel is about $3.7/gallon, in gas stations in College Station TX on June 15 2014. Therefore the reduced fuel cost for dual-fuel engines can eventually offset the cost of additional gasoline supply system.

3.2 Data acquisition and calculation

The determination of important parameters is described in Table 2, and some parameters are introduced afterwards. All crank angle resolved measurements (cylinder volume, rail pressure, needle lift, injection current, and in-cylinder pressure) are collected for 300 consecutive cycles. The analysis is performed on the average of the 300 cycles to remove cyclic variation and get a good measurement of the true steady-state operation.

In-cylinder pressure

In-cylinder pressure is measured from all 4 cylinders every 0.2º CA using Kistler 6056A piezo-electric pressure transducers. The ordinary calibration and fidelity checks are carried out according to [61]. The reported pressure data are from a collection of 300 consecutive cycles. A low-pass zero-phase IIR (infinite impulse response) filter is used to remove high frequency reverberations so that relatively smooth heat release rate profiles can be obtained (it is noted such pressure filtering is carefully monitored to prevent data shifting or excessive loss of signal). A filter order of three is used with a cutoff frequency of about 10% of the sampling frequency (1800 samples/revolution). The filter properties are determined so that the peak value and width of the pressure derivative maximums associated with combustion events are minimally affected.

Table 2 *Determination of important parameters*

Parameter	Determination
engine speed	Measured using speed sensor.
torque	Measured using dyno-mounted load cell.
air temperature, humidity and barometric pressure	Measured using OMEGA EWS-RH relative humidity, temperature transmitter and OMEGA EWS-BP-A barometric pressure transmitter.
temperature	The temperature of intake gas, fuel, oil and exhaust gas, etc. is measured using K type thermocouples in respective positions.
pressure	The pressure of intake gas and exhaust gas is measured using pressure sensors in respective positions.
fuel flow rate	Measured using Max Machinery flow meter.
fuel consumption	Detailed below.
gasoline fraction	Detailed below.
air flow rate	Measured using Meriam air flow meter.
A/F ratio and equivalence ratio	Detailed below.
EGR level	Detailed below.
crank angle	Measured using AVL angle encoder with 0.2° resolution.
in-cylinder pressure	Detailed below.
needle lift	Measured using needle lift sensor.
diesel fuel rail pressure	Measured via engine controller sensor.
start or end of injection	Calculated from measured needle lift.
SOC	The crank angle where the heat release rate reaches the lowest local value after SOI.
end of combustion	Considered as CA90.
ignition delay	Crank angles from SOI to SOC.
combustion duration	Crank angles from SOC to end of combustion.
bulk gas temperature	Calculated using ideal gas equation.
combustion efficiency	Detailed below.
heat release rate and MFB	Detailed below.
brake fuel conversion efficiency	Detailed below.
smoke number	Measured using AVL smoke meter.
PM emission	Measured using mini dilution tunnel.
NOx emission	Measured using Horiba emission bench: heated chemiluminescence.
HC emission	Measured using Horiba emission bench: FID. Reported on propane basis.
CO and CO_2 emission	Measured using Horiba emission bench: NDIR.
O_2 emission	Measured using Horiba emission bench: magneto-pneumatic method.
brake specific emissions of NOx, HC and CO	The exhaust gas emissions measured are expressed as volumetric or mole fractions. NOx and HC fractions are on wet basis, while the other fractions are on dry basis. First, the dry fractions are converted into wet fractions. Second, the molecular weight of exhaust gas is calculated. Third, the mass fractions and mass flow rates of NOx, HC, CO are calculated. Finally, their brake specific emissions are calculated through dividing mass flow rates by brake power.

Brake fuel conversion efficiency

Brake fuel conversion efficiency ($\eta_{f,b}$) is defined as brake power divided by the fuel energy delivery rate, as shown in Equation (3.1). It is abbreviated as "efficiency" in the following parts of the dissertation.

$$\eta_{fb} = \frac{P_b}{\dot{E}_f} = \frac{P_b}{\dot{m}_d LHV_d + \dot{m}_g LHV_g} \tag{3.1}$$

Where, $\dot{E}_f$: fuel energy delivery rate (kW); LHV_d, LHV_g: lower heating values (kJ/kg) of diesel fuel and gasoline, respectively; $\dot{m}_d, \dot{m}_g$: diesel fuel and gasoline flow rates (kg/s); P_b: brake power (kW).

Fuel consumption

Usually the fuel consumption is represented by BSFC (g/kWh), as shown in Equation (3.2). The symbols are not explained because their meanings are already shown under equation (3.1). In Section 3.2 same symbols have same meanings, so not each symbol in a certain equation is explained after that equation.

$$BSFC = \frac{\dot{m}_d + \dot{m}_g}{P_b} \tag{3.2}$$

Since dual-fuel tests involve two kinds of fuels with different heating value, the fuel consumption can be represented more suitably by BSEC (brake specific energy consumption, kJ/kWh), as shown in Equation (3.3).

$$BSEC = \frac{\dot{m}_d LHV_d + \dot{m}_g LHV_g}{P_b} \tag{3.3}$$

Diesel and gasoline used in this research have similar heating values, 43.01 and 41.68 MJ/kg respectively, so BSEC is almost proportional to BSFC, and BSFC is used to report fuel consumption for simplicity.

Gasoline fraction

Gasoline fraction is defined as the fraction of gasoline in all the fuel including gasoline and diesel. The fraction can be in terms of mass (r_m) and energy (r_e), as shown

in Equations (3.4) and (3.5). Diesel and gasoline have similar heating values, so the two fractions are very close, and gasoline fraction based on mass is used because it is more common.

$$r_m = \frac{\dot{m}_g}{\dot{m}_d + \dot{m}_g} \tag{3.4}$$

$$r_e = \frac{\dot{m}_g LHV_g}{\dot{m}_d LHV_d + \dot{m}_g LHV_g} \tag{3.5}$$

A/F ratio and Equivalence ratio

The A/F ratio and equivalence ratio of the air-fuel mixture are defined in Equations (3.6) and (3.7).

$$A/F = \frac{\dot{m}_a}{\dot{m}_d + \dot{m}_g} \tag{3.6}$$

$$\phi = \frac{\dot{m}_d (A/F)_{stoic,d} + \dot{m}_g (A/F)_{stoic,g}}{\dot{m}_a} \tag{3.7}$$

Where, $\dot{m}_a$ is air mass flow rate (kg/s); $(A/F)_{stoic,d}$ and $(A/F)_{stoic,g}$ are stoichiometric A/F ratio of diesel and gasoline.

EGR level

The EGR level is defined in Equation (3.8).

$$EGR = \frac{\dot{m}_{EGR}}{\dot{m}_{trapped}} \tag{3.8}$$

Where, $\dot{m}_{EGR}$ is mass flow rate of recirculated exhaust gas; $\dot{m}_{trapped}$ is mass flow rate of intake mixture of fresh air, recirculated exhaust gas and residual gas.

EGR level can be calculated with measured exhaust and intake gas concentrations using a standard method described in [62, 63].

Heat release rate and MFB

Heat release rate is calculated using the in-cylinder pressure data along with the First Law of Thermodynamics, with consideration of cylinder mixture from IVC to EVO (exhaust valve opening) as a control volume, and assumption of single zone mixture, ideal gas behavior, and no mass transfer (i.e., no blow-by, crevice flow, or mass addition from injection) [64, 65]. It is shown in Equation (3.9).

$$\frac{\delta Q_{ch}}{d\theta} = \frac{\delta W_{cv}}{d\theta} + \frac{dU_{cv}}{d\theta} + \frac{\delta Q_{ht}}{d\theta} \tag{3.9}$$

The four terms are heat release rate, work rate, internal energy change rate and heat transfer rate. The terms in the right will be introduced below respectively.

The work rate can be written as Equation (3.10).

$$\frac{\delta W_{cv}}{d\theta} = p\frac{dV}{d\theta} \tag{3.10}$$

The measurement and processing of in-cylinder pressure p is mentioned above. Cylinder volume change rate $\frac{dV}{d\theta}$ is calculated from engine geometric data.

The internal energy change rate can be written as Equation (3.11).

$$\frac{dU_{cv}}{d\theta} = \sum_i m x_i c_{v,i} \frac{dT}{d\theta} \tag{3.11}$$

Where, m: total trapped mixture mass; x_i: species mass fraction; $c_{v,i}$: species specific heat; T: bulk gas temperature. $T = \frac{pV}{mR}$ (R is mixture gas constant).

Both x_i and $c_{v,i}$ are calculated based on information in the JANAF tables [66]. These computerized tables have detailed equation fits for experimentally determined species properties. Also included in the tables are species equilibrium mechanism constants that aid in determining the equilibrium concentrations for a specific reaction. These equations allow for the simultaneous solution of a number of important species equilibrium mechanisms that are included in the calculation. Subsequently, knowing the species concentrations that correspond to a given temperature and pressure along with the species specific heats allow for the calculation of the mixture internal energy [67].

The heat transfer rate can be written as Equations (3.12) and (3.13). Equation (3.13) is a well-established correlation developed by Hohenberg ([68]). It is widely used and can reflect the influence of gas temperature, wall temperature, and in-cylinder fluid motion. Equations (3.12) and (3.13) do not directly assess radiation heat transfer, whose influence is reflected in the change of temperature.

$$\frac{\delta Q_{ht}}{d\theta} = h_c A_s (T - T_w) \tag{3.12}$$

$$h_c = 3.26 V^{-0.06} p^{0.8} T^{-0.4} (\bar{S}_p + 1.40)^{0.8} \tag{3.13}$$

Where, h_c: heat transfer coefficient; *As*: heat transfer area, including the surfaces of cylinder head bottom, cylinder wall and piston top, calculated from engine geometric data; *Tw*: temperature of the heat transfer area. It is assumed to be constant because the tests are run at steady state conditions; $\bar{S}_p$: mean piston speed.

MFB is calculated through dividing the amount of fuel burned from SOC till a certain crank angle by the amount of fuel burned from SOC till EVO, as shown in Equation (3.14). The crank angle where MFB equals *N*% is denoted as CA*N*. The most common ones are CA10, CA50, and CA90.

$$MFB = \frac{m_{fuel,CA,i}}{m_{fuel,i}} = \frac{\dfrac{\sum_{\theta=SOC}^{CA} \dot{Q}_i * \Delta CA}{LHV_{fuel}}}{\dfrac{\sum_{\theta=SOC}^{EVO} \dot{Q}_i * \Delta CA}{LHV_{fuel}}} = \frac{\sum_{\theta=SOC}^{CA} \dot{Q}_i * \Delta CA}{\sum_{\theta=SOC}^{EVO} \dot{Q}_i * \Delta CA} \tag{3.14}$$

Where, $m_{fuel,CA,i}$: cumulative mass of fuel burned from SOC till a certain crank angle in cylinder *i* within a cycle; $m_{fuel,i}$: total mass of fuel burned from SOC till EVO in cylinder *i* within a cycle; θ: crank angle; $\dot{\zeta}_i$: heat release rate at a certain crank angle in cylinder *i*; ΔCA: crank angle resolution, 0.2º; LHV_{fuel}: fuel lower heating value.

3.3 Fuel

Standard #2 diesel fuel and 87 AKI (anti-knock index) gasoline (both acquired from local fuel stations) are used in this study. The same batches of both fuels were used consistently throughout the study. Their properties are measured by Southwest Research Institute, and shown in Table 3. The standards used are shown in the brackets. A few gasoline properties are calculated by the author based on the measured properties assuming the fuel contains only pure gasoline and ethanol, and the pure gasoline contains only carbon and hydrogen elements. Ethanol is considered as pure substance, and its density and LHV are adopted as 789 kg/m^3 [69] and 27 MJ/kg [70], respectively. The calculated properties are also shown in Table 3 as denoted by *.

3.4 Work plan

The topic of this research is "simultaneous efficiency, NOx, and smoke improvements through diesel/gasoline dual-fuel operation in a diesel engine". Therefore the test plan is made to find the influencing factors of the efficiency and emissions, at 1400 rpm and each of three loads (BMEP of 1.88, 5.65 and 8.52 bar, called low load, medium load, and high load respectively), in both diesel baseline tests and dual-fuel tests, and then compare the results and get conclusions. Engine speed of 1400 rpm is chosen because max torque occurs at this speed, and many previous tests were done at this speed offering many data for reference. Higher loads are not adopted considering safety.

First, DOE and relevant statistical techniques were applied to tests, to identify and quantify the parameter settings for efficiency and emissions. Second, parametric studies of gasoline fraction and injection timing were done to find their influence on efficiency and emissions. Finally, individual cycle data were analyzed to study cyclic variability and its influence on dual-fuel efficiency and emissions.

Detailed information is shown in Chapter 4 - 6 respectively.

Table 3 *Diesel fuel and gasoline properties*

Note:
① The standards for diesel fuel and gasoline are SAE J1829 and ASTM D5291 CH respectively.
② The standard for diesel fuel is SAE J1829, while the values for gasoline are calculated.
N/A 1: not available.
N/A 2: not applicable.

property (standard)	unit	diesel fuel	gasoline
carbon mass concentration (①)	%	85.81	83.1
hydrogen mass concentration (①)	%	13.41	13.75
oxygen mass concentration (②)	%	0.78	3.15
H/C mole ratio (②)	-	1.862	1.986
sulfur concentration (ASTM D5453)	ppm	5.3	18.1
density @ 15ºC (ASTM D4052s)	kg/m^3	825.5	748.9
net heating value (ASTM D240N)	MJ/kg	43.008	41.678
gross heating value (ASTM D240N)	MJ/kg	45.853	N/A 1
stoichiometric A/F ratio (SAE J1829)	-	14.44	N/A 1
cetane number (ASTM D613)	-	51.3	N/A 1
initial boiling point (ASTM D1160)	°C	173.4	N/A 1
final boiling point (ASTM D1160)	°C	340.5	N/A 1
viscosity (ASTM D445 40C)	cSt	2.247	N/A 1
ethanol mole fraction *	%	N/A 2	8.49
pure gasoline mole fraction *	%	N/A 2	91.51
ethanol mass fraction *	%	N/A 2	8.94
pure gasoline mass fraction *	%	N/A 2	91.06
carbon mass concentration in pure gasoline *	%	N/A 2	86.18
hydrogen mass concentration in pure gasoline *	%	N/A 2	13.82
pure gasoline LHV *	MJ/kg	N/A 2	43.12
pure gasoline stoichiometric A/F ratio *	-	N/A 2	14.17

4. METHODOLOGY TO IDENTIFY SETTINGS FOR BETTER EFFICIENCY AND EMISSIONS

4.1 Overview

The flow diagram of the study is shown in Figure 5, similar to the one in [71]. DOE and relevant statistical techniques were applied to tests, to identify the parameter settings for better engine efficiency and emissions through varying certain factors. Four sets of tests were done: diesel baseline tests and dual-fuel tests both at low load and medium load.

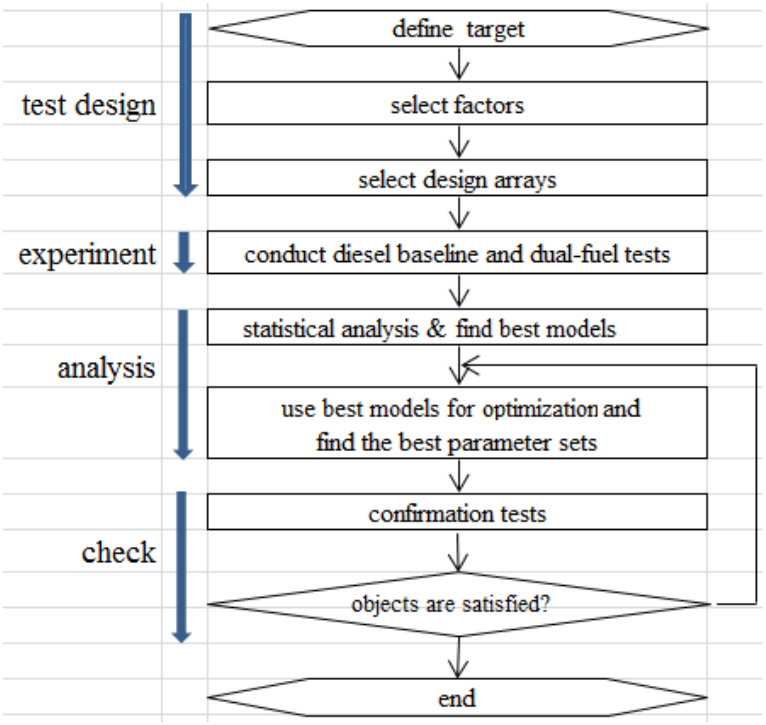

Figure 5 *Flow diagram of the study*

The factors are chosen considering their influence on the targets and the easiness of operation, as shown in Table 4 . The highlighted cells indicate the factors adjusted in

each group of tests. The intake pressure was adjusted through VGT vane position, and the EGR level was adjusted through EGR valve position, because the latter ones are much easier to adjust in tests. Each factor is set at five levels, different for different tests. The actual levels are determined based on previous test data, literature review, as well as safety, noise, combustion timing, and interaction, and are shown in the later corresponding sections. The symbols of the factors are used in regression equations. The targets and their symbols in the regression equations are shown in Table 5. Because the tests will involve various combinations of factors, the engine performance is not so predictable. Therefore, some parameters will be monitored to ensure they are within constraints, as shown in Table 6. Excessive turbo speed, MPRR, and peak cylinder pressure might affect engine structure integrity. Excessive exhaust pressure will increase pumping loss and drive a lot of exhaust gas into the intake manifold even if EGR valve only opens slightly. IMEPn COV is an indicator of how well cylinders are balanced. The constraints of NOx, smoke number, HC, and CO are the upper limits of the measuring ranges of respective instruments.

There are several possible methods to carry out the tests, as shown in Table 7. Single factor alternate method is a commonly used method. Factor 1 is varied while the other factors are fixed to find factor 1's best value; then factor 2 is varied while the other factors are fixed (factor 1 is fixed at its best value) to find factor 2's best value; repeat until all the best values are found. Orthogonal design and uniform design are two kinds of DOE. The arrays are chosen because they are fit for the number of factors and levels in the presented study. In the symbols, L means orthogonal design, U means uniform design, and the three numbers mean the number of test runs for an array, the number of levels, and the number of factors respectively. With much less tests to do, uniform design is chosen to be used in this research with its arrays shown in Table 8 [72], but at the expense of more complex data analysis than orthogonal design. The numbers in Table 8 represent levels of factors. Compared to testing all combinations and single factor alternate method, DOE has a few advantages: the number of test runs and thus time and cost are greatly reduced so more factors can be studied; interactions between

factors can be analyzed; global optimum point can be obtained while the point obtained with single factor alternate method could be a local optimum; useful statistical analysis can be done, such as prediction of system responses to variable settings.

The statistical analysis and confirmation tests will be explained in detail in Sections 4.2 – 4.6.

Table 4 *The factors and symbols*

intake pressure	rail pressure	SOI for diesel baseline tests	SOI for dual-fuel tests	EGR level	gasoline fraction
bar	bar	° ATDC	° ATDC	-	-
x1	x2	x3	x4	x5	x6
diesel baseline test					
dual-fuel test					

Table 5 *The targets and symbols*

efficiency	NOx	smoke number	HC	CO
-	ppm	-	ppm	ppm
y1	y2	y3	y4	y5

Table 6 *Constraints of parameters*

turbo speed	MPRR	peak cylinder pressure	exhaust pressure	IMEPn COV	NOx	smoke number	HC	CO
rpm	bar/°	bar	bar	-	ppm	-	ppm	ppm
75000	15	100	2.5	5%	4896	10	6000	4950

Table 7 *Possible test methods*

test method	array	number of test runs	calculation
all the combinations of factors are tested	-	15000	$(5^4+5^5)*2*2$
single factor alternate method	-	152	[(5+4*3)+(5+4*4)]*2*2
orthogonal design	$L_{25}(5^6)$	108	25*2*2+2*2*2
uniform design	$U_{10}(5^4)$ and $U_{10}(5^5)$	48	10*2*2+2*2*2

Table 8 *Uniform design arrays*

	$U_{10}(5^4)$				$U_{10}(5^5)$				
test #	**x1**	**x2**	**x3**	**x5**	**x1**	**x2**	**x4**	**x5**	**x6**
1	1	2	3	1	3	1	2	4	5
2	2	1	4	5	2	3	5	2	5
3	5	4	2	1	5	2	4	1	3
4	3	3	4	3	3	5	2	1	2
5	4	5	3	5	2	1	3	2	1
6	3	3	2	3	4	3	1	5	2
7	1	4	1	4	5	5	3	4	4
8	5	2	5	4	1	4	1	3	4
9	4	1	1	2	1	2	4	5	3
10	2	5	5	2	4	4	5	3	1

4.2 Results and discussion for dual-fuel tests at low load at 1400 rpm

The uniform design array used to do the dual-fuel tests at low load and the values of targets acquired from the tests are shown in Table 9. Note that the codes of levels in Table 8 are replaced with actual values in Table 9, with a few adjustments in SOI levels. Tests were done in the order shown in Table 9 which is different from Table 8, because this could facilitate testing.

Data analysis procedures:

1. In Minitab 17 software, do linear regression for each y with all x's.
2. In Minitab, do quadratic regression for each y with all x's and two x interactions: the interaction between intake pressure and EGR level, and that between rail pressure and SOI. The two interactions are considered the most significant among the interactions between any two x's. Intake pressure affects the flow of EGR gas, and rail pressure affects actual injection timing.

   The results from the above linear and quadratic regressions are the same as the results acquired through "regression" function in Microsoft EXCEL software, but with more details.
3. In Minitab, use all x's to find the best linear model through "best subsets" function.

4. In Minitab, use all x's and their quadratic terms (square terms and interaction terms) to find the best model through "stepwise regression" function.
5. In Minitab, try some measures to improve the models if necessary based on the following criteria, such as standardizing factors, reducing factors, weighting, and partial least square.
6. Evaluate the models using the following criteria and determine the best model for each y.
7. y1 - y5 represent efficiency, NOx, smoke number, HC, and CO respectively. The improvement of the first three is the focus of this study. HC and CO are also studied by the way, because they are related to NOx and smoke number, and are also regulated by emission regulations like the latter two. Therefore in addition to the best models for individual y, the best models for y1 - y3 and y1 - y5 are found in Minitab using "response optimizer" function, and later confirmation tests are done to verify the models.

Table 9 *The uniform design array used to do dual-fuel tests at low load and the values of targets*
OL: over measurement limit.

test #	intake pressure	rail pressure	SOI	EGR level	gasoline fraction	efficiency	NOx	smoke number	HC	CO
	bar	bar	° ATDC	-	-	-	ppm	-	ppm	ppm
	x1	x2	x4	x5	x6	y1	y2	y3	y4	y5
1	0.969	1000	-15	0.126	0.359	0.225	632.9	0.019	10.9	3270
2	0.97	800	-10	0.162	0.306	0.219	288.3	0.022	18	3386
3	0.982	700	-9	0.093	0.131	0.237	305.9	0.029	11	1287
4	0.982	900	-9	0.094	0.497	0.203	271.4	0.011	35	OL
5	1.019	1100	-7	0	0.216	0.224	418.5	0.008	13.4	2077
6	1.007	700	-9	0.204	0.484	0.221	179.8	0.027	39.8	OL
7	1.044	1000	-7	0.24	0.107	0.231	278.2	0.019	8.2	1303
8	1.035	900	-7	0.253	0.195	0.236	187.9	0.029	14.6	2250
9	1.176	800	-7	0	0.302	0.203	228.5	0.025	24.9	2708
10	1.076	1100	-7	0.37	0.401	0.213	145.6	0.026	21.7	OL

The criteria to evaluate a model [73]:

1. P-value for the regression and each factor should be as low as possible. Here its limit is set to 0.05. P-value is the probability of obtaining a test statistic that is at least as extreme as the calculated value if the null hypothesis is true in a hypothesis test.
2. R-sq, R-sq(adj), and R-sq(pred) should be as close to 100% as possible. They also should be close to each other although R-sq > R-sq(adj) > R-sq(pred). R-sq is coefficient of determination, indicating how well data points fit a statistical model. R-sq of n% means the factors explain n% of the variance of the target. R-sq(adj) is adjusted R-sq, accounting for the number of factors in the model. R-sq(pred) is predicted R-sq. It is close to R-sq and R-sq(adj) if the model is not overfit and has adequate predictive ability.
3. Data should not be ill-conditioned, namely VIF for the coefficients of the equation should be as close to 1 as possible. VIF is variance inflation factor, indicating the extent to which multicollinearity (correlation among factors) is present in a regression analysis. Multicollinearity is problematic because it can increase the variance of the regression coefficients, making them unstable and difficult to interpret.
4. The fitted values should be close to measured values.
5. Residuals should have constant variance.
6. Residuals should be independent of (not correlated with) one another.
7. Residuals should be normally distributed.
8. No unusual observations or outliers.
9. Better model should contain more factors so it will be easier to verify through tests.

The above procedures and criteria were also used in the other tests.

The results from the regression of y2 versus x2, x4, x5, and x6 are shown in Figure 6 and Figure 7 as an example. Such examples will not be given for the other y's and for the other tests to save space. The conclusions are shown below.

```
Analysis of Variance
Source      DF  Adj SS  Adj MS  F-Value  P-Value
Regression   4  179162   44791    81.57    0.000
  x2         1   32374   32374    58.96    0.001
  x4         1  112247  112247   204.43    0.000
  x5         1   28515   28515    51.93    0.001
  x6         1   13036   13036    23.74    0.005
Error        5    2745     549
Total        9  181908

Model Summary
      S    R-sq  R-sq(adj)  R-sq(pred)
23.4324  98.49%     97.28%      93.02%

Coefficients
Term        Coef  SE Coef  T-Value  P-Value   VIF
Constant  -327.6     58.5    -5.60    0.003
x2        0.4150   0.0541     7.68    0.001  1.06
x4        -47.57     3.33   -14.30    0.000  1.13
x5        -505.8     70.2    -7.21    0.001  1.09
x6        -294.1     60.4    -4.87    0.005  1.13

Regression Equation
y2 = -327.6 + 0.4150 x2 - 47.57 x4 - 505.8 x5 - 294.1 x6

Fits and Diagnostics for Unusual Observations
                          Std
Obs     y2    Fit  Resid  Resid
  6  179.8  145.6   34.2   2.11  R
R  Large residual
```

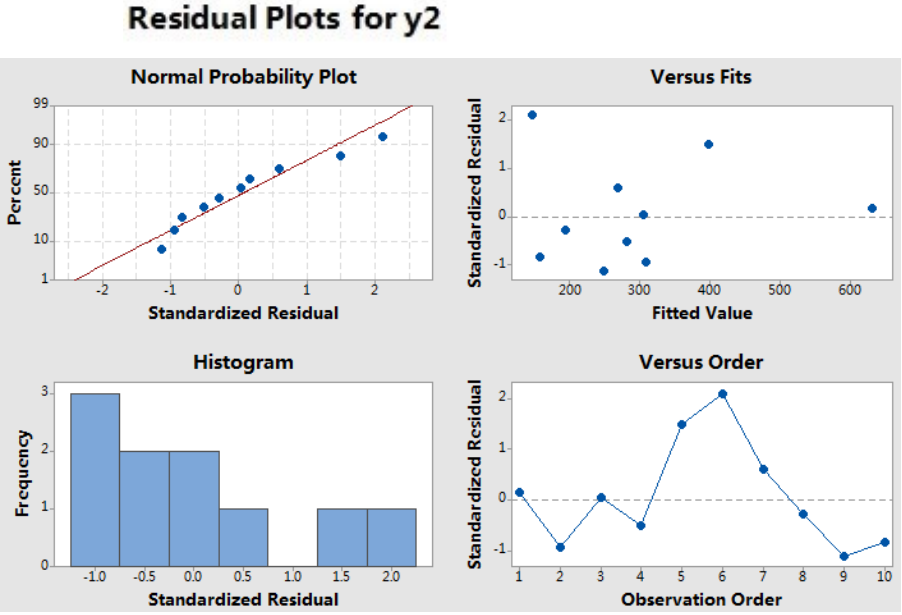

Figure 6 *The results from the regression of y2 versus x2, x4, x5, x6 (NOx versus rail pressure, SOI, EGR level, gasoline fraction), in dual-fuel tests at low load*

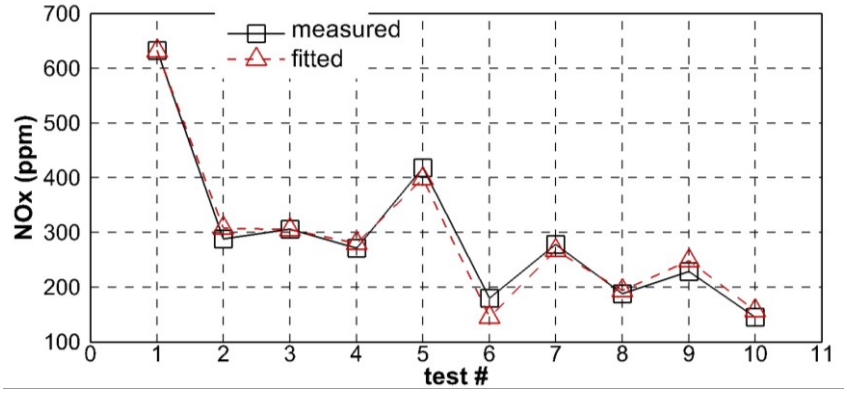

Figure 7 *Measured and fitted y2 (NOx) in dual-fuel tests at low load*

1. The p-value for the regression model is 0.000, showing that the model is significant at an α-level of 0.05. This indicates at least one coefficient is different from zero.
2. The p-values for the estimated coefficients of all x's are much smaller than 0.05, indicating that all the x's are significantly related to y2.
3. The VIFs are all close to 1, indicating the factors are not correlated.
4. The R-sq indicates that the factors explain 98.49% of the variance in y2. R-sq and R-sq(adj) are close to 100%, indicating the model fits the data well.
5. R-sq(pred) is 93.02%, close to R-sq and R-sq(adj), so the model does not appear to be overfit and has adequate predictive ability.
6. Observation 6 is identified as unusual because the absolute value of the standardized residual is greater than 2, indicating it might be an outlier.
7. The normal probability plot shows an approximately linear pattern consistent with a normal distribution. The two points in the upper-right corner may be outliers, corresponding to the upper two points in the versus fits and versus order plots. The two points are from observations 5 and 6.
8. In the versus fits plot, the residuals do not show obvious pattern with the fitted values, indicating the residuals have constant variance.

9. The histogram indicates that outliers may exist in the data, shown by the two bars on the far right side.
10. The versus order plot shows the order that the data was collected and can be used to find non-random error, especially of time-related effects. This plot does not display a pattern (A positive correlation is indicated by a clustering of residuals with the same sign. A negative correlation is indicated by rapid changes in the signs of consecutive residuals).
11. Since the number of observations is only 10, much lower than 50, the residual plots may show substantial variation and nonlinearity even if the residuals are normally distributed.
12. The fitted and measured y2 are very close as shown in Figure 7, indicating the model fits the data well.
13. In summary, the regression results in a good model of y2.

The best model for each y is shown in Table 10, with indicators of regression quality, and intercepts and coefficients of regression equations. Note there are two best models for y1. The applicable x ranges are shown in Table 11, which are the limits of the values actually used in the tests. All the regression p-values are lower than 0.05, meaning all the models are significant at an α-level of 0.05. The three R-sq values in each model for y2 - y5 are very high, meaning the models fit the data well and have adequate predictive ability. Such values in the models for y1 are not very high, meaning the models fit the data poorly and have inadequate predictive ability. Most p-values for the coefficients are lower than 0.05, meaning the corresponding x's or quadratic terms of x's are significantly related to y's. The regression quality reflected by the p-values of the coefficients is consistent with what reflected by the R-sq values: most p-values in the models for y2 - y5 are lower than the p-values in the models for y1.

The model for y3 is used as an example to explain the significance of factors. Such explanation will not be given for the other y's and the other tests to save space, but the summary of the significance of factors is provided in Section 4.6. x1, x2, x5, x6, x5*x5,

x1*x2, x1*x5, and x1*x6 are included in the model. This means smoke emission is a complex phenomenon, affected by quite a few items. Intake pressure, rail pressure, EGR level, gasoline fraction, quadratic term of EGR level, interaction between intake pressure and rail pressure, interaction between intake pressure and EGR level, interaction between intake pressure and gasoline fraction, are significantly related to smoke emission. x4 is not included in the model, meaning SOI does not have significant influence on smoke emission. The signs of coefficients indicate complex influence of each factor. The net influence of each factor on smoke emission depends on the relative magnitude of the positive and negative terms. Positive coefficients of x1, x1*x5, and x1*x6 mean increasing intake pressure will increase smoke emission. This is counterintuitive because increasing intake pressure should provide more air to the combustion chamber, improve the combustion, and decrease smoke emission. Fortunately, negative coefficient of x1*x2 mean increasing intake pressure will decrease smoke emission. Moreover, x2 is much higher than x1, x5, or x6, so generally increasing intake pressure will decrease smoke emission, even considering the much smaller negative coefficient. By the way, three of the four interaction terms include x1, meaning intake pressure has an especially important role in smoke emission. Positive coefficient of x2 means increasing rail pressure will increase smoke emission, while negative coefficient of x1*x2 means increasing rail pressure will decrease smoke emission. This perhaps infers that high rail pressure will cause the fuel spray to impinge the cylinder wall, resulting in incomplete combustion, but high intake pressure will cause high cylinder pressure, and alleviate the impingement. Because x1 is around 1 and the absolute values of the two coefficients are equal, generally rail pressure does not have much influence on smoke emission. Positive coefficients of x5 and x1*x5 mean increasing EGR level will increase smoke emission, while negative coefficient of x5*x5 means increasing EGR level decrease smoke emission. x1 is around 1, but x5 is no more than 0.37, so x1*x5 is greater than x5*x5. Also considering the relative magnitude of coefficients, generally increasing EGR level will increase smoke emission. Positive coefficient of x6 means increasing gasoline fraction will increase smoke emission, while

negative coefficient of x1*x6 means increasing gasoline fraction will decrease smoke emission. Also considering x1 is around 1 and the absolute values of coefficients are close, gasoline fraction has a little negative influence on smoke emission. Note the conclusion about the significance of factors is only applicable within the ranges shown in Table 11. Caution should be exerted when the conclusion is extended outside the ranges.

Table 10 *Best model for each y in dual-fuel tests at low load*

	y1 (efficiency)				**y2 (NOx)**	
regression p-value	0.046		0.015		0	
R-sq	81.21%		80.67%		98.49%	
R-sq(adj)	66.18%		71.01%		97.28%	
R-sq(pred)	35.68%		54.28%		93.02%	
intercept	0.3153		0.3302		-327.6	
	coefficient	**p-value**	**coefficient**	**p-value**	**coefficient**	**p-value**
x1 (intake pressure)	-0.0801	0.15	-0.0909	0.039		
x2 (rail pressure)					0.415	0.001
x4 (SOI)	-0.0005	0.721			-47.57	0
x5 (EGR level)	0.0325	0.181	0.0306	0.155	-505.8	0.001
x6 (gasoline fraction)	-0.0701	0.012	-0.0678	0.005	-294.1	0.005
x2*x2						
x5*x5						
x1*x2						
x1*x5						
x1*x6						
x4*x6						

Table 10 continued

	y3 (smoke number)		y4 (HC)		y5 (CO)	
regression p-value	0.001		0		0.011	
R-sq	100.00%		99.42%		99.46%	
R-sq(adj)	100.00%		98.69%		98.39%	
R-sq(pred)	99.99%		88.24%		84.15%	
intercept	-0.554		120		3324	
	coefficient	**p-value**	**coefficient**	**p-value**	**coefficient**	**p-value**
x1 (intake pressure)	0.6029	0.008			-2849	0.096
x2 (rail pressure)	0.001	0.001	-0.1168	0.001		
x4 (SOI)			6.96	0	105.2	0.069
x5 (EGR level)	-0.2782	0.001			1831	0.065
x6 (gasoline fraction)	-0.8381	0.005	-55.5	0	11405	0.005
x2*x2			4.80E-05	0.149		
x5*x5	0.1469	0.008				
x1*x2	-0.001	0.001				
x1*x5	0.2864	0.004				
x1*x6	0.8083	0.002				
x4*x6			-15.65	0.014		

Table 11 *Applicable x ranges in dual-fuel tests at low load*

	lower limit	upper limit
x1 (intake pressure)	0.97	1.18
x2 (rail pressure)	700	1100
x4 (SOI)	-15	-7
x5 (EGR level)	0	0.37
x6 (gasoline fraction)	0.1	0.5

The goal is to maximize y1, while make y2 - y5 as close to 0 as possible. From the best models (equations) in Table 10, it is easy to optimize individual y and corresponding x's. For linear equations, just use the lower limits for x's with negative coefficients, and upper limits for x's with positive coefficients, to maximize y, and

opposite method to minimize y. For quadratic equations, take derivative of y over certain x in quadratic terms, and find the extreme value of y. The "response optimizer" function of Minitab was also used because it can provide more information.

The combination of x's that jointly optimize y1 - y5, as well as y1 - y3, were found with the above best models (the first best model for y1 was used) using the "response optimizer" function. The optimization plot obtained from optimizing y1 - y3 is given in Figure 8 as an example. The optimization plots will not be provided for the other y's or the other tests to save space. The blue text and horizontal lines, and red text and vertical lines, indicate the better y's and corresponding x's respectively. The black curves and lines indicate how all the y's or individual y change with the change of each x and fixed other x's. The gray regions indicate where y has zero desirability. As mentioned in [73], D is composite desirability, evaluating how the factor settings optimize a set of targets overall. d is individual desirability, evaluating how the factor settings optimize a single target. Desirability has a range of zero to one. One represents the ideal case; zero indicates that one or more targets are outside their acceptable limits. The composite desirability (0.7702) is not close to 1, which indicates the settings do not appear to achieve favorable results for all targets as a whole. The individual desirability indicates that the settings are more effective at minimizing y3 than maximizing y1 and minimizing y2. The importance of y1 - y3 was all set as 1 before drawing the optimization plot. Since maximizing y1 is more important than minimizing y2 and y3, the importance of y1 can be set to be higher than that of y2 and y3, to achieve higher individual desirability for y1. The optimization plot allows the user to interactively change the factor settings to perform sensitivity analysis and check the corresponding y's, by moving the vertical red lines. By the way, in the optimization for better y1 - y5, the importance of y1 - y3 was set as 1, while the importance of y4 and y5 was set as 0.5, to reflect the fact that y1 - y3 are more important than y4 and y5.

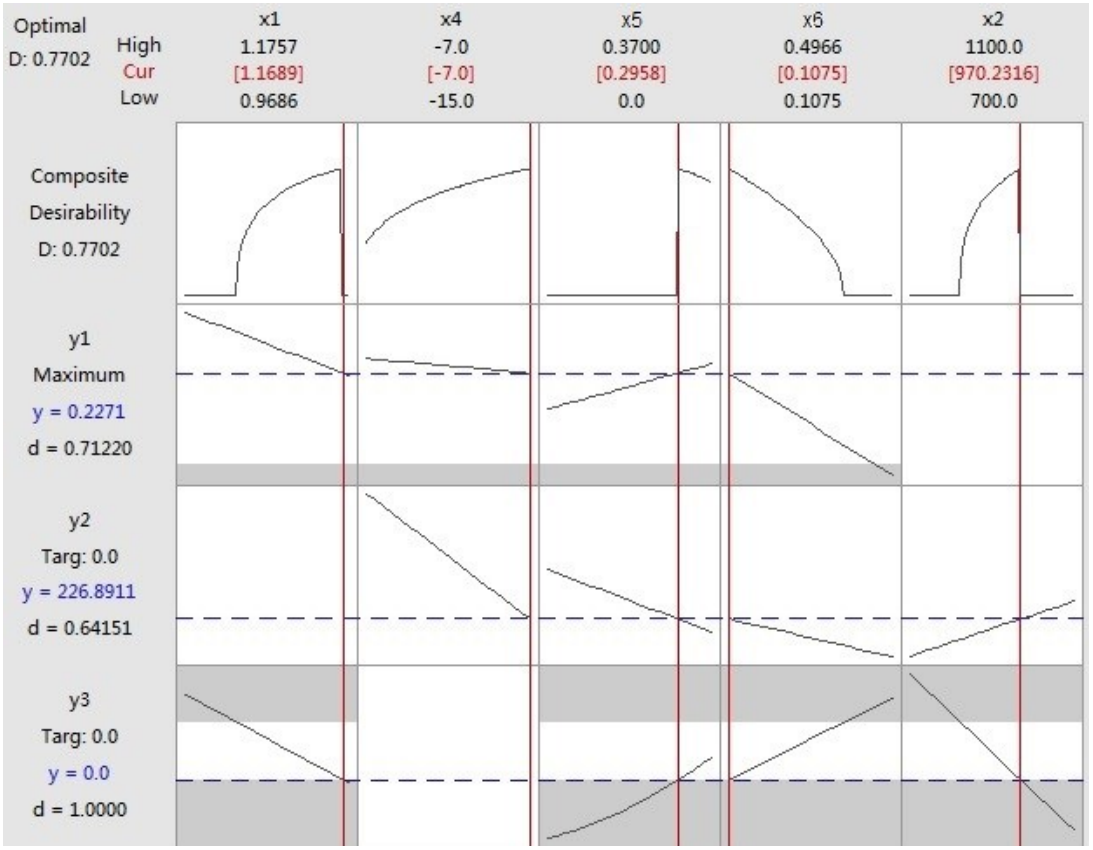

Figure 8 *The optimization plot for better y's (y1: efficiency; y2: NOx; y3: smoke number) and corresponding x's (x1: intake pressure; x2: rail pressure; x4: SOI; x5: EGR level; x6: gasoline fraction) in dual-fuel tests at low load*

The results from the optimization are summarized in Table 12. As mentioned in [73], SE Fit is standard error of fits, namely the variation in the estimated mean target for a given set of factor levels. CI is confidence interval of the prediction, representing a range that the mean target is likely to fall with specified settings of factors. PI is prediction interval, representing a range that a single new observation of target is likely to fall with specified settings of factors. Take y1 as an example, with these settings: x1=0.969, x4=-15, x5=0.370, x6=0.107, you can be 95% confident that the mean efficiency will fall into the range of (0.2217, 0.2771), and you can be 95% confident that a single new observation of efficiency will fall into the range of (0.2163, 0.2825). Better y1 - y5 were determined with Microsoft EXCEL instead of Minitab because y5 has less available

observations than the other y's. Therefore there is no SE Fit, 95% CI, 95% PI, and composite desirability for better y1 - y5. Composite desirability values for individual y are about 1, obviously higher than those for multiple y's. The results for better multiple y's are more realistic than the results for better individual y. The above two facts are expected because there has to be compromise when optimizing multiple y's with conflicting requirements on suitable x's. y1 (fuel conversion efficiency) seems to have the best results from all three optimizations. Although y3 (smoke number) and y4 (HC) can approach 0 as shown in certain tests, it is doubtful that y2 (NOx) and y5 (CO) can approach 0. This question can be answered by confirmation tests.

Table 12 *Summary of optimization results in dual-fuel tests at low load*

(a) Better individual y

	y1 (efficiency)	**y2 (NOx)**	**y3 (smoke number)**	**y4 (HC)**	**y5 (CO)**
	0.249	0.554	0	0	5.82
x1 (intake pressure)	0.969		1.176		1.054
x2 (rail pressure)		700	839	717	
x4 (SOI)	-15	-7		-14.9	-15
x5 (EGR level)	0.370	0.295	0.069		0
x6 (gasoline fraction)	0.107	0.497	0.107	0.242	0.111
SE Fit	0.0108	21.5	4.4E-05	2.58	295
95% CI	(0.2217, 0.2771)	(-54.6, 55.7)	(-0.000554, 0.000554)	(-7.16, 7.16)	(-1265, 1277)
95% PI	(0.2163, 0.2825)	(-81.1, 82.2)	(-0.000562, 0.000562)	(-7.92, 7.92)	(-1348, 1359)
composite desirability	1	0.999	1	1	0.998

Table 12 continued

(b) Better y1 - y3

x1 (intake pressure)	1.169
x2 (rail pressure)	970
x4 (SOI)	-7
x5 (EGR level)	0.296
x6 (gasoline fraction)	0.107
composite desirability	0.77

		SE Fit	**95% CI**	**95% PI**
y1 (efficiency)	0.227	0.0082	(0.20601, 0.24818)	(0.19928, 0.25491)
y2 (NOx)	226.9	16.9	(183.4, 270.4)	(152.6, 301.2)
y3 (smoke number)	0	4.9E-05	(-0.000619, 0.000619)	(-0.000626, 0.000626)

(c) Better y1 - y5

x1 (intake pressure)	1.12
x2 (rail pressure)	1100
x4 (SOI)	-7
x5 (EGR level)	0.37
x6 (gasoline fraction)	0.1

y1 (efficiency)	0.234
y2 (NOx)	245
y3 (smoke number)	0.00154
y4 (HC)	6.29
y5 (CO)	1215

Confirmation tests were done using the factor settings shown in Table 12 (b) and (c) for better y1 - y3 and for better y1 - y5. The results are plotted in Figure 9 together with the results from uniform design tests shown in Table 9 and optimization results shown in Table 12 (b) and (c). Uniform design tests, confirmation test for better y1 - y3, and confirmation test for better y1 - y5 are test 1 - 10, test 11, and test 12, respectively. Optimization result points are denoted with letter “o”, and some have vertical bars indicating 95% PI. Such assignment and denotation are also used in Figure 10, Figure 11, and Figure 12, even if some results are not available, so that different kinds of results can be easily identified.

In the confirmation test for better y1 - y3, compared to the values in uniform design tests, the efficiency, NOx and CO are lower than the medians, while smoke number and HC are the highest. Compared to the optimization results, efficiency and NOx are lower, while smoke number is higher. In the confirmation test for better y1 - y5, the efficiency

is about the median, NOx and CO are lower than the medians, smoke number is higher than the median, while HC is among the highest. Compared to the optimization results, efficiency and NOx are lower, while smoke number, HC and CO are higher. It seems NOx is predicted with more accuracy: the confirmation test result is close to the optimization result, and fall into 95% PI. It is hoped the values are close to prediction, efficiency is higher than the median, NOx, smoke number, HC, and CO are lower than the medians. This goal is not fully realized.

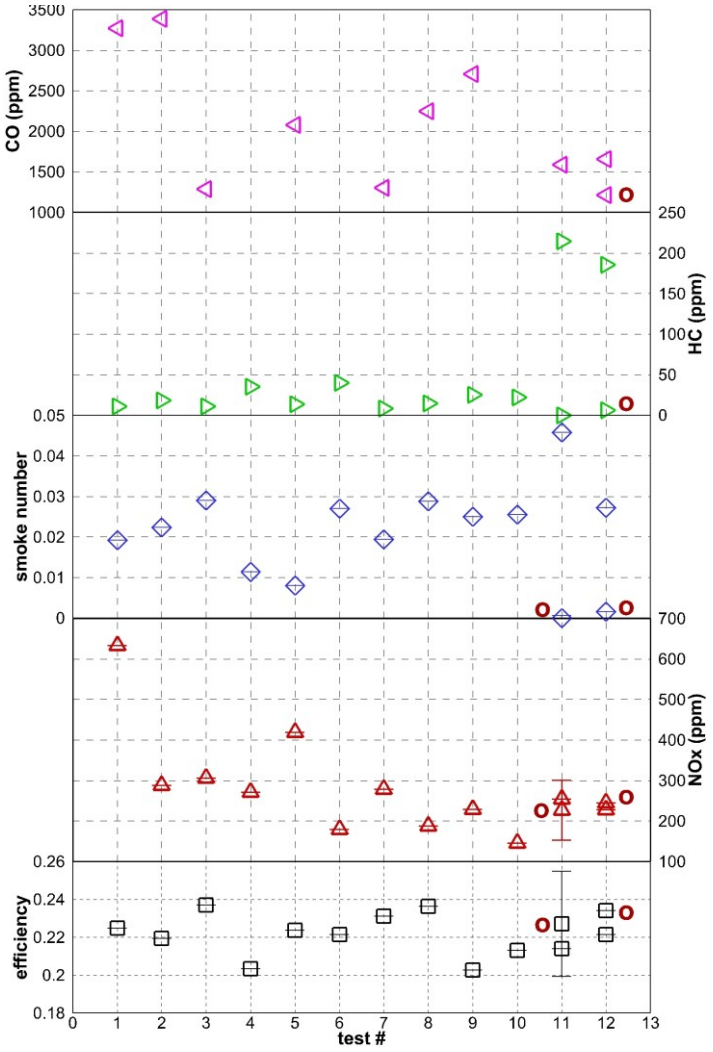

Figure 9 *Results from dual-fuel low load uniform design tests, confirmation tests, and optimization*

The difference between the prediction and measurement could be caused by the following problems, which can be improved in future study.

1. Small number of uniform design tests affects the quality of the regression models.
2. “Stepwise” function of Minitab was used to get some best models. The terms specified by the user are candidates for the final model. Stepwise removes and adds terms to the model for the purpose of identifying a useful subset of the terms. As mentioned in [73], it is a valuable tool in data analysis, particularly in the early stages of building a model. But it presents certain dangers: because the procedures automatically "snoop" through many models, the model selected may fit the data "too well." That is, the procedure can look at many variables and select ones which, by pure chance, happen to fit well; the procedures are heuristic algorithms, which often work very well but which may not select the model with the highest R-sq for a given number of factors; the procedures cannot take into account special knowledge about the data. Therefore, the model selected may not be the best from a practical point of view.
3. The best models should have been verified through engine tests with specified factor settings, before they were used for optimization.
4. Some of the test conditions for the uniform design tests and confirmation tests are different, such as atmospheric temperature, pressure and humidity.

4.3 Results and discussion for dual-fuel tests at medium load at 1400 rpm

The uniform design array used to do the dual-fuel tests at medium load and the values of targets acquired from the tests are shown in Table 13. Note that the codes of levels in Table 8 are replaced with actual values in Table 13, with a few adjustments in SOI levels, and test 8 in Table 8 is ignored because it is similar to test 7. Tests were done in the order shown in Table 13 which is different from Table 8, because this could facilitate testing.

Table 13 *The uniform design array used to do dual-fuel tests at medium load and the values of targets*

test #	intake pressure	rail pressure	SOI	EGR level	gasoline fraction	efficiency	NOx	smoke number	HC	CO
	bar	bar	° ATDC	-	-	-	ppm	-	ppm	ppm
	x1	x2	x4	x5	x6	y1	y2	y3	y4	y5
1	1.037	1000	-7	0.119	0.407	0.357	576	0.231	295	1408
2	1.045	900	-8	0.133	0.209	0.358	454	0.772	197	1390
3	1.062	700	-8	0.145	0.494	0.366	443	0.277	379	1677
4	1.074	1100	-8	0.144	0.205	0.358	501	0.471	160	1198
5	1.126	700	-10	0.109	0.115	0.366	510	0.677	116	1025
6	1.109	1100	-7	0.173	0.394	0.359	442	0.231	270	1645
7	1.229	800	-8	0	0.303	0.355	536	0.189	238	2536
8	1.22	900	-8	0.202	0.503	0.363	416	0.195	318	1381
9	1.211	1000	-9	0.285	0.108	0.36	268	1.116	107	865

The best model for each y is shown in Table 14, with indicators of regression quality, and intercepts and coefficients of regression equations. Note there are three best models for y4. The applicable x ranges are shown in Table 15, which are the limits of the values actually used in the tests. Note for y5 the values except R-sq are not shown. The regression equation contains 8 terms with factors, the degree of freedom for the regression is 8, so the degree of freedom for error is 0, and the p-values, R-sq(adj) and R-sq(pred) cannot be calculated. The following statement applies to y1 - y4. All the regression p-values are lower than 0.05, meaning all the models are significant at an α-level of 0.05. The three R-sq values in each model are very high, meaning the models fit the data well and have adequate predictive ability. Most p-values for the coefficients are lower than 0.05, meaning the corresponding x's or quadratic terms of x's are significantly related to y's.

The results from the optimization are summarized in Table 16 (the first best model for y4 was used). Again, composite desirability for better individual y is higher than that for better multiple y's, but the former results are less realistic than the latter results. y1

seems to have the best results. Although y3 and y4 can approach 0 as shown in certain tests, it is doubtful that y2 and y5 can approach 0. This question can be answered by confirmation tests.

Table 14 *Best model for each y in dual-fuel tests at medium load*

	y1 (efficiency)		**y2 (NOx)**		**y3 (smoke number)**	
regression p-value	0.005		0.016		0.004	
R-sq	96.02%		99.99%		98.91%	
R-sq(adj)	92.05%		99.95%		97.09%	
R-sq(pred)	84.41%		87.92%		91.21%	
intercept	0.3284		302		4.451	
	coefficient	**p-value**	**coefficient**	**p-value**	**coefficient**	**p-value**
x1 (intake pressure)	-0.01931	0.021			0.1443	0.661
x2 (rail pressure)			1.087	0.026	-0.0017	0.016
x4 (SOI)	-0.00542	0.001	6.5	0.061	0.2794	0.032
x5 (EGR level)	0.01425	0.044	2740	0.017	3.474	0.003
x6 (gasoline fraction)	0.02427	0.002	-2028	0.07	-2.856	0.003
x4*x4						
x5*x5						
x6*x6			5518	0.046		
x1*x5						
x2*x4						
x2*x5			-5.252	0.018		
x4*x6			196	0.029		
x5*x6						

Table 14 continued (coeff.: coefficient)

	y4 (HC)						y5 (CO)	
regression p-value	0.002		0.001		0		*	
R-sq	99.38%		99.63%		99.37%		100.00%	
R-sq(adj)	98.35%		99.01%		98.75%		*	
R-sq(pred)	93.18%		84.67%		96.00%		*	
intercept	758		707		727		5164	
	coeff.	**p-value**	**coeff.**	**p-value**	**coeff.**	**p-value**	**coeff.**	**p-value**
x1 (intake pressure)			-71.12	0.246			1190	*
x2 (rail pressure)	-0.312	0.033	-0.2405	0.023	-0.2694	0.01		
x4 (SOI)	52.5	0.051	40.04	0.046	48.3	0.016	483.1	*
x5 (EGR level)	150.5	0.203	135	0.139	156.9	0.101	31528	*
x6 (gasoline fraction)	392.9	0.01	421.7	0.004	390	0.002	-7007	*
x4*x4							29.69	*
x5*x5							120972	*
x6*x6								
x1*x5							-68431	*
x2*x4	-0.0057	0.872						
x2*x5								
x4*x6								
x5*x6							57259	*

Table 15 *Applicable x ranges in dual-fuel tests at medium load*

	lower limit	**upper limit**
x1 (intake pressure)	1.04	1.23
x2 (rail pressure)	700	1100
x4 (SOI)	-10	-7
x5 (EGR level)	0	0.28
x6 (gasoline fraction)	0.1	0.5

Table 16 *Summary of optimization results in dual-fuel tests at medium load*

(a) Better individual y

	y1 (efficiency)	y2 (NOx)	y3 (smoke number)	y4 (HC)	y5 (CO)
	0.379	0	0	0.00247	0.244
x1 (intake pressure)	1.037		1.228		1.229
x2 (rail pressure)		1100	700.0	1100	1100
x4 (SOI)	-10	-8.752	-7.238	-10	-10
x5 (EGR level)	0.2852	0.2820	0	0	0
x6 (gasoline fraction)	0.5030	0.2429	0.5030	0.1208	0.108
SE Fit	0.002	13.7	0.0716	49.4	30.1
95% CI	(0.37331, 0.38444)	(-174.0, 174.0)	(-0.2277, 0.2277)	(-157.1, 157.1)	(-95.6, 96.1)
95% PI	(0.37259, 0.38516)	(-175.8, 175.8)	(-0.2889, 0.2889)	(-161.7, 161.7)	(-100.1, 100.5)
composite desirability	1	1	1	1.0000	0.9994

(b) Better y1 - y3

x1 (intake pressure)	1.037
x2 (rail pressure)	1100
x4 (SOI)	-9.6
x5 (EGR level)	0.254
x6 (gasoline fraction)	0.285
composite desirability	0.951

		SE Fit	95% CI	95% PI
y1 (efficiency)	0.371	0.00125	(0.36737, 0.37429)	(0.36630, 0.37536)
y2 (NOx)	0.4	19.9	(-253.0, 253.7)	(-254.3, 255.0)
y3 (smoke number)	0.155	0.147	(-0.312, 0.623)	(-0.344, 0.655)

Table 16 continued

(c) Better y1 - y5

x1 (intake pressure)	1.23
x2 (rail pressure)	858
x4 (SOI)	-9.6
x5 (EGR level)	0.16
x6 (gasoline fraction)	0.38
composite desirability	0.801

		SE Fit	**95% CI**	**95% PI**
y1 (efficiency)	0.368	0.00105	(0.36516, 0.37100)	(0.36395, 0.37221)
y2 (NOx)	200	17.7	(-25.1, 424.4)	(-26.6, 425.8)
y3 (smoke number)	0.0018	0.0991	(-0.3137, 0.3173)	(-0.3603, 0.3639)
y4 (HC)	211	22.1	(140.7, 281.7)	(131.0, 291.4)
y5 (CO)	262	*	(*, *)	(*, *)

In the confirmation tests for better y1 - y3, the settings of x1 and x5 could not be achieved simultaneously, because low intake pressure is needed to achieve high EGR level. 1.037 bar is the lowest possible intake pressure achievable with the extreme position of the VGT vanes, while 0.15 is the highest EGR level achieved even with the fully opened EGR valve. Therefore only the confirmation test results for better y1 - y5 are shown here. The results are plotted together with the results from uniform design tests and optimization, as shown in Figure 10.

In the confirmation test for better y1 - y5, the efficiency is higher than the median of the results from uniform design tests, NOx is among the highest, smoke number and HC are among the lowest, CO is about the median. Efficiency and HC are lower than the prediction, while NOx, smoke number, and CO are higher. None of the targets seem to be predicted with accuracy: the confirmation test results are far from the optimization results, and most do not fall into 95% PI.

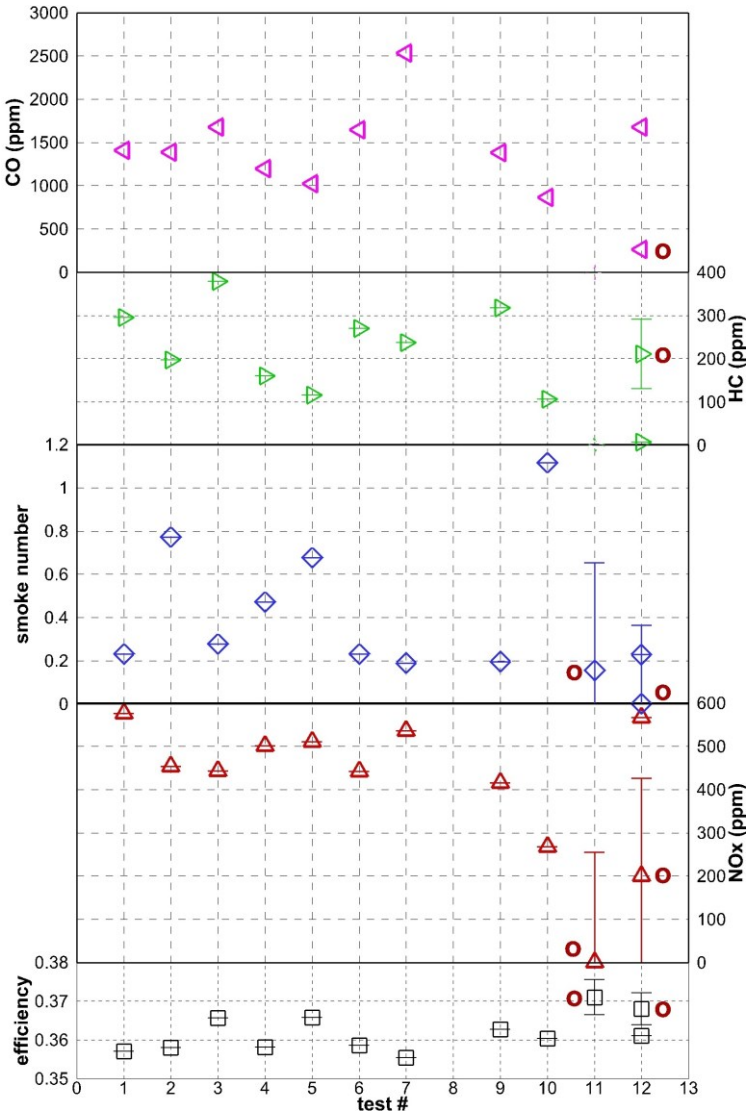

Figure 10 *Results from dual-fuel medium load uniform design test, confirmation tests, and optimization*

4.4 Results and discussion for diesel baseline tests at low load at 1400 rpm

The uniform design array used to do the diesel baseline tests at low load and the values of targets acquired from the tests are shown in Table 17. Note that the codes of levels in Table 8 are replaced with actual values in Table 17. Tests were done in the order shown in Table 17 which is different from Table 8, because this could facilitate testing.

Table 17 *Uniform design array used for diesel baseline tests at low load and values of targets*

test #	intake pressure	rail pressure	SOI	EGR level	efficiency	NOx	smoke number	HC	CO
	bar	bar	° ATDC	-	-	ppm	-	ppm	ppm
	x1	x2	x3	x5	y1	y2	y3	y4	y5
1	0.970	700	-10	0.000	0.240	472.7	0.041	62.1	201
2	0.978	1100	-4	0.179	0.229	302.9	0.010	63.6	509
3	0.995	1300	-16	0.155	0.209	988.4	0.012	45.3	138
4	0.990	500	-13	0.213	0.256	251.5	0.380	49.3	273
5	1.018	900	-13	0.285	0.236	387.4	0.056	40.5	237
6	1.021	900	-7	0.284	0.236	238.2	0.063	47.4	321
7	1.083	500	-4	0.410	0.238	90.8	0.266	60.1	471
8	1.048	1300	-10	0.504	0.221	136.0	0.121	49.9	417
9	1.355	1100	-7	0.000	0.170	447.6	0.049	46.8	92
10	1.036	700	-16	0.598	0.240	40.4	1.345	68.8	922

The best model for each y is shown in Table 18, with indicators of regression quality, and intercepts and coefficients of regression equations. The applicable x ranges are shown in Table 19, which are the limits of the values actually used in the tests. All the regression p-values are lower than or about 0.05, meaning all the models are significant at an α-level of 0.05. The R-sq and R-sq(adj) values are very high, but R-sq(pred) values are low except for y1, meaning the models fit the data well, but the models for y2 - y5 do not have adequate predictive ability. Most p-values for the coefficients in the models for y1 - y4 are lower than 0.05, meaning the corresponding x's or quadratic terms of x's are significantly related to y's. All the models involve some quadratic terms, meaning the influence of factors is complex and the interactions between some factors are important.

Table 18 *Best model for each y in diesel baseline tests at low load*

	y1 (efficiency)	y2 (NOx)	y3 (smoke number)
regression p-value	0	0.001	0.007
R-sq	99.80%	95.76%	95.95%
R-sq(adj)	99.41%	92.37%	90.88%
R-sq(pred)	86.85%	65.30%	0.00%
intercept	0.3914	775	1.331

Table 18 continued

	coefficient	p-value	coefficient	p-value	coefficient	p-value
x1 (intake pressure)	-0.1411	0.002				
x2 (rail pressure)	-4.20E-05	0	-0.533	0.016	-0.00053	0.019
x3 (SOI)	-0.00392	0.034	46.7	0.004	0.1451	0.062
x5 (EGR level)	0.404	0.003	-963	0.001	-1.867	0.031
x3*x3	-0.00023	0.011			0.00507	0.135
x5*x5						
x1*x2						
x1*x5	-0.3566	0.035				
x2*x3			-0.0841	0.007		
x2*x5						
x3*x5					-0.261	0.008

	y4 (HC)		y5 (CO)	
regression p-value	0.056		0.053	
R-sq	94.25%		99.94%	
R-sq(adj)	82.74%		99.48%	
R-sq(pred)	0.00%		0.00%	
intercept	137.2		7755	
	coefficient	**p-value**	**coefficient**	**p-value**
x1 (intake pressure)	-73.4	0.02	-6257	0.465
x2 (rail pressure)	0.0165	0.538	-5.44	0.391
x3 (SOI)	1.361	0.027	193.8	0.078
x5 (EGR level)	-57.2	0.748	-8099	0.049
x3*x3			6.993	0.087
x5*x5	232.7	0.011		
x1*x2			5.24	0.167
x1*x5			6994	0.118
x2*x3				
x2*x5	-0.0752	0.078		
x3*x5			-154	0.057

Table 19 *Applicable x ranges in diesel baseline tests at low load*

	lower limit	upper limit
x1 (intake pressure)	0.97	1.35
x2 (rail pressure)	500	1300
x3 (SOI)	-16	-4
x5 (EGR level)	0	0.598

The results from the optimization are summarized in Table 20. Again, the results for better multiple y's are more realistic than the results for better individual y. y1 seems to have the best results. Although y3 and y4 can approach 0 as shown in certain tests, it is doubtful that y2 and y5 can approach 0. This question can be answered by confirmation tests.

Table 20 *Summary of optimization results in diesel baseline tests at low load*

(a) Better individual y

	y1 (efficiency)	y2 (NOx)	y3 (smoke number)	y4 (HC)	y5 (CO)
	0.285	0	0	11.94	0.68
x1 (intake pressure)	0.97			1.35	1.01
x2 (rail pressure)	500	1264	635	1300	815
x3 (SOI)	-8.73	-6.68	-4	-16	-15.5
x5 (EGR level)	0.598	0.517	0.598	0.332	0
SE Fit	0.00497	66.8	0.165	7.14	26.4
95% CI	(0.26955, 0.30118)	(-171.8, 171.8)	(-0.458, 0.458)	(-10.77, 34.66)	(-335.2, 336.5)
95% PI	(0.26852, 0.30221)	(-258.4, 258.4)	(-0.572, 0.572)	(-13.97, 37.86)	(-402.0, 403.4)
composite desirability	1	1	1	0.826	0.999

Table 20 continued

(b) Better y1 - y3

x1 (intake pressure)	0.970
x2 (rail pressure)	900
x3 (SOI)	-4
x5 (EGR level)	0.426
composite desirability	0.991

		SE Fit	**95% CI**	**95% PI**
y1 (efficiency)	0.254	0.00348	(0.24253, 0.26467)	(0.24110, 0.26610)
y2 (NOx)	0	50.2	(-129.1, 129.1)	(-232.2, 232.2)
y3 (smoke number)	0	0.107	(-0.298, 0.298)	(-0.454, 0.454)

(c) Better y1 - y5

x1 (intake pressure)	1.039
x2 (rail pressure)	500
x3 (SOI)	-11.0
x5 (EGR level)	0.223
composite desirability	0.729

		SE Fit	**95% CI**	**95% PI**
y1 (efficiency)	0.247	0.00123	(0.24310, 0.25093)	(0.24002, 0.25402)
y2 (NOx)	241	43.6	(128.8, 352.9)	(17.7, 464.0)
y3 (smoke number)	0.305	0.0833	(0.0740, 0.5367)	(-0.1080, 0.7187)
y4 (HC)	44.6	3.09	(34.76, 54.41)	(28.70, 60.47)
y5 (CO)	164.3	31.1	(-231.5, 560.0)	(-289.6, 618.1)

In the confirmation tests for better y1 - y3, the settings of x1 and x5 could not be achieved simultaneously, because low intake pressure is needed to achieve high EGR level. 0.983 bar is the lowest possible intake pressure achievable with the extreme position of the VGT vanes, while 0.201 is the highest EGR level achieved even with fully opened EGR valve. Therefore only the confirmation test results for better y1 - y5 are shown here. The results are plotted together with the results from uniform design tests and optimization, as shown in Figure 11. Because a few points are very close, the letters “u” or “l” are used to indicate the optimization points are the upper points or lower points.

In the confirmation test for better y1 - y5, compared to the values in uniform design tests, the efficiency and smoke number are among the highest, NOx is in the lower half,

HC is the lowest, and CO is about the median. Compared to the values in Table 20 (c), efficiency and NOx are close to the prediction, smoke number and HC are lower, while CO is higher. It seems all the targets except HC are predicted with accuracy: optimization results are close to confirmation test results which fall into 95% PI.

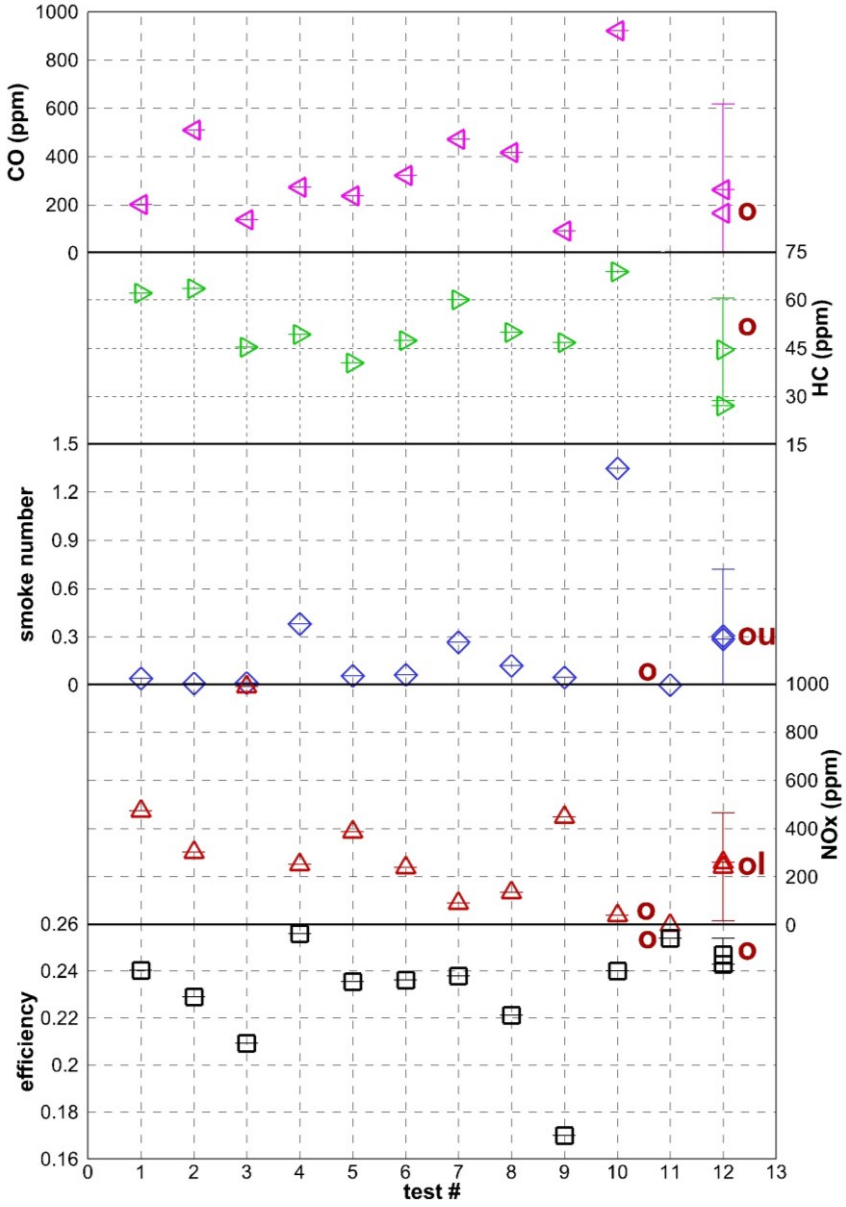

Figure 11 *Results from diesel baseline low load uniform design tests, confirmation tests, and optimization*

4.5 Results and discussion for diesel baseline tests at medium load at 1400 rpm

The uniform design array used to do the diesel baseline tests at medium load and the values of targets got from the tests are shown in Table 21. Note that the codes of levels in Table 8 are replaced with actual values in Table 21. Test 10 was done but could not reach the desired load with the factor settings, so its information is not shown here. Tests were done in the order shown in Table 21 which is different from Table 8, because this could facilitate testing.

Table 21 *The uniform design array used to do diesel baseline tests at medium load and the values of targets*

OL: over limit.

test #	intake pressure	rail pressure	SOI	EGR level	efficiency	NOx	smoke number	HC	CO
	bar	bar	° ATDC	-	-	ppm	-	ppm	ppm
	x1	x2	x3	x5	y1	y2	y3	y4	y5
1	1.029	800	-12	0.000	0.363	1085	0.388	256.6	143
2	1.040	1000	-8	0.138	0.357	412	1.083	185.1	267
3	1.072	1100	-16	0.134	0.350	1279	0.430	83.8	128
4	1.074	700	-14	0.174	0.367	502	1.317	72.6	253
5	1.120	900	-14	0.238	0.364	447	1.193	59.6	245
6	1.133	900	-10	0.229	0.358	283	1.595	67.4	307
7	1.253	700	-8	0.365	0.326	76	6.609	153.9	2668
8	1.159	1100	-12	0.427	0.244	44	9.618	1099.4	OL
9	1.462	1000	-10	0.000	0.319	OL	0.307	3.2	101

The best model for each y is shown in Table 22, with indicators of regression quality, and intercepts and coefficients of the regression equations. The applicable x ranges are shown in Table 23, which are the limits of the values actually used in the tests. Note for y5 the values except R-sq are not shown. The regression equation contains 7 terms with factors, the degree of freedom for the regression is 7, so the degree of freedom for error is 0, and the p-values and R-sq(adj) and R-sq(pred) cannot be calculated. The following statement applies to y1 - y4. The regression p-values of the models for y1, y2, and y4 are lower than 0.05, meaning these models are significant at an α-level of 0.05. The R-sq

values in each model are very high, meaning the models fit the data well, but the models for y3 and y4 do not have adequate predictive ability indicated by low R-sq(pred). Most p-values for the coefficients are lower than 0.05 except in the model for y3, meaning the corresponding x's or quadratic terms of x's are significantly related to y's. All the models involve some quadratic terms, meaning interactions between some factors are important for all y's.

The results from the optimization are summarized in Table 24. Better y1 - y3 and y1 - y5 were acquired from Microsoft EXCEL instead of Minitab because y2 and y5 have less available observations than the other y's. Therefore there is no SE Fit, 95% CI, 95% PI, and composite desirability for y1 - y3 and y1 - y5. Anyway, again the results for better multiple y's are more realistic than the results for better individual y. y1 seems to have the best results. Although y3 and y4 can approach 0 as shown in certain tests, it is doubtful that y2 and y5 can approach 0. This question can be answered by confirmation tests.

The confirmation test results for better y1 - y3 and for better y1 (represented by test 13) are plotted together with the results from uniform design tests and optimization, as shown in Figure 12. Confirmation test for better y1 - y5 was not done because its x settings are similar to those of confirmation test for better y1 - y3. So the results are expected to be similar. Then the confirmation test for better y1 was done, with the settings in Table 24 (a). The intake pressure and SOI could be set freely, being 1.085 bar and -12º ATDC respectively. SOI was set so that CA50 in each cylinder was within 5 - 10º ATDC.

Interestingly, the confirmation test results for better y1 - y3 and for better y1 are similar. Compared to the values in uniform design tests, the efficiency is the highest, NOx is above the median, smoke number is about the median, HC and CO are among the lowest. In the confirmation test for better y1 - y3, efficiency is lower than the prediction, NOx is higher, smoke number is close. In the confirmation test for better y1, efficiency is lower than the prediction. It seems efficiency and smoke number are

predicted with accuracy: optimization results are close to confirmation test results which fall into 95% PI.

Table 22 *Best model for each y in diesel baseline tests at medium load*

	y1 (efficiency)		y2 (NOx)		y3 (smoke number)	
regression p-value	0.001		0.003		0.126	
R-sq	94.42%		98.83%		95.61%	
R-sq(adj)	91.07%		97.27%		82.43%	
R-sq(pred)	75.79%		89.52%		0.00%	
intercept	0.4232		3842		-61.67	
	coefficient	**p-value**	**coefficient**	**p-value**	**coefficient**	**p-value**
x1 (intake pressure)					-6.849	0.11
x2 (rail pressure)	-9.00E-05	0.02	-3.721	0.152	0.07327	0.133
x3 (SOI)			262.4	0.018	-4.984	0.349
x5 (EGR level)	0.3584	0.012	-2775	0.001	-292.8	0.136
x2*x2						
x5*x5	-1.245	0.002				
x1*x3						
x1*x5					264.8	0.119
x2*x3			-0.3465	0.012	0.00512	0.154
x2*x5						

	y4 (HC)		y5 (CO)	
regression p-value	0.004		*	
R-sq	96.20%		100%	
R-sq(adj)	92.41%		*	
R-sq(pred)	49.71%		*	
intercept	1040		24065	
	coefficient	**p-value**	**coefficient**	**p-value**
x1 (intake pressure)			-8733	*
x2 (rail pressure)	-0.987	0.178	-30.96	*
x3 (SOI)			925.2	*
x5 (EGR level)	-7937	0.013	-8095	*
x2*x2			0.01746	*
x5*x5	6327	0.021	38230	*
x1*x3			-790.4	*
x1*x5				
x2*x3				
x2*x5	7.17	0.012		

Table 23 *Applicable x ranges in diesel baseline tests at medium load*

	lower limit	upper limit
x1 (intake pressure)	1.03	1.46
x2 (rail pressure)	700	1100
x3 (SOI)	-16	-8
x5 (EGR level)	0	0.5

Table 24 *Summary of optimization results in diesel baseline tests at medium load*

(a) Better individual y

	y1 (efficiency)	y2 (NOx)	y3 (smoke number)	y4 (HC)	y5 (CO)
	0.384	0	0	12.9	0
x1 (intake pressure)			1.149		1.029
x2 (rail pressure)	700	805	911	700	1082
x3 (SOI)		-12.4	-8.7		-15.7
x5 (EGR level)	0.142	0.378	0	0.229	0.173
SE Fit	0.00738	55.6	1.09	60.9	*
95% CI	(0.36514, 0.40307)	(-176.8, 176.8)	(-4.68, 4.68)	(-156.1, 181.9)	(*, *)
95% PI	(0.34845, 0.41977)	(-293.6, 293.6)	(-7.57, 7.57)	(-296.3, 322.2)	(*, *)
composite desirability	1	1	1	0.988	1

(b) Better y1 - y3

x1 (intake pressure)	1.03
x2 (rail pressure)	700
x3 (SOI)	-16
x5 (EGR level)	0.2

y1 (efficiency)	0.380
y2 (NOx)	364.7
y3 (smoke number)	0.942
y4 (HC)	18.6
y5 (CO)	86.2

(c) Better y1 - y5

x1 (intake pressure)	1.08
x2 (rail pressure)	700
x3 (SOI)	-15
x5 (EGR level)	0.25

y1 (efficiency)	0.370
y2 (NOx)	245.8
y3 (smoke number)	1.508
y4 (HC)	15.0
y5 (CO)	808.9

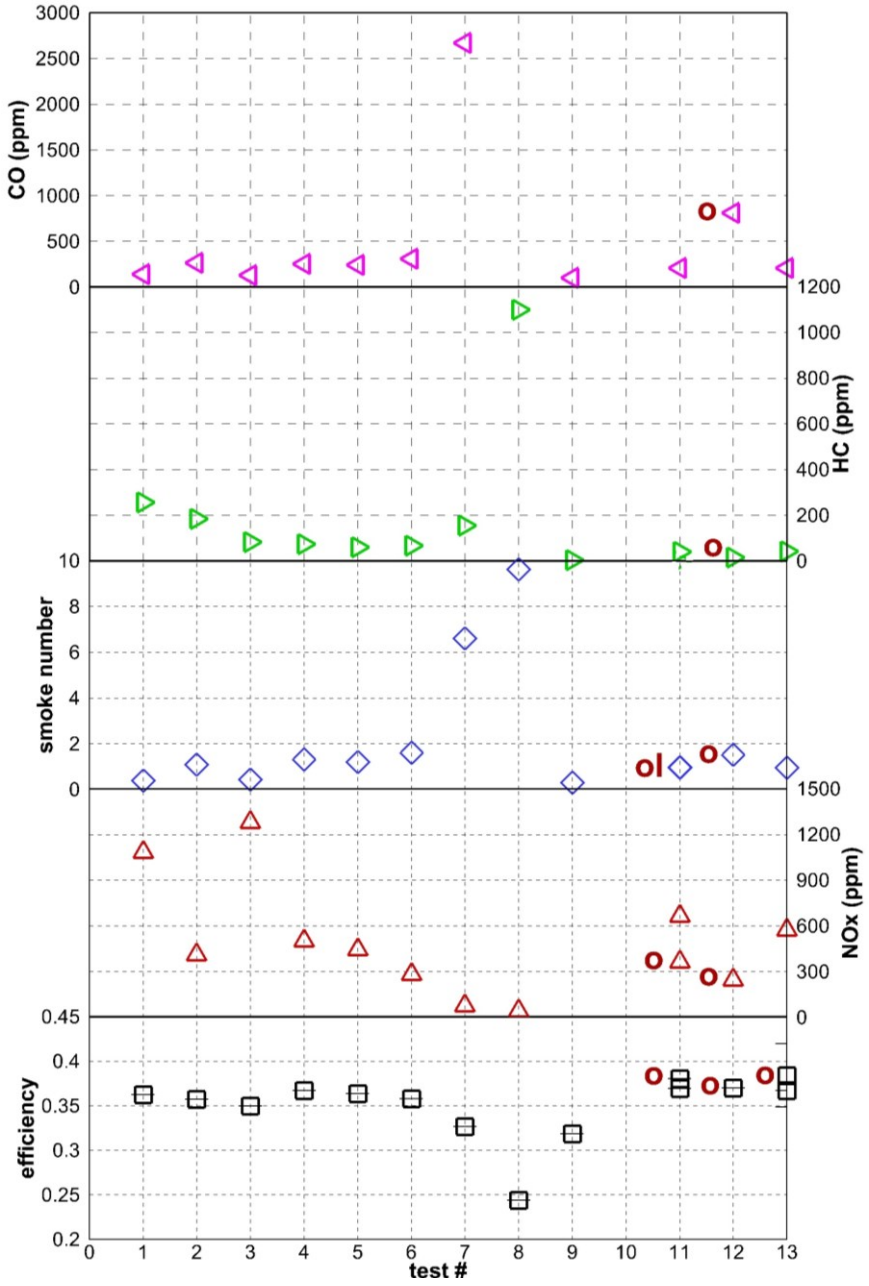

Figure 12 *Results from diesel baseline medium load uniform design tests, confirmation tests, and optimization*

4.6 Summary

The confirmation test results and the corresponding factor settings from diesel baseline tests and dual-fuel tests at low load and medium load are summarized in Table

25 for comparison. At low load, of the two dual-fuel tests, the test for better y1 - y5 achieves better results. Compared to the diesel baseline test at low load, it improves NOx slightly, improves smoke number significantly, but deteriorates efficiency, HC and CO. It needs higher intake pressure, rail pressure, and EGR level, retarded SOI, and low gasoline fraction. At medium load, compared to the two similar diesel baseline test results, dual-fuel operation does not influence efficiency, improves NOx slightly, improves smoke number and HC significantly, but deteriorates CO. It needs higher intake pressure and rail pressure, similar EGR level, retarded SOI, and medium gasoline fraction. These observations are basically consistent with those from earlier tests shown in Chapter 5. In summary, the optimization effort makes some achievements, but needs further improvement which can be made with the help of Table 26.

Table 26 shows 23 best models: y1 has 5 models; y2, y3, and y5 each has 4 models; y4 has 6 models. It summarizes the influence of each factor on each target indicated by best models. It shows the relative importance of the factors, and how to adjust the factors to get better targets.

Table 25 *The confirmation test results and the corresponding factor settings from diesel baseline tests and dual-fuel tests at low load and medium load*

confirmation test		**diesel, low load, for y1-y5**	**dual-fuel, low load, for y1-y3**	**dual-fuel, low load, for y1-y5**	**diesel, medium load, for y1-y3**	**diesel, medium load, for y1**	**dual-fuel, medium load, for y1-y5**
efficiency	-	0.243	0.214	0.221	0.369	0.367	0.361
NOx	ppm	259	255	228	666	575	566
BSNOx	g/kWh	4.41	4.38	3.42	3.94	3.61	3.28
smoke number	-	0.286	0.046	0.027	0.969	0.941	0.228
HC	ppm	27.1	215	186	39.5	41.3	7.52
CO	ppm	262	1585	1656	209	211	1679
intake pressure	bar	1.039	1.169	1.12	1.03	1.085	1.23
rail pressure	bar	500	970	1100	700	700	858
SOI	° ATDC	-11	-7	-7	-16	-12	-9.6
EGR level	-	0.223	0.296	0.37	0.2	0.142	0.16
gasoline fraction	-		0.107	0.1			0.38

Table 26 *The influence of each factor on each target indicated by the best models in dual-fuel tests and diesel baseline tests at low load and medium load*

Note:
Numbers: coefficients.
Both x3 and x4 are used to represent SOI, but only x3 is used here to avoid repetition.
significant and positive: p-value is lower than 0.05 and coefficient is positive.
insignificant and positive: p-value is higher than 0.05 and coefficient is positive.
significant and negative: p-value is lower than 0.05 and coefficient is negative.
insignificant and negative: p-value is higher than 0.05 and coefficient is negative.
not applicable. x6 is gasoline fraction and not applicable to diesel baseline tests.

	dual-fuel tests at low load						dual-fuel tests at medium load							diesel baseline tests at low load					diesel baseline tests at medium load				
	y1 (efficiency)		**y2 (NOx)**	**y3 (smoke number)**	**y4 (HC)**	**y5 (CO)**	**y1 (efficiency)**	**y2 (NOx)**	**y3 (smoke number)**	**y4 (HC)**			**y5 (CO)**	**y1 (efficiency)**	**y2 (NOx)**	**y3 (smoke number)**	**y4 (HC)**	**y5 (CO)**	**y1 (efficiency)**	**y2 (NOx)**	**y3 (smoke number)**	**y4 (HC)**	**y5 (CO)**
x1 (intake pressure)	↓ -0.0801	-0.0909		↓ 0.6029		↑ -2849	↓ -0.01931		↓ 0.1443		↑ -71.12		↓ 1190	↓ -0.1411			↑ -73.4	— -6257			↓ -6.849		— -8733
x2 (rail pressure)			↓ 0.415	— 0.001	↑ -0.1168			— 1.087	↑ -0.0017	-0.312	↑ -0.2405	-0.2694		↓ -4. 20E-05	↑ -0.533	↑ -0.00053	— 0.0165	— -5.44	↓ -9.00E-05	↑ -3.721	— 0.07327	— -0.987	↑ -30.96
x3 (SOI)	↓ -0.0005		↑ -47.57		↓ 6.96	↓ 105.2	↓ -0.00542	↑ 6.5	↓ 0.2794	52.5	↓ 40.04	48.3	↓ 483.1	↓ -0.00392	↑ 46.7	↓ 0.1451	↓ 1.361	↓ 193.8		— 262.4	↓ -4.984		— 925.2
x5 (EGR level)	↑ 0.0325	0.0306	↑ -505.8	↓ -0.2782		↓ 1831	↑ 0.01425	↑ 2740	↓ 3.474	150.5	↓ 135	156.9	— 31528	— 0.404	↑ -963	↑ -1.867	↓ -57.2	↓ -8099	— 0.3584	↑ -2775	— -292.8	— -7937	— -8095
x6 (gasoline fraction)	↓ -0.0701	-0.0678	↑ -294.1	↑ -0.8381	↑ -55.5	↓ 11405	↑ 0.02427	↑ -2028	↑ -2.856	392.9	↓ 421.7	390	— -7007										
x2*x2					4.80E-05																		0.01746
x3*x3													29.69	-0.00023		0.00507		6.993					
x5*x5				0.1469									120972				232.7		-1.245			6327	38230
x6*x6								5518															
x1*x2				-0.001														5.24					
x1*x3																							-790.4
x1*x5				0.2864									-68431	-0.3566				6994			264.8		
x1*x6				0.8083																			
x2*x3										-0.0057					-0.0841					-0.3465	0.00512		
x2*x5								-5.252									-0.0752					7.17	
x3*x5																-0.261		-154					
x3*x6					-15.65			196															
x5*x6													57259										

First, check Table 26 horizontally. Intake pressure is included in 13 models: 4 models of y1, no model of y2, 3 models of y3, 2 models of y4, and 4 models of y5. It can be deduced that intake pressure is important for efficiency and CO, somewhat important for smoke and HC, but least important for NOx.

Rail pressure is included in 18 models. These models contain all the models in diesel baseline tests, meaning rail pressure is especially important in diesel tests. Rail pressure is important for NOx, smoke, and HC in dual-fuel tests, but least important for efficiency and CO.

SOI is included in 19 models. It is less important for efficiency in dual-fuel tests at low load, least important for smoke number in dual-fuel tests at low load, efficiency and HC in diesel baseline tests at medium load.

EGR level is included in 22 models, meaning it is a very important factor influencing almost all the performance in different tests. It is only least important for HC in dual-fuel tests at low load.

Among all the 15 possible quadratic terms, only 2 terms do not appear in these models: x1*x1 and x2*x6. Quadratic terms appear in every model in diesel baseline tests, but do not appear in a few models in dual-fuel tests. This is unexpected. Because dual-fuel tests involve more factors, the models were expected to be more complex. Anyway, this makes predicting performance in dual-fuel tests easier, especially efficiency. Among the 4 square terms, x5*x5 and x3*x3 appear far more times than the other terms. Interestingly, the signs of coefficients for x3 are the same as the signs of coefficients for x3*x3, and the signs for x5 are the opposite of the signs for x5*x5, with one exception. Considering x3 is negative and x5 is positive, the above phenomenon further confirms the importance of SOI and EGR level in certain models. Among the 9 interaction terms, x1*x5 and x2*x3 appear more times than the other terms, meaning the interaction between intake pressure and EGR level and that between rail pressure and SOI are more important. This confirms the idea about the two interactions as mentioned in data analysis procedures in Section 4.2. The other quadratic terms are sparsely distributed, so it is hard to obtain any conclusions.

Second, check Table 26 vertically. In the dual-fuel tests at medium load, to improve efficiency, intake pressure needs to be decreased, injection timing advanced, EGR level and gasoline fraction increased.

To improve NOx, injection timing needs to be retarded. EGR level and gasoline fraction need to be increased. No comment for rail pressure because its influence is mixed.

To improve smoke, intake pressure and EGR level need to be decreased, injection timing advanced, rail pressure and gasoline fraction increased.

To improve HC, intake pressure and rail pressure need to be increased, EGR level and gasoline fraction decreased, and injection timing advanced.

To improve CO, intake pressure needs to be decreased, injection timing advanced. No comment for EGR level and gasoline fraction because their influence is mixed.

Increasing, decreasing, and no comment are indicated by upward arrows, downward arrows, and short lines respectively.

In the dual-fuel tests at low load, and diesel baseline tests at low load and medium load, the measures to improve efficiency and emissions can be explained similarly, so will not be detailed here.

Based on the data analysis in Sections 4.2 - 4.5, especially the problems mentioned in the end of Section 4.2, better regression models can be obtained with following methods.

1. Increase the number of tests whose results are used to create models. Increase the number of factors.
2. Be careful about using “Stepwise” function of Minitab.
3. Use other functions of Minitab such as partial least square, or try to create nonlinear models.
4. Although regression and optimization can provide useful information, they are not substitutes for subject matter expertise. Relevant background information, theoretical principles, and knowledge gained through experience should be used when applying these methods, especially for complex system as an engine. Some

literature use similar models as the ones in this study. Further literature review might find better models.

5. THE INFLUENCE OF GASOLINE FRACTION AND INJECTION TIMING ON EFFICIENCY AND EMISSIONS *

This chapter describes the parametric studies of gasoline fraction and injection timing to find their influence on efficiency and emissions.

5.1 Test matrix

Tests were done at an engine speed of 1400 rpm and three BMEPs - 1.88, 5.65 and 8.52 bar. Several parameters were adjusted, including gasoline fraction, diesel injection timing, and rail pressure. At each load with a certain injection timing and rail pressure, gasoline was added and diesel fuel was decreased gradually to increase gasoline fraction. Therefore the influence of gasoline fraction is not only related to gasoline, but also related to diesel. Increasing gasoline fraction infers decreasing diesel fraction and thus decreased diesel premixed and diffusion burning and decreased fuel spray penetration (refer to Section 6.3). The test matrix is shown in Table 27. The test name format is mentioned in Page 27. The desired gasoline fractions are 0, 0.16, 0.27, 0.33 and 0.5. The actual values are slightly different, and are used in calculations and reporting data. All the tests were done twice, on two days with similar atmospheric conditions, to reduce the uncertainty and verify the repeatability of results, except the test with -15.3º ATDC injection timing at high load. The uncertainty is shown as the pink, dark green, and light green error bars in the curves for efficiency and measured emissions in Figure 13, Figure 21, Figure 22, Figure 28. Most of the error bars are very short, meaning good repeatability and low uncertainty of the results.

At each load with certain injection timing, the influence of gasoline fraction is similar. So when discussing the influence of gasoline fraction in Sections 5.3 and 5.4, one injection timing is chosen for each load for brevity, as shown in Table 27. At each load with certain gasoline fraction, the influence of injection timing is similar. So when discussing the influence of injection timing in Sections 5.5 and 5.6, one gasoline fraction

* Part of this section is reprinted with permission from SAE Paper 2013-01-0273 © 2013 SAE International: Sun, J., Bittle, J.A., and Jacobs, T.J., 2013, "Influencing Parameters of Brake Fuel Conversion Efficiency with Diesel / Gasoline Operation in a Medium-Duty Diesel Engine". SAE paper No. 2013-01-0273. Further use or distribution of this material is not permitted without prior permission from SAE.

is chosen for each load for brevity, as shown in Table 27. Table 27 also shows tests whose results are used for analyzing cyclic variability as detailed in Chapter 6.

Table 27 *Test matrix of all the tests*

Note:
A: for analyzing influence of gasoline fraction.
B: for analyzing influence of injection timing.
C: for analyzing cyclic variability.

No.	test name	actual gasoline fraction	A	B	C
1	1.88-827--8-0	0			C
2	1.88-827--8-0.27	0.273			C
3	1.88-827--8-0.5	0.495		B	C
4	1.88-827--5-0	0	A		
5	1.88-827--5-0.27	0.266	A		
6	1.88-827--5-0.5	0.487	A	B	
7	1.88-827--3-0	0			
8	1.88-827--3-0.27	0.282			
9	1.88-827--3-0.5	0.501		B	
10	1.88-827-0-0	0			
11	1.88-827-0-0.27	0.275			
12	1.88-827-0-0.5	0.504		B	
13	5.65-1124--9.4-0	0	A		C
14	5.65-1124--9.4-0.27	0.284	A		C
15	5.65-1124--9.4-0.5	0.496	A	B	C
16	5.65-1124--6-0	0			
17	5.65-1124--6-0.27	0.276			
18	5.65-1124--6-0.5	0.500		B	
19	5.65-1124--3-0	0			
20	5.65-1124--3-0.27	0.279			
21	5.65-1124--3-0.5	0.488		B	
22	5.65-1124-0-0	0			
23	5.65-1124-0-0.27	0.280			
24	5.65-1124-0-0.5	0.476		B	
25	8.52-1000--15.3-0	0	A		
26	8.52-1000--15.3-0.27	0.256	A		
27	8.52-1000--15.3-0.33	0.327	A	B	
28	8.52-1000--3.5-0	0			C
29	8.52-1000--3.5-0.16	0.172			
30	8.52-1000--3.5-0.33	0.333		B	C
31	8.52-1000-0-0	0			
32	8.52-1000-0-0.16	0.174			
33	8.52-1000-0-0.33	0.331		B	

5.2 Energy balance

Brake power is nominally held constant during parameter sweeps (i.e., gasoline fraction and injection timing) at each load, so based on Equation (3.1), the differences in efficiency mainly result from differences in fuel energy delivery rates.

The fuel energy is distributed among brake power, incomplete combustion, friction loss, exhaust, and heat transfer [75]. The relative magnitudes of the losses affect brake power, and thus efficiency. Energy balance was done to analyze the influencing factors of efficiency, with reference to the methods outlined in [12, 26, 30, 34, 35, 37, 75], shown in Equations (5.1) - (5.4).

Incomplete combustion is the energy carried by incomplete combustion products including HC, CO, H_2, and soot in the exhaust gas. In the calculation soot is neglected because it has low amount and it is difficult to determine its amount and property. This neglecting is common in the references mentioned in the above paragraph. Anyway, in the future PM will be measured and its constituents will be analyzed, so that the contribution of soot to incomplete combustion can be accounted. Friction loss is the difference between net indicated work from all four cylinders and brake power. Exhaust is the difference between the enthalpy of intake air and exhaust gas. Heat transfer involves several factors and is considered as the difference of fuel energy and the other losses, so the heat transfer fraction includes uncertainty.

$$\dot{E}_{IC} = \dot{m}_{exh}(x_{HC} LHV_{HC} + x_{CO} LHV_{CO} + x_{H2} LHV_{H2}) \tag{5.1}$$

$$\dot{E}_{FL} = \dot{W}_{in} - P_b \tag{5.2}$$

$$\dot{E}_{exh} = \dot{m}_{exh} \sum_{i=1}^{6} x_i h_i - \dot{m}_{air} h_{air} \tag{5.3}$$

$$\dot{E}_{HT} = \dot{E}_f - P_b - \dot{E}_{FL} - \dot{E}_{IC} - \dot{E}_{exh} \tag{5.4}$$

Where, $\dot{E}_{exh}$, $\dot{E}_{FL}$, $\dot{E}_{HT}$, $\dot{E}_{IC}$:, exhaust, friction loss, heat transfer, and incomplete combustion (kW); h_{air}: enthalpy of intake air (kJ/kg), from [66]; h_i: enthalpy of N_2, O_2, CO_2, H_2O, CO and NO in exhaust gas (kJ/kg), from [66]; LHV_{HC}, LHV_{CO}, LHV_{H2}: lower heating values of HC (considered the same as fuel), CO and H_2; $\dot{m}_{exh}$, $\dot{m}_{air}$: exhaust gas and air flow rates (kg/s); $\dot{W}_{in}$: net indicated work rate (kW); x_{HC}, x_{CO}, x_{H2} : mass

concentrations of HC, CO and H_2 in exhaust gas; x_i: mass concentrations of N_2, O_2, CO_2, H_2O, CO and NO in exhaust gas. Actually CO and NO have very low concentrations compared to other gases, so do not have large influence. HC also has very low concentration, and its enthalpy is unknown, so it is not considered for the calculation of exhaust enthalpy loss.

5.3 Influence of gasoline fraction on efficiency

As shown in Figure 13, efficiency decreases with increasing gasoline fraction. The test names are in the format of "BMEP-rail pressure-SOI", which applies to all the figures in Section 5.3. As expected, efficiency increases with increasing load. It's also interesting to note the worsening effect of gasoline fraction at low load, where efficiency at high load even with high gasoline fraction is comparable to single-diesel fuel operation.

The fractions of losses in total fuel energy are also shown in Figure 13. Exhaust and heat transfer are the largest. The incomplete combustion fraction is significant in dual-fuel operation at low load. Friction loss fraction is significant at low load. These losses have the most significant influence on efficiency.

Incomplete combustion fraction, i.e., combustion inefficiency, is one minus combustion efficiency. Combustion efficiency decreases with increasing gasoline fraction at low load. Combustion efficiency still decreases at medium and high loads but remains over 0.97 at maximum studied gasoline fraction. With increasing gasoline fraction, heat transfer fraction decreases at low load, but increases at medium and high loads. Except heat transfer fraction, the other loss fractions generally show clear trends at all loads, namely friction loss and exhaust fractions decrease, while incomplete combustion fraction increases. The change is no less than 3% with maximum gasoline fraction for friction loss fraction at low load, for combustion and exhaust fractions at low and medium loads, and for heat transfer fraction at all loads. The increase of incomplete combustion fraction is by far the most substantial. For example, at low load, the

incomplete combustion fraction increases from 0.7% in diesel operation to 8.7% with 0.27 gasoline fraction and to 15.9% with 0.5 gasoline fraction.

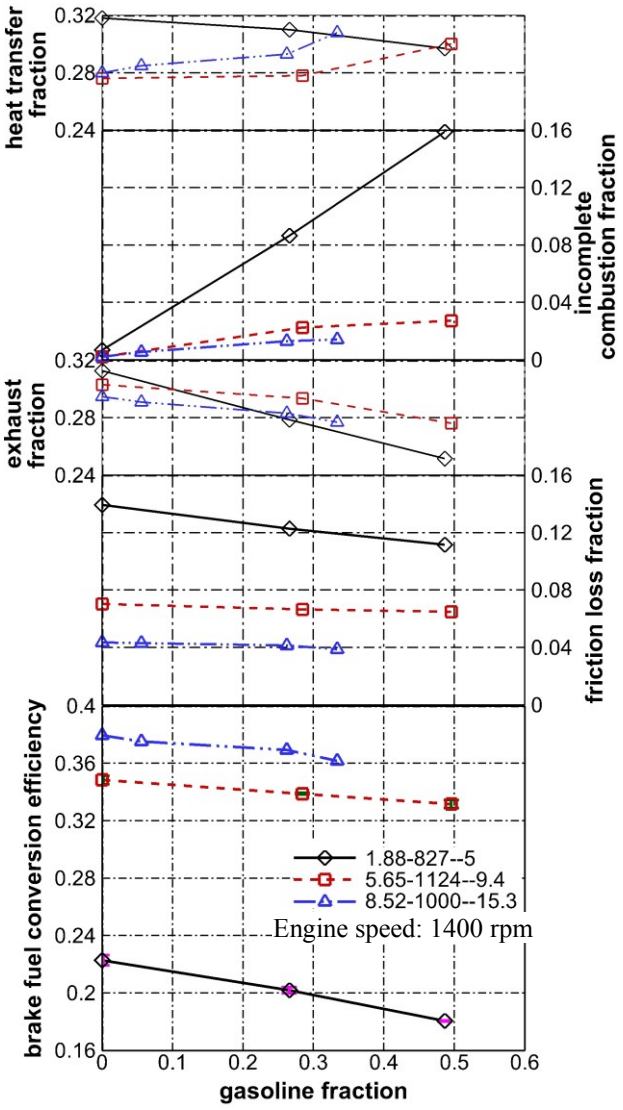

Figure 13 *Efficiency and loss fractions as function of gasoline fraction at variable loads and injection timings*

In summary, in dual-fuel operation high incomplete combustion and heat transfer are mainly responsible for lowered efficiency, while low exhaust and friction loss mitigate

decreases in efficiency. These losses will be analyzed in Sections "Incomplete combustion", "Friction loss", "Exhaust", and "Heat transfer", sometimes applying techniques used by Bittle, et al. [67]. That study [67] demonstrates a systematic analysis of the most significant factors affecting efficiency in biodiesel operation: heat loss, mixture properties, pumping work, friction, combustion efficiency, and combustion timing.

Incomplete combustion

Incomplete combustion results from the significant and almost linear increase in HC and CO emissions with gasoline fraction, as shown in Figure 21. The emissions at low load are much higher and influenced more seriously by dual-fuel operation than medium and high loads. The concentration increase of CO is higher than HC. The reasons for the high HC and CO emissions include poor flammability of lean mixture mentioned in the next paragraph, the uneven fuel distribution mentioned in Section 3.1, less diesel to ignite gasoline, and shorter diesel fuel spray to reach gasoline vapor near combustion chamber wall.

The global mixture at low load is very lean, with equivalence ratio less than 0.31. The premixed gasoline/air mixture at all loads are very lean, with equivalence ratio less than 0.15 for low load, and 0.15 - 0.25 for medium and high loads. Equivalence ratio of about 0.8 is the lower flammability limit for gasoline/air mixture. Gasoline is likely to exist in overly lean and cool areas which are difficult to ignite, and it is hard for the mixture to burn completely.

The heat release rate profiles in Figure 14, Figure 15, and Figure 16 also offer some clues about diesel and gasoline combustion and the corresponding effect on incomplete combustion. There is an interesting phenomenon with increasing gasoline fractions. The heat release rate peaks decrease at low load. The first (premixed) peaks increase, while the second (diffusion) peaks decrease and become more advanced at medium and high loads (medium load with 50% gasoline has only one peak). This probably infers that relatively less gasoline is burned in the premixed process at low load, while relatively

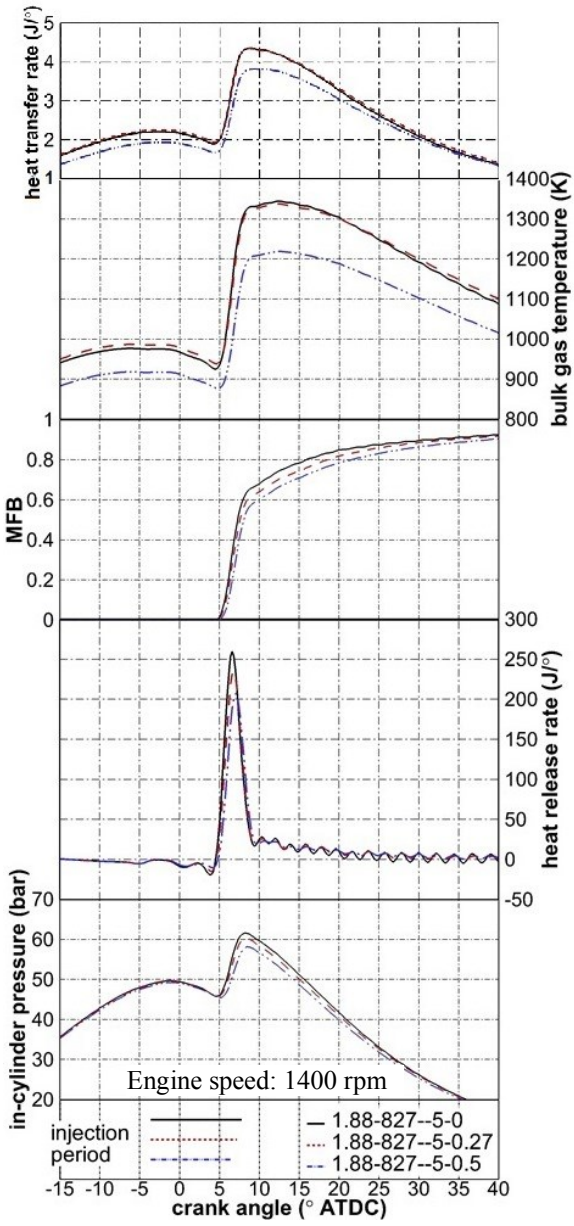

Figure 14 *Injection timing, in-cylinder pressure, heat release rate, MFB, bulk gas temperature, and heat transfer rate at low load with variable gasoline fractions*

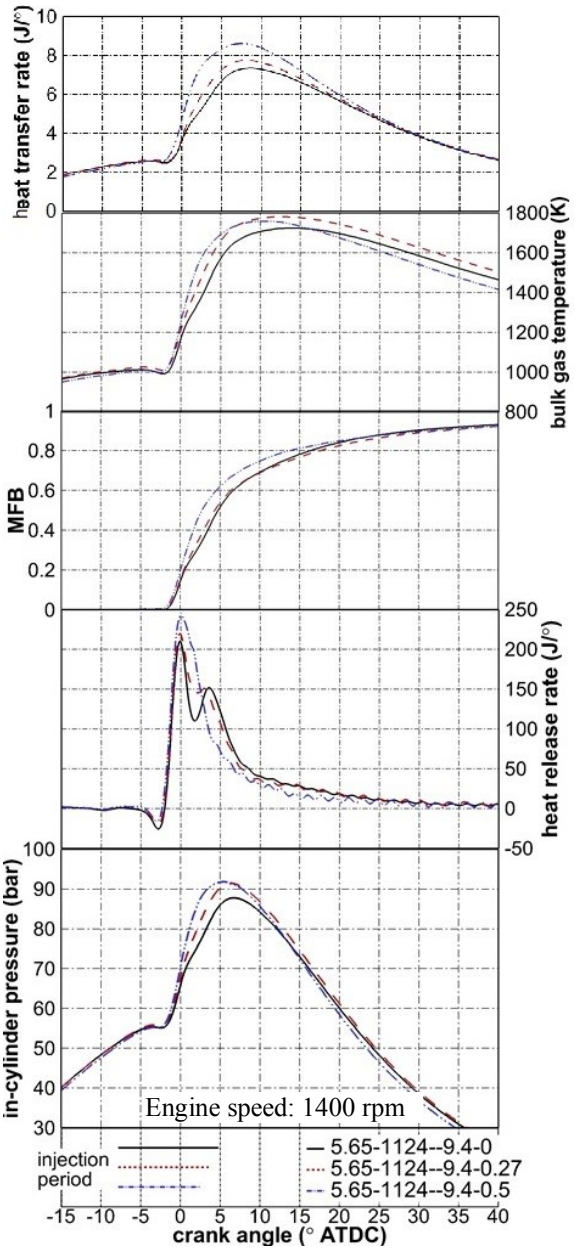

Figure 15 *Injection timing, in-cylinder pressure, heat release rate, MFB, bulk gas temperature, and heat transfer rate at medium load with variable gasoline fractions*

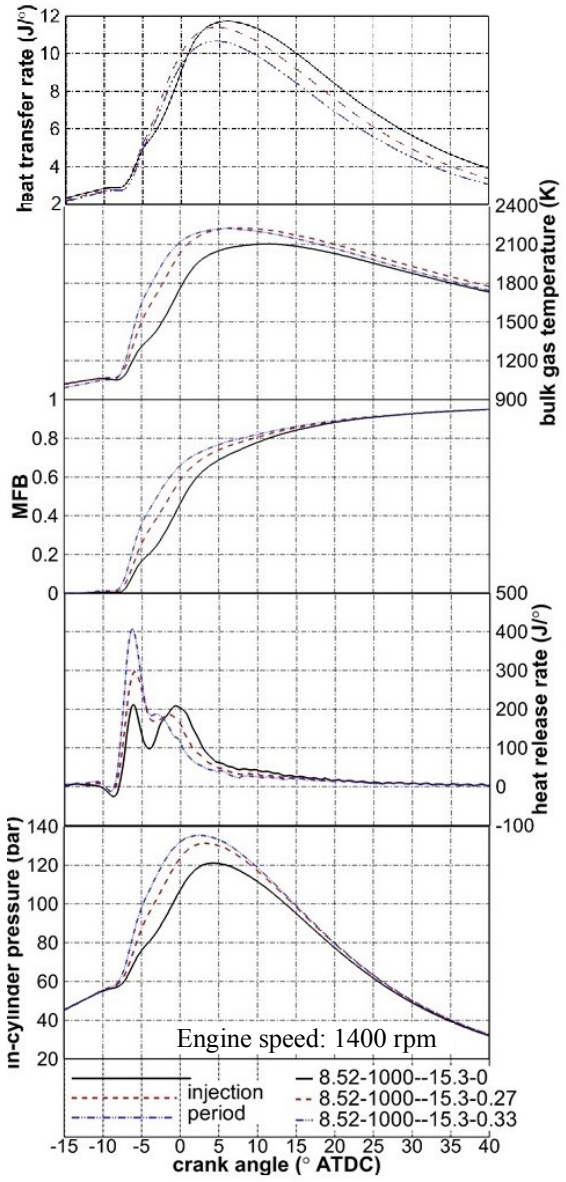

Figure 16 *Injection timing, in-cylinder pressure, heat release rate, MFB, bulk gas temperature, and heat transfer rate at high load with variable gasoline fractions*

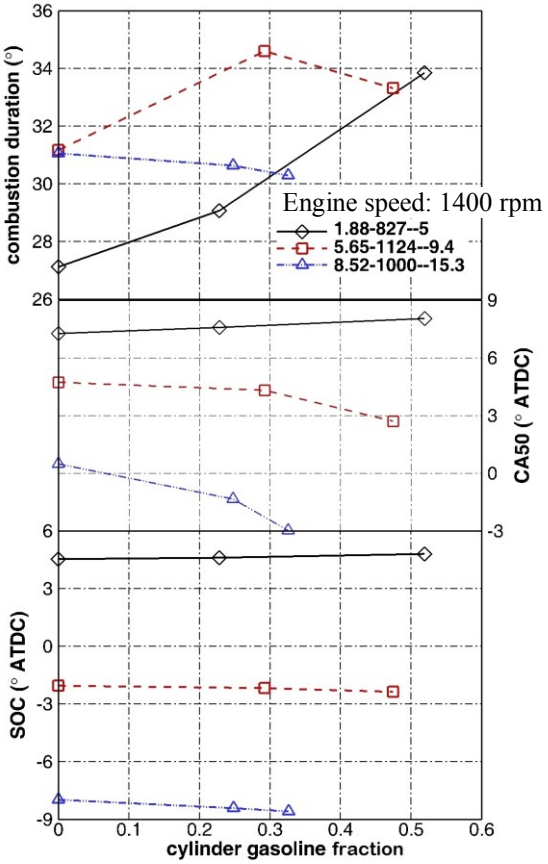

Figure 17 *SOC, CA50 and combustion duration as function of cylinder gasoline fraction at variable loads and injection timings*

more gasoline is burned in the premixed process at medium and high loads, considering probably less diesel is burned in the premixed process due to increasing gasoline. This seems to be indicative of less complete combustion at low load. The phenomenon at

medium and high load can be explained by the theory mentioned in [33]: the gasoline vapor is subject to slow oxidation during the long period of compression, producing intermediate combustion products such as peroxides and aldehydes. The heat generated in such reactions is less but these intermediate combustion products react more rapidly with oxygen than the original hydrocarbon. In dual-fuel operation, at medium and high loads, the reactions are intense enough due to favorable conditions: high pressure, temperature and gasoline/air equivalence ratio. Therefore, once the mixture is ignited by diesel, a lot of intermediate combustion products react in a short time, causing higher first peaks of heat release rate than diesel operation. The second peaks mainly represent the combustion of remaining diesel, so their termination advance as less diesel is burned. In summary, two peaks in some heat release rate curves show tradeoffs in premixed / mixing controlled burns, demonstrating the combustion is conventional diesel combustion.

Combustion phasing can also have a significant impact on efficiency. For any given operating condition, there is optimal combustion timing and phasing that optimizes the tradeoff between high heat losses with too early a timing and high expansion losses with too late a timing. This is often observed in SOC, CA50, and combustion duration data, as shown in Figure 17. Such parameters are calculated from heat release rate and MFB data.

As shown by MFB curves in Figure 14, Figure 15, and Figure 16, as well as Figure 17, SOC remains unchanged with increasing gasoline fraction at each load. Since SOI is the same at each load, ignition delay also remains unchanged. This indicates that gasoline does not affect the compressed-ignition of diesel and the mixture is still ignited by diesel in dual-fuel operation. In the combustion process following ignition, both CA50 and combustion duration generally do not change at medium and high loads. At low load, however, combustion duration is extended up to 7º, caused by the lack of rapid reaction of intermediate combustion products as mentioned above. Considering SOC already occurs at over 4º after TDC, the extension will have large negative effect on combustion, and thus efficiency.

In summary, it seems that poor mixture flammability, prolonged combustion, and less diesel burning are mainly responsible for the incomplete combustion at low load.

Friction loss

The friction loss is the energy used to overcome the resistance to relative motion of all the moving parts of the engine and to drive the engine accessories [75]. When gasoline fraction changes at a certain load, the power to drive diesel fuel supply system including pump, common rail, and injectors might be the only significant changing factor affecting friction loss. With increasing gasoline fraction, less diesel fuel is pumped and injected, thus less power requirement and less friction loss. As shown in Figure 13, the only significant change of friction loss occurs at medium and high loads with high gasoline fractions as expected, especially at medium load, when the rail pressure is the highest. It is noted that the energy balance does not capture the energy supplied to power the gasoline pump, which is electrically driven.

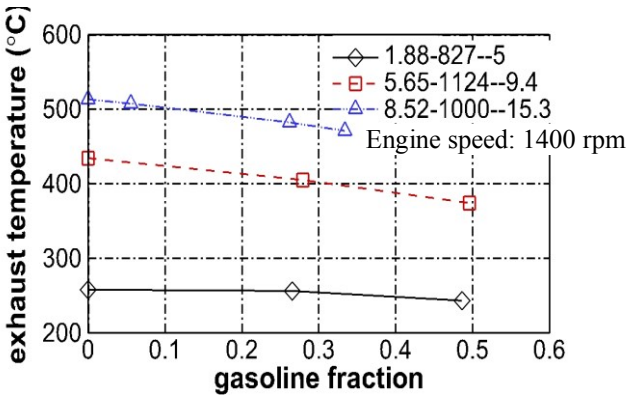

Figure 18 *Exhaust temperature as function of gasoline fraction at variable loads and injection timings*

Exhaust

As shown in Figure 13, exhaust decreases with increasing gasoline fraction. The decrease is mainly due to decreased exhaust temperature, as shown in Figure 18. At all

loads the exhaust temperature decreases with increasing gasoline fraction, especially at medium and high loads, up to 50ºC. Dual-fuel operation has lower exhaust temperature due to less complete combustion at low load and sooner end of combustion at medium and high loads.

Heat transfer

Heat transfer results in the transfer of thermal energy from the system, which ultimately lowers the mixture pressure and therefore the capability to convert to useful work (brake torque). With increasing gasoline fraction, heat transfer fraction decreases at low load, but increases at medium and high loads. Heat flux and heat transfer are plotted in Figure 19 and Figure 20 respectively to verify the accuracy of calculation.

Currently instantaneous heat flux based on crank angle is not measured, but time-averaged heat flux defined as heat transfer (from energy balance) divided by the area of heat transfer surface (cylinder head, piston crown, and exposed cylinder wall) can be calculated. The min and max values correspond to the position where the heat transfer surface area is largest and smallest, namely BDC (bottom dead center) and TDC. These values are comparable to those in [74] and [76].

As mentioned in Section 3.2, heat transfer rate is estimated by Equations (3.12) and (3.13). The heat transfer rate profiles are shown in Figure 14, Figure 15, and Figure 16. With changing gasoline fraction, wall temperature T_w does not change with assumption of constant, mean piston speed $\bar{S}_p$ does not change because engine speed does not change, instantaneous surface area A_s and volume V respectively remain the same at a certain crank angle. Bulk gas temperature T is calculated using ideal gas equation, different for operations with different gasoline fractions due to different in-cylinder pressure p, trapped mass m, and gas constant R. So the difference in heat transfer rate is actually related to difference in T and p. The calculated heat transfer is shown in Figure 20, together with the values from energy balance. The former is lower than the latter, but the trend is similar, which indicates Equations (3.12) and (3.13) might be suitable for qualitative analysis. It can be found that heat transfer rate increases with increasing

cylinder temperature and pressure by substituting equation (3.13) into equation (3.12). It is proportional to ($T^{0.6}$-$T_w/T^{0.4}$) and $p^{0.8}$.

As shown in Figure 14, Figure 15, and Figure 16, the bulk gas temperature at dual-fuel operation is lower than diesel operation at low load, but generally higher at medium and high loads. While it is hard to explain the trend, decreased smoke number can be one of the causes. As shown in Figure 21, smoke number decreases with increasing gasoline fraction, and much more significantly at medium and high loads. With gasoline fraction increasing, ignition delay remains constant, meaning premixing time is not reduced which helps to reduce local rich regions (since the fraction of diesel fuel decreases). Similarly, less diesel fuel is burning with less diffusion combustion indicated by dwindling second peaks of heat release rate curves in Figure 14, Figure 15, and Figure 16, which helps to reduce smoke generation. As mentioned in [45], fuel composition plays a role in soot formation for both premixed and diffusion flames. The more carbon a fuel molecule contains, the more likely it is to produce soot. Conversely, oxygen within a fuel decreases the tendency of a fuel to produce soot. Of lesser importance than oxygen, but clearly important is that increasing hydrogen in the fuel decreases the fuels tendency to soot. As shown in Table 3, compared to diesel fuel, gasoline has less carbon, more hydrogen and oxygen. All these factors can explain partly dual-fuel combustion produces less smoke. Less smoke infers less in-cylinder soot formation, and thus less in-cylinder radiation heat transfer. A change in radiation heat transfer will manifest a change in cylinder temperature, and thus indirectly affect the heat transfer rates [67].

As shown in Figure 14, Figure 15, and Figure 16, the trend of in-cylinder pressure is similar to that of in-cylinder temperature. At low load, in-cylinder pressure decreases as gasoline fraction increases. At medium and high loads, the trend is just the opposite; cylinder pressure increases as gasoline fraction increases.

The higher temperature and pressure at medium and high loads in dual-fuel operation can partly explain the higher heat transfer shown in Figure 13 and Figure 20. Heat transfer tends to increase as combustion duration increases. So prolonged combustion at low and medium loads can also partly explain the higher heat transfer.

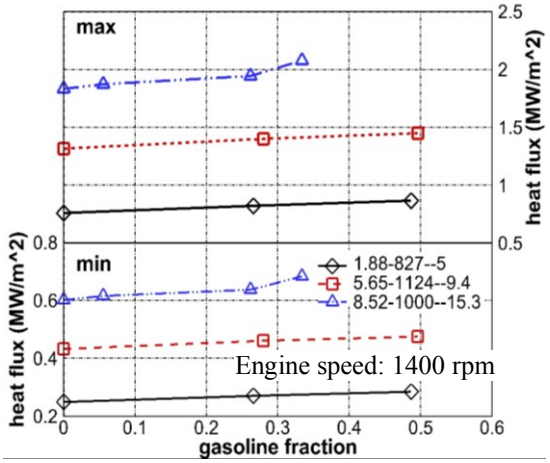

Figure 19 *Min and max heat flux as function of gasoline fraction at variable loads and injection timings*

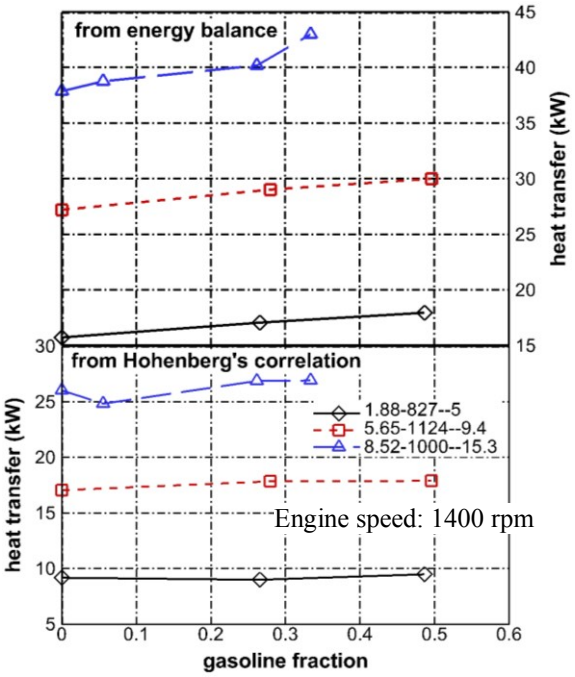

Figure 20 *Heat transfer as function of gasoline fraction at variable loads and injection timings*

Summary

1. the efficiency generally decreases as gasoline fraction increases, by between no change to 1.4% (relative to pure diesel operation) at medium and high loads with gasoline fraction increasing from 0 to 0.5 and 0.33 respectively, and by between 2.0% to 4.0% (relative to pure diesel operation) at low load with gasoline fraction increasing from 0 to 0.5.
2. With increasing gasoline fraction, heat transfer fraction decreases at low load, but increases at medium and high loads. The other loss fractions generally show clear trends at all loads, namely friction loss and exhaust fractions decrease, while incomplete combustion fraction increases. The increase of incomplete combustion fraction is the most substantial. For example, at low load it increases from 0.7% at pure diesel operation to 8.7% with 0.27 gasoline fraction and to 15.9% with 0.5 gasoline fraction.

3. At dual-fuel operation high incomplete combustion and heat transfer are mainly responsible for low efficiency, while low exhaust and friction loss are beneficial for efficiency.
4. Premixed gasoline/air mixture at all loads are very lean, with equivalence ratio less than 0.15 for low load, and 0.15 - 0.25 for medium and high loads. SOC almost does not change at a certain load with different gasoline fractions. Poor mixture flammability and late combustion are mainly responsible for the incomplete combustion at low load.
5. The decrease in the power to drive diesel fuel supply system at dual-fuel operation is sufficient to result in significant decrease in friction loss.
6. The higher temperature and pressure at medium and high loads in dual-fuel operation can partly explain the higher heat transfer. The prolonged combustion at low and medium loads can also partly explain the higher heat transfer.

5.4 Influence of gasoline fraction on emissions

The measured emissions and brake specific emissions as function of gasoline fraction, and the NOx-smoke trade-offs are shown in Figure 21.

The trends of the emissions with increasing gasoline fraction are generally the same for each pollutant, whether in terms of volumetric concentration or normalized by brake power. NOx emission decreases slightly with gasoline fraction at low load, but increases a little at medium and high loads. Correspondingly, the bulk gas temperature at dual-fuel operation is lower than diesel operation at low load, but generally higher at medium and high loads. Therefore, the strong influence of temperature on NOx emission is confirmed. The smoke, HC and CO emissions and their causes are explained in Section 5.3.

NOx-smoke trade-off curves show that generally low load tests produce both lower NOx and smoke emissions.

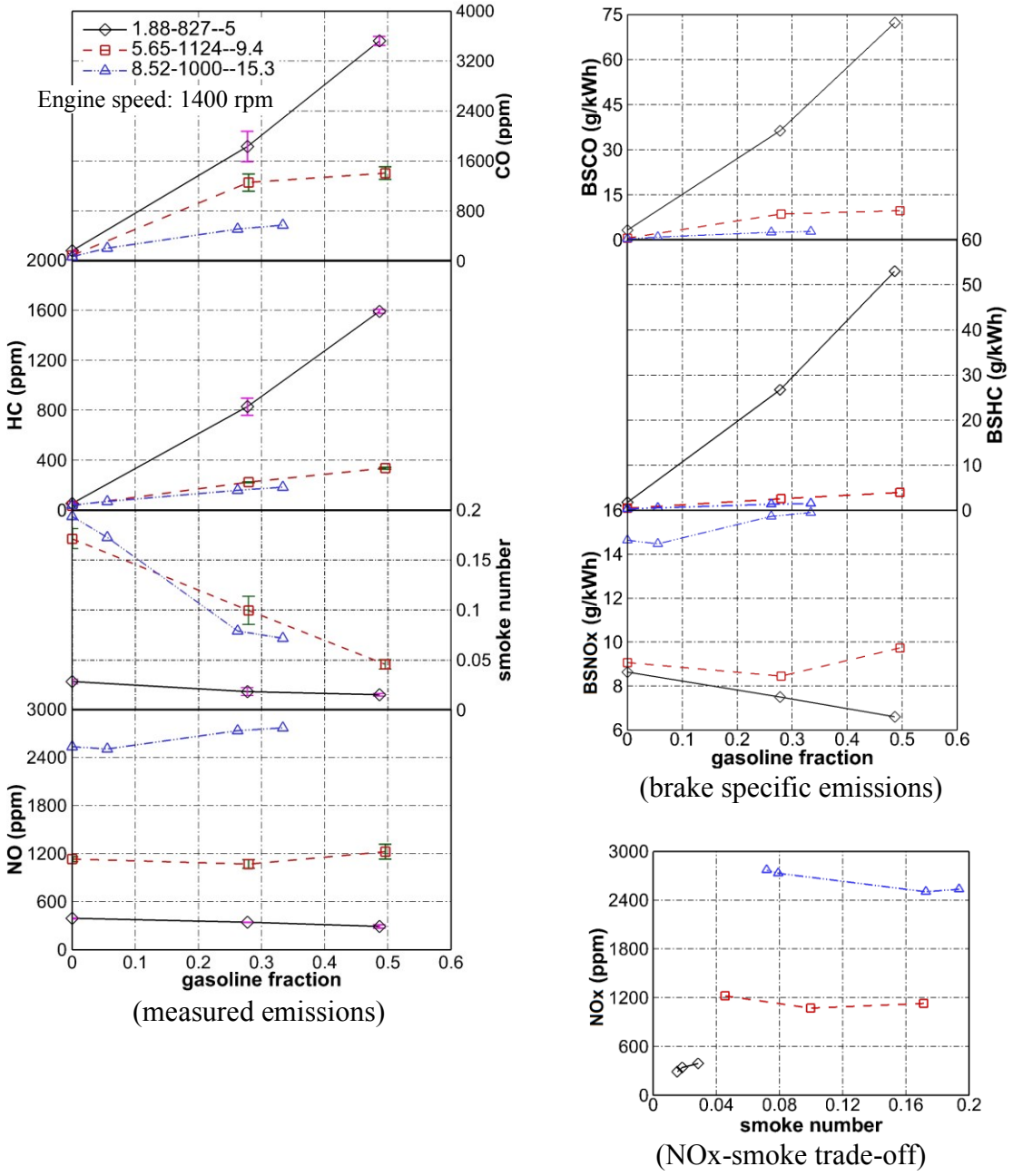

Figure 21 *Emissions as function of gasoline fraction, at variable loads*

5.5 Influence of injection timing on efficiency

As shown in Figure 22, efficiency decreases with retarding SOI at low load, by up to 2.6%. But the change is almost negligible at medium and high loads. So retarding SOI

only has significant influence on efficiency at low load, while efficiency at medium and high loads even with SOI after TDC is comparable to efficiency with SOI of -15.3º ATDC.

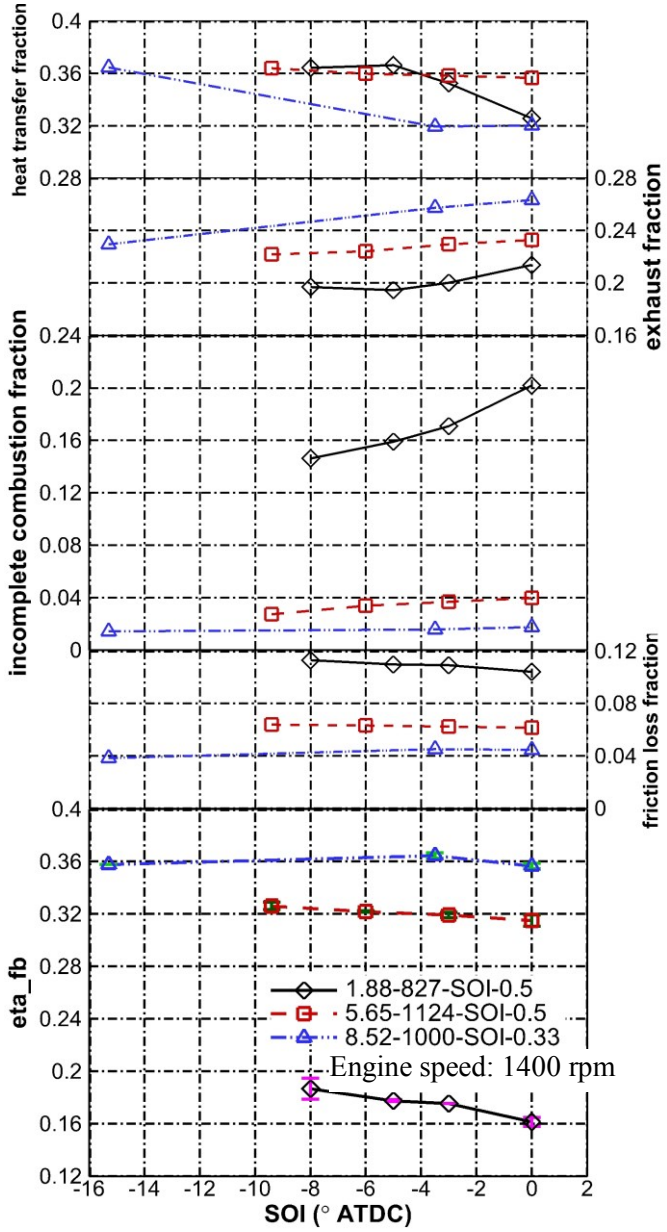

Figure 22 *Efficiency and loss fractions as function of SOI at variable loads and gasoline fractions*

The energy balance method mentioned in Section 5.3 is also used to analyze the influencing factors of efficiency.

With retarding SOI, exhaust fraction increases slightly at low and medium loads, while increases by up to 4% relative to the most advanced SOI at high load. Heat transfer fraction decreases slightly at medium load, while decreases by up to 4% and 5% relative to the most advanced SOI at low and high loads respectively. Actually the slopes of these lines are similar. The higher changes at high load are mainly due to its advanced SOI of -15.3º ATDC. Incomplete combustion fraction increases by up to 5% at low load, but almost does not change at medium and high loads. Friction loss fraction almost does not change at all loads. In summary, with the increase in exhaust and decrease in heat transfer counteracting each other, the decrease of efficiency is only demonstrated by the increase in incomplete combustion.

Incomplete combustion indicated by the significant increase in HC emission at low load and in CO emission at medium and high loads with retarding SOI, as shown in Figure 28. The following factors might be partly responsible for the high HC and CO emissions. The mixture at low load is very lean, with equivalence ratio less than 0.32. And the premixed gasoline/air mixture is also very lean, with equivalence ratio less than 0.16. Gasoline is likely to exist in overly lean and cool areas which are difficult to ignite, and it is hard for the mixture to burn completely. Moreover, much less diesel fuel is injected at low load compared to medium and high loads although the gasoline fractions are comparable, so it is possible that the shorter spray does not reach the gasoline/air mixture at the edge of combustion chamber at low load.

The heat release rate profiles are shown in Figure 23, Figure 24, and Figure 25. At low load the profile with the latest SOIs are considerably lower than those with advanced SOIs at all loads. Moreover, CA50 and CA90 are retarded further away from TDC with retarding SOI, as shown in Figure 26. Therefore the slower heat release and non-optimal combustion timing cause low efficiency.

The increase in exhaust can be attributed to the increase in exhaust temperature, as shown in Figure 27. With retarding SOI, the heat release process is retarded, but exhaust

valves open at the same time, so gases with higher temperature are expelled when the exhaust valves open.

The bulk gas temperature and in-cylinder pressure decrease significantly with retarded SOI at high load as shown in Figure 23, Figure 24, and Figure 25. This might partly contribute to the decrease in heat transfer.

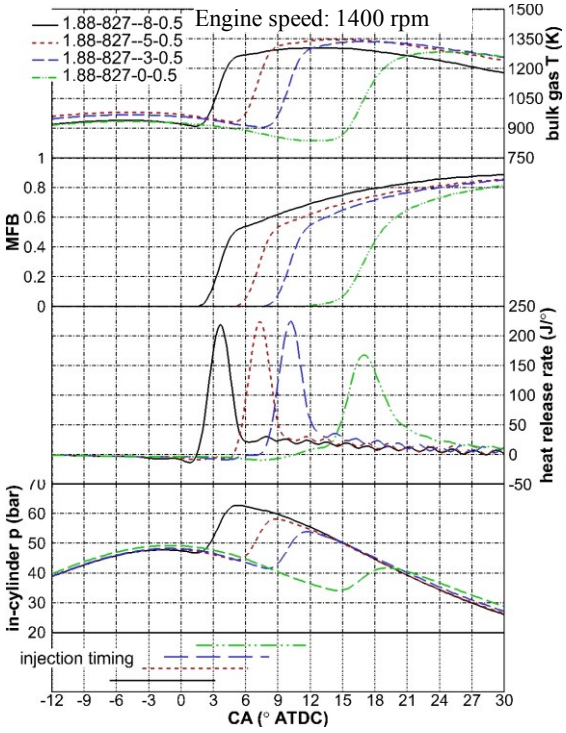

Figure 23 *Injection timing, in-cylinder pressure, heat release rate, MFB, and bulk gas temperature at 1.88-827-SOI-0.5 with variable SOIs*

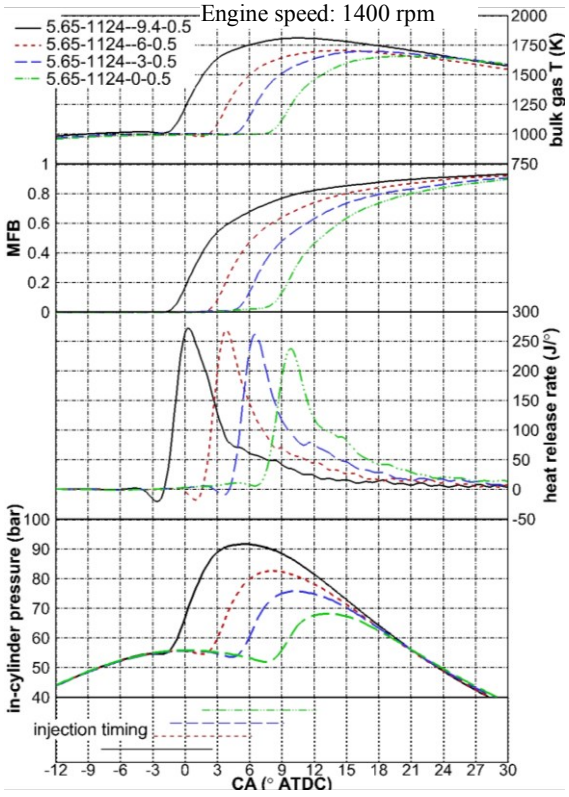

Figure 24 *Injection timing, in-cylinder pressure, heat release rate, MFB, and bulk gas temperature at 5.65-1124-SOI-0.5 with variable SOIs*

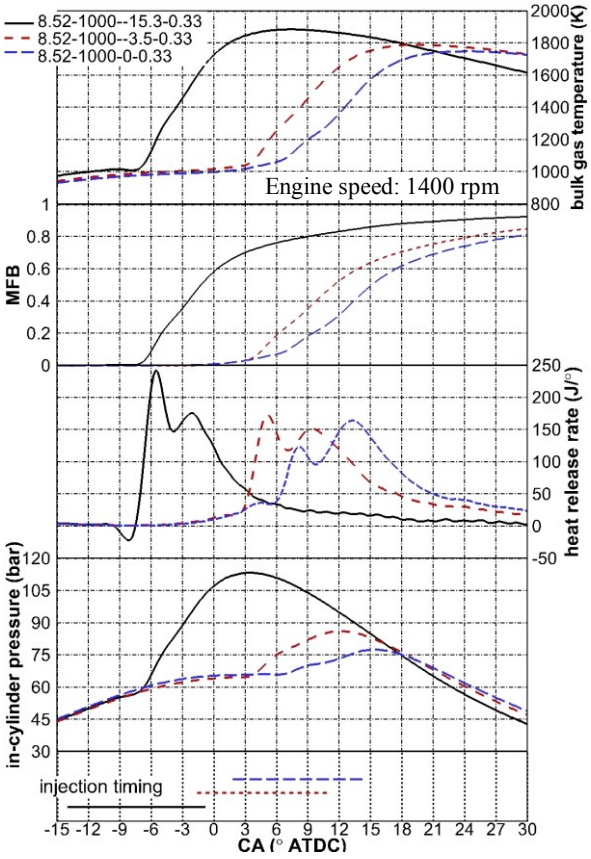

Figure 25 *Injection timing, in-cylinder pressure, heat release rate, MFB, and bulk gas temperature at 8.52-1000-SOI-0.33 with variable SOIs*

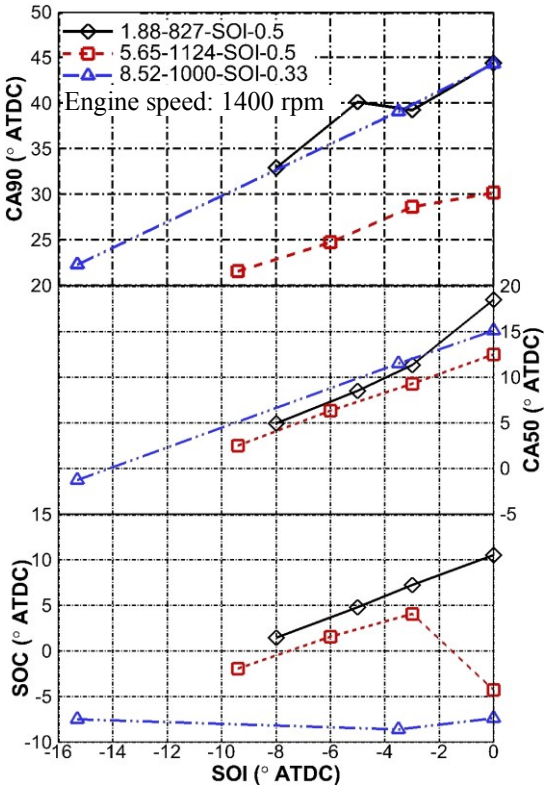

Figure 26 *Combustion timings as function of SOI at variable loads and gasoline fractions*

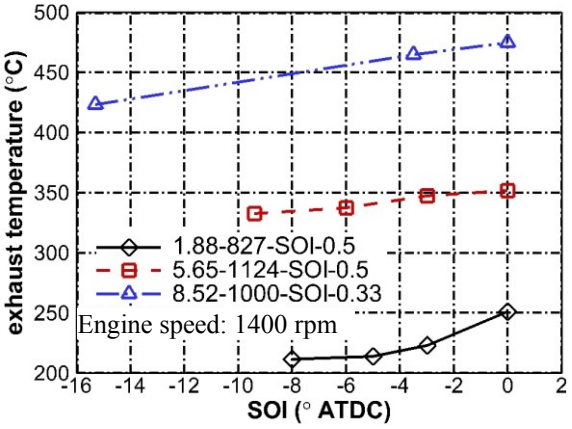

Figure 27 *Exhaust temperature as function of SOI at variable loads and gasoline fractions*

5.6 Influence of injection timing on emissions

The measured emissions and brake specific emissions as function of SOI, and the NOx-smoke trade-offs are shown in Figure 28.

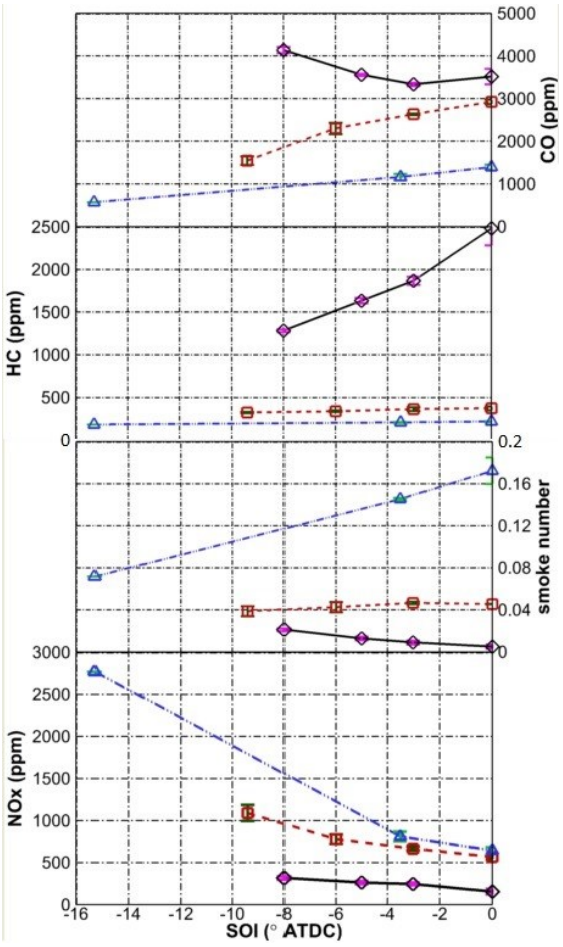

(measured emissions)

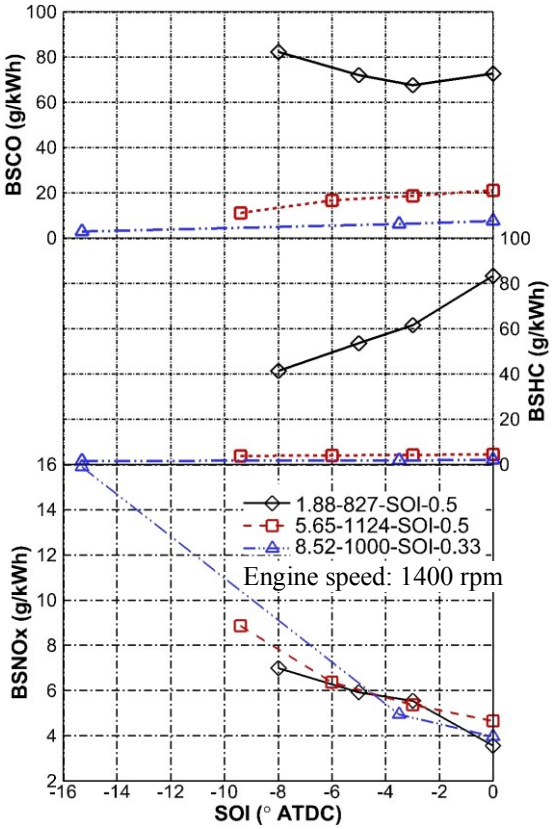

(brake specific emissions)

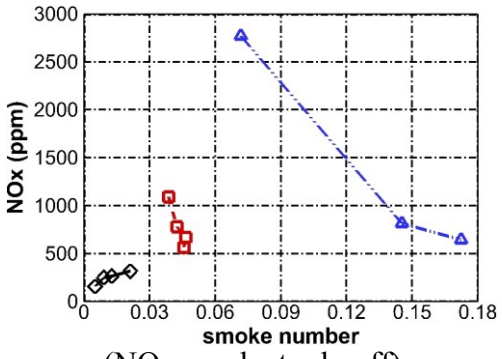

(NOx-smoke trade-off)

Figure 28 *Emissions as function of SOI, at variable loads*

The trends of the emissions with retarding SOI are generally the same for each pollutant, whether in terms of volumetric concentration or normalized by brake power. NOx decreases with retarding SOI, especially at medium and high loads. Smoke number decreases a little at low load, does not change at medium loads, while increases a lot at high load. HC increases significantly at low load, but does not change at medium and high loads. CO does not show consistent trend at low load, but increases a lot at medium and high loads.

NOx-smoke trade-off shows that low load tests produce low NOx and smoke emissions.

6. THE INFLUENCE OF CYCLIC VARIABILITY ON DUAL-FUEL EFFICIENCY AND EMISSIONS *

6.1 Introduction

Cyclic variability (CV) can be considered as non-repeatability of engine behavior (e.g., combustion, pressure, power output, and emissions) between different cycles at nominally identical operating conditions. CV has long been identified as a limiting factor in determining the performance of an engine [16]. Figure 29 shows the influence of CV in combustion on engine performance. Much of Figure 29's content is from [77], with a few modifications. The lower efficiency and higher HC and CO emissions with dual-fuel operation compared to single-fuel operation discussed in Section 5 could be due to increased CV in combustion through the paths in the right side of Figure 29. This motivates the study of CV.

Moreover, as to the differences between dual-fuel operation and single-fuel operation, the discussions in most papers focus on time-averaged results. Because fuel properties and combustion modes are different, the CV is expected to be different in the two operations. But few papers discuss the results on cycle-to-cycle basis, three of which are discussed below. Dunbeck and Reitz [25] did tests on a single-cylinder diesel engine with gasoline port injection and diesel fuel direct injection. Changing standard deviation of IMEP is shown for 100 individual cycles with increasing gasoline fraction, at 75% load and two intake port temperatures - 48 °C and 57 °C. At 10% and 25% load points, the standard deviation of IMEP showed less dramatic response than at high load to the amount of gasoline. Leermakers et al. [13] did tests on one cylinder of a six-cylinder 12.6 L diesel engine. Several data show mean values and standard deviations of CA50 values from 50 cycles per operating point, as function of SOA (start of diesel injection activation) for four injection strategies. Splitter [14] did RCCI and HCCI tests on a single-cylinder heavy-duty diesel engine with 45% EGR level and different intake

* Most of this section is reprinted with permission from ASME paper: Sun, J., Bittle, J.A., and Jacobs, T.J., 2013, "Cyclic Variability in Diesel/Gasoline Dual-Fuel Combustion on a Medium-Duty Diesel Engine", Proceedings of the ASME 2013 Internal Combustion Engine Division Fall Technical Conference, Dearborn, Michigan, USA, October 13-16, 2013. ICEF2013-19095.

temperature. Box plot statistical analysis and P test of PPRR (peak pressure rise rate) were done, and it is found that RCCI and HCCI have similar PPRR behavior, but different magnitudes and spreads. The variability in PPRR shows that the combustion process of HCCI is less stable.

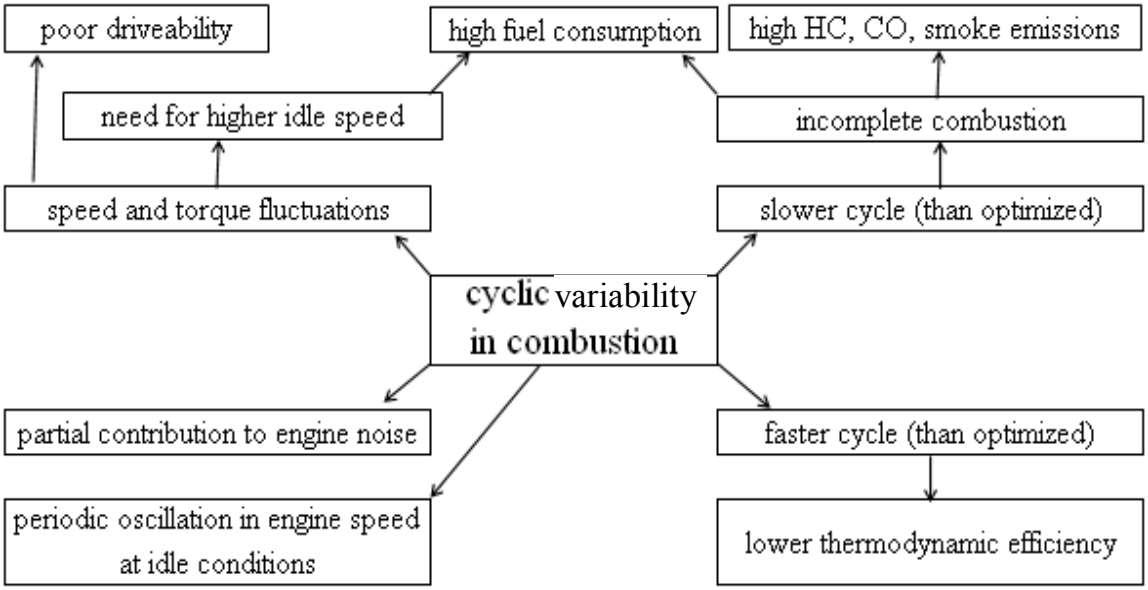

Figure 29 *The influence of CV in combustion on engine performance (adapted from [77])*

On the other hand, relatively more studies are done on CV in diesel/natural gas (or methane) engines [78, 79, 80, 81]. These papers study the influence of engine settings (engine load, compression ratio, pilot diesel injection timing, pilot diesel quantity, engine speed, and EGR ratio) on CV of some parameters (peak pressure or PP, maximum pressure rise rate or MPRR, IMEP, ignition phasing, combustion phasing, and peak heat release rate). These papers also provide useful information on test design and data analysis to the present study, because diesel/gasoline operation and diesel/natural gas operation are similar in that both use diesel direct injection and the premixing of another kind of fuel.

This study aims to investigate the CV in both dual-fuel and single-fuel operations, to compare their potential differences, and to find out the causes. Next, the test methodology to acquire high-speed data from consecutive cycles is described, then the sources of CV and their differences in the two operations are elaborated, and finally the CV is discussed in terms of magnitude and determinism sequentially.

6.2 Test methodology

In most of the tests shown in Table 27, the data for analysis of CV were obtained. High-speed data including in-cylinder pressure, heat release rate, MFB, needle lift, and rail pressure, were collected for about 150 consecutive cycles, with crank angle resolution of 0.2º. Certain tests shown in Table 27 are chosen to be analyzed for brevity.

The following 10 parameters are calculated for each cycle from the high-speed data: SOI, maximum heat release rate (MHRR), SOI-CA10, CA10-CA50, CA50, PP and its location (LPP), MPRR and its location (LMPRR), and gross indicated mean effective pressure (IMEPg). SOI-CA10 is the period from SOI to CA10, representing combustion initiation process. CA10-CA50 is the period from CA10 to CA50. These parameters are used for the analysis of CV.

6.3 Sources of CV

The sources of CV are summarized in [16, 76, 82, 83]. Table 28 lists the major factors that either cause CV in combustion, or influence its magnitude. In Table 28 , “fuel” includes both gasoline and diesel fuels. These factors are classified into three groups, which are slightly different from the groups related to CV in SI combustion as mentioned in [16]; the statements are changed so the factors could be applicable to CI engines as well. Most of the content in the “factor” column is from [77, 82] which center on spark ignition; thus statements regarding spark plugs are removed and statements regarding injectors are added to the content of Table 28 . The “description” column shows the mechanism and behavior of the factors in the present study. Some factors need detailed descriptions, which are provided in the prose following Table 28 .

Table 28 *Causing and influencing factors of CV (adapted from [77, 82])*

factor		description
group 1: variation of gas motion in the cylinder due to swirl and turbulence		
causing factors	CV of flow vector	These factors cause variations of mixture preparation, flame properties, and flame development. The charge components in single-fuel operation and dual-fuel operation are different: air in the former, and air and gasoline vapor in the latter. So the variation of gas motion should be different for the two operations. But special techniques are needed to evaluate the gas motion, such as large-eddy simulation and optical engine [84, 85]. Thus these factors are not analyzed.
	turbulence intensity and scales	
influencing factors	mean flow vector	
	averaged turbulence intensity	
	overall flow pattern	
group 2: variation of the amounts of air, fuel, residual gas, and EGR gas in the cylinder		
causing factors	CV of cylinder charging	Refer to the following paragraphs.
	CV of overall A/F ratio	Refer to the following paragraphs.
	CV of overall fractions of diluents	No comment as related to the current study.
influencing factors	overall A/F ratio	The higher gasoline fraction or load, the lower A/F ratio. The decrease of A/F ratio with increasing gasoline fraction at low load is more significant than that at medium or high load. It is mentioned in [82] that close to stoichiometric A/F ratio is best for minimum CV in SI engines, through influencing initial flame kernel development and turbulent flame propagation. This may also be true for the current study's apparatus, but stoichiometric overall A/F ratios are not studied.
	overall fractions of diluents	No comment as related to the current study.
group 3: variation of mixture preparation, namely the mixing of gas and fuel in the cylinder		
causing factors	CV of fuel injection timing	Refer to the following paragraphs.
	CV of fuel spray characteristics	No capability to assess in present study.
	mixture spatial inhomogeneity	No capability to assess in present study.
influencing factors	mean fuel injection timing	It influences the interaction of fuel spray with turbulence, and combustion phasing. It is the same for both single-fuel and dual-fuel operations, so not related to the difference of CV in the two operations.
	mean fuel spray characteristics	Refer to the following paragraphs.
	fuel type	Single-fuel operation uses diesel fuel, while dual-fuel operation uses gasoline and diesel fuel. The two fuels have different physical properties. For example, gasoline has higher volatility and lower viscosity than diesel fuel, which might help decrease CV of mixture preparation in dual-fuel operation.
	fuel injector locations	The three factors influence fuel spray characteristics and its interaction with gas mixture and combustion chamber. They are the same for single-fuel and dual-fuel operations, so not related to the difference of CV in the two operations.
	nozzle features	
	combustion chamber geometry	

The measurements of the causing factors in group 2 need special techniques such as cycle-based fuel consumption measurement [86]. But such techniques are not used in this study, so only two rough estimations were made.

One estimation calculates the CV of cylinder charging amount by evaluating in-cylinder pressure before SOC. The variation of charge amount is related to the variation of in-cylinder pressure and temperature through ideal gas equation, but only the pressure is measured, so its coefficients of variation (COV) were calculated at crank angles before SOC. As shown in Figure 30, the COVs are very small, less than 0.22%. So perhaps there is little variation in the charge amount among all the cycles in all the tests. On the other hand, the COV increases with increasing gasoline fraction, meaning the CV of charge amount in dual-fuel operation is higher than that in single-fuel operation. Finally, it is noted that the COV of in-cylinder pressure during injection was also used as a measure of mixture preparation variation in [87].

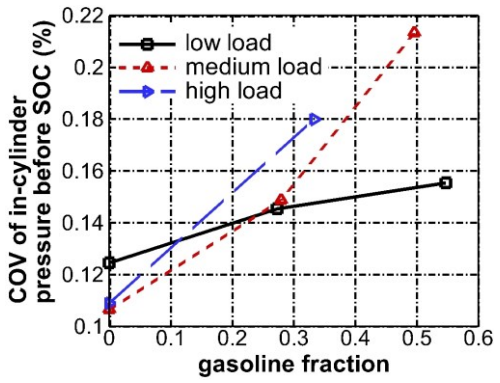

Figure 30 *COV of in-cylinder pressure before SOC as function of gasoline fraction in all the tests at 1400 rpm*

The other estimation calculates CV of fuel amount, and thus overall A/F ratio. The amount of fuel entering a certain cylinder in a cycle is related to the total heat release, which is obtained through integrating heat release rate from SOC to EVO. As shown in Figure 31, the COV of total heat release is not negligible, especially at low load. Moreover, the COV is higher in dual-fuel operation than in single-fuel operation. These

indicate considerable CV of fuel amount. The injection of diesel injector is considered to be fairly stable, while the gasoline vapor has to travel some distance from the injector to each cylinder. So it is believed the variation of gasoline amount is the major contributor to the higher CV of fuel amount in dual-fuel operation. The injection of less diesel is less stable than more diesel on cycle-to-cycle basis, and could be another contributor.

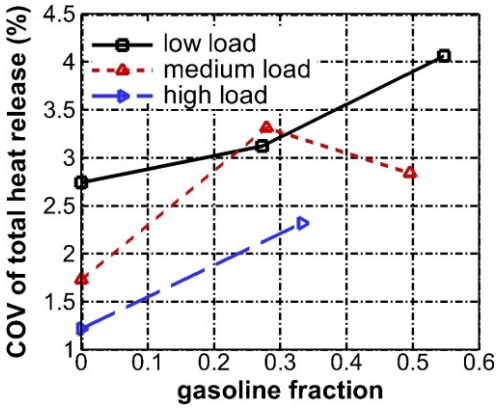

Figure 31 *COV of total heat release as function of gasoline fraction in all the tests at 1400 rpm*

Among the factors in group 3, injection timing and fuel spray characteristics can be calculated from the measured data. Figure 32 shows the standard deviation of SOI among all the cycles in each test. They range from 0.2 to 0.45º, namely one time to two times crank angle resolution of 0.2º. They decrease slightly with increasing gasoline fraction at low and high loads, while increase slightly at medium load. The values are obviously the highest at low load. The high standard deviation at low load could be caused by significantly lower diesel fuel flow rate, so SOI is more vulnerable to CV of fuel supply system.

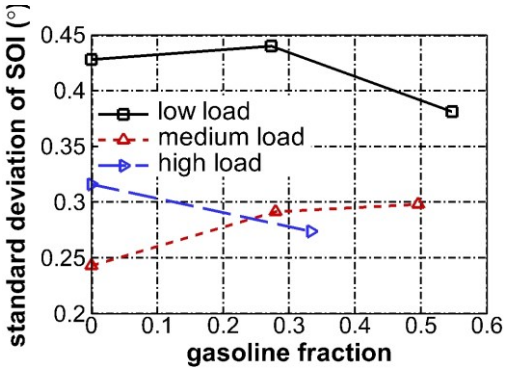

Figure 32 *Standard deviation of SOI as function of gasoline fraction in all the tests at 1400 rpm*

Diesel fuel spray characteristics are represented by three parameters: fuel spray cone angle (θ), fuel spray penetration (S), and Sauter mean diameter (D_{32}). They were calculated using equations (6.1) - (6.8), provided by [88, 89]. The results do not necessarily reflect true values because the present test conditions are not exactly the same as those under which these equations were derived, and the results are not validated with experimental spray data. But the results should be sufficient for analyzing the trends of the variables affecting CV.

$$\tan(\theta/2) = 0.31(\rho_f/\rho_g)^{0.19} \tag{6.1}$$

$$x^* = \frac{0.905 d_0 \sqrt{\rho_f/\rho_g}}{0.66\tan(\theta/2)} \tag{6.2}$$

$$t^* = x^*/U_f \tag{6.3}$$

$$U_f = 0.68\sqrt{2(p_f - p_g)/\rho_f} \tag{6.4}$$

$$\tilde{t} = \tilde{S}/2 + \sqrt{1+16\tilde{S}^2}\,\tilde{S}/4 + \ln(4\tilde{S} + \sqrt{1+16\tilde{S}^2})/16 \tag{6.5}$$

$$\tilde{S} = S/x^* \tag{6.6}$$

$$\tilde{t} = t/t^* \tag{6.7}$$

$$D_{32} = 214.9\Delta p^{-0.61}\rho_g^{\,0.036} d_0^{\,0.31} x^{0.7} \tag{6.8}$$

Where, θ: fuel spray cone angle, º; ρ_f, ρ_g: density of fuel and gas respectively, kg/m^3; x^*, t^*: characteristic penetration length and time respectively; C_a: nozzle orifice area

contraction coefficient; d_0: orifice exit diameter, mm; U_f: injected fuel velocity, m/s; p_f, p_g: pressure of fuel and gas respectively, bar; $\tilde{s}$, $\tilde{t}$: non-dimensional penetration length and time respectively; S, t: penetration length and time respectively; D_{32}: Sauter mean diameter, μm; Δp: pressure drop across the nozzle, bar; x: axial position, mm. It is considered as the penetration length traveled by the spray during injection duration in this study.

As shown in Figure 33 (a), θ changes very little with increasing gasoline fraction, with the maximum variation being smaller than 0.2º, caused by similar ρ_g in single-fuel and dual-fuel operations. On the other hand, ρ_g is significantly higher at high load than at low and medium loads, so θ is larger by about 0.8º. θ affects the mixing of fuel spray with cylinder charge. The fuel spray mixes with cylinder charge in a larger space with large θ, which helps decrease CV of mixture preparation.

S is calculated assuming t is injection duration. As shown in Figure 33 (b), S decreases with increasing gasoline fraction because less diesel fuel is injected in dual-fuel operation than in single-fuel operation. On the other hand, S is apparently smaller at low load than medium and high loads, because less diesel fuel is injected at low load. Larger S means the fuel spray will mix with more cylinder charge in the outer regions of the cylinder, good for decreasing CV of mixture preparation.

As shown in Figure 33 (c), D_{32} changes slightly with increasing gasoline fraction. Moreover, D_{32} is the smallest at medium load due to low ρ_g and highest Δp, second smallest at low load, and largest at high load. Small fuel droplet size leads to fast vaporization because less heat transfer is required. This in turn results in good mixing of fuel and cylinder charge, and less CV of mixture preparation.

In summary, among the factors analyzed above, fuel spray penetration and CV of cylinder charging, overall A/F ratio, and fuel injection timing, tend to increase CV in dual-fuel operation. On the other hand, fuel type (less volatile and more viscous diesel fuel) tends to increase CV in single-fuel operation. Based on the former observations, it is postulated that the CV in dual-fuel operation is more serious than that in single-fuel operation, which is confirmed and discussed in detail in the next section.

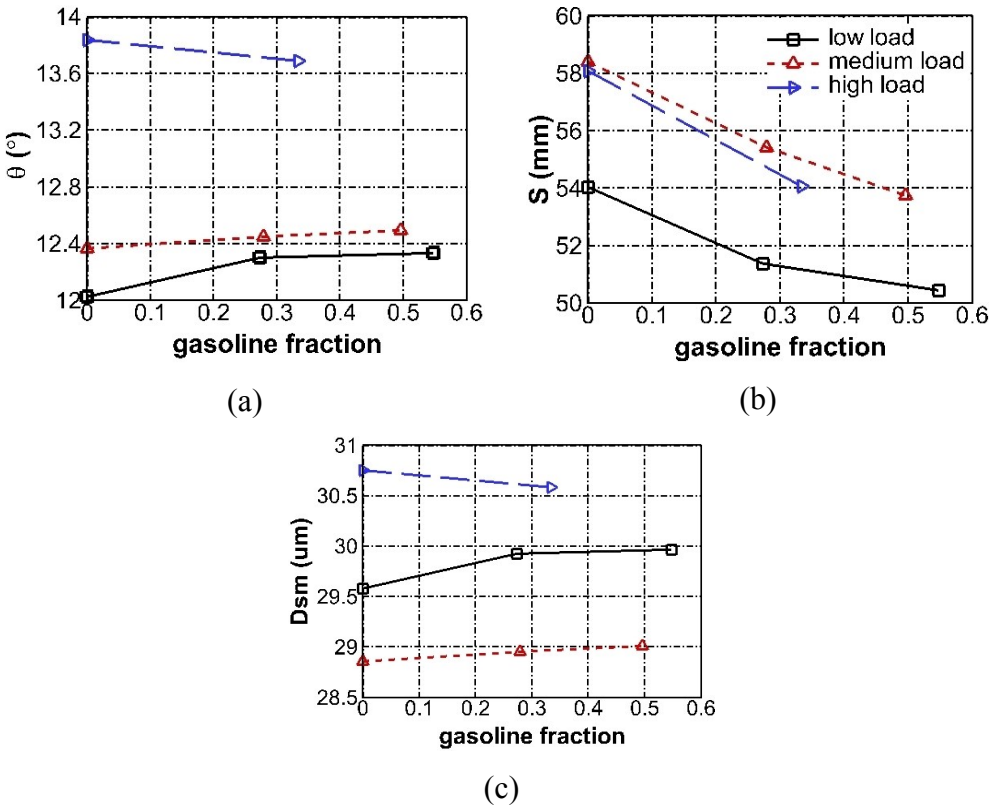

Figure 33 *(a) Fuel spray cone angle, (b) fuel spray penetration, and (c) Sauter mean diameter as function of gasoline fraction at all the loads at 1400 rpm*

6.4 CV in terms of magnitude

The CV of crank angle-based data can be shown directly when the profiles from all the cycles are plotted together. As shown in Figure 34, the heat release rate profiles from all the cycles overlie each other forming the areas of "cyclic spread". The areas after SOC (which can be inferred from heat release rate profiles) indicate CV in combustion. Such areas generally increase with increasing gasoline fraction at medium and high loads, while the areas at low load do not change much. This means CV of heat release rate in dual-fuel operation is generally higher than single-fuel operation at medium and high loads. In an average profile, each value at a crank angle is the average of the values at the same crank angle from all the cycles.

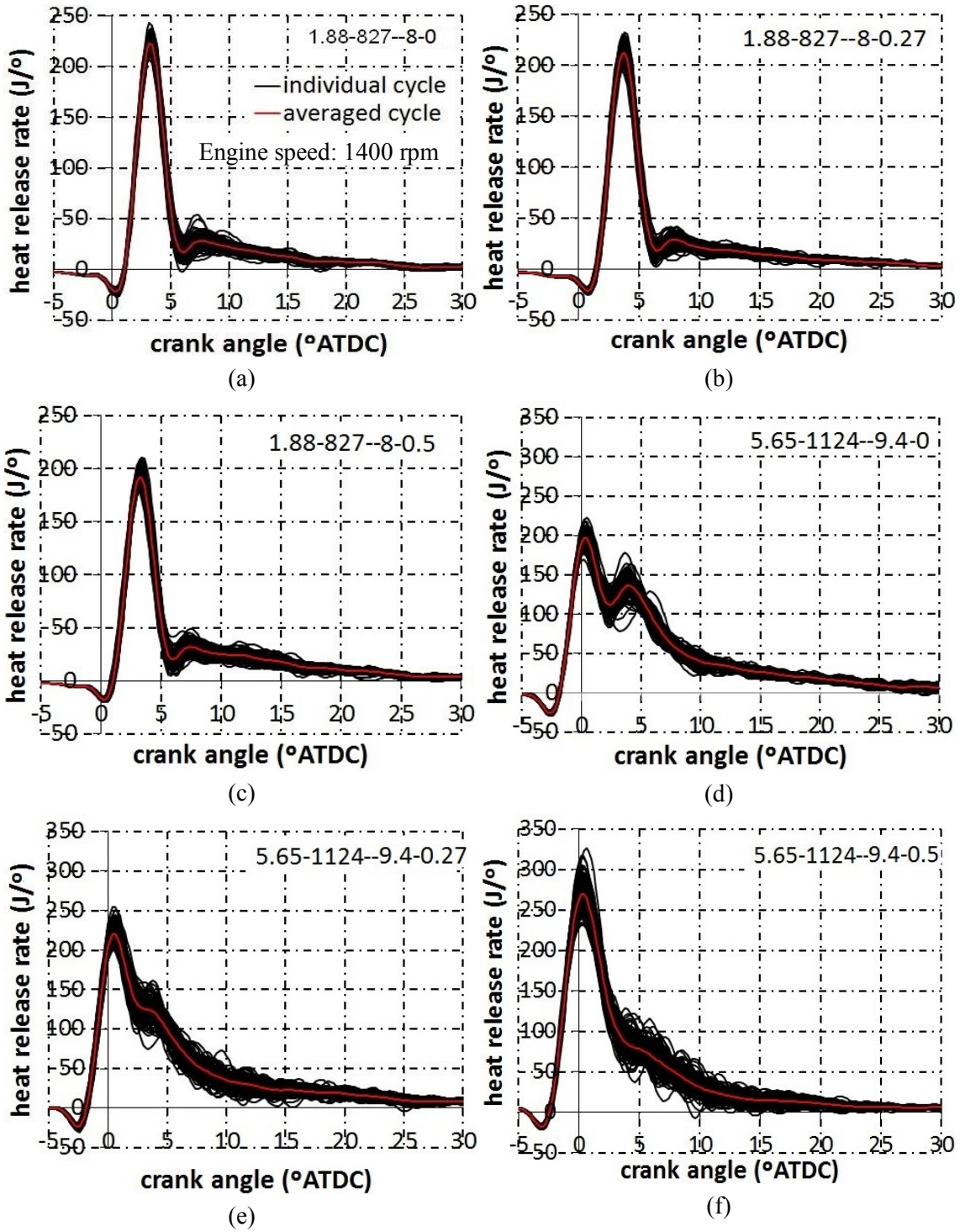

Figure 34 *Cyclic heat release rate profiles (black) and the corresponding average profiles (red) at low load with (a) single-fuel operation, (b) nominally 27% gasoline, and (c) nominally 50% gasoline; at medium load with (d) single-fuel operation, (e) nominally 27% gasoline, and (f) nominally 50% gasoline; at high load with (g) single-fuel operation and (h) nominally 33% gasoline*

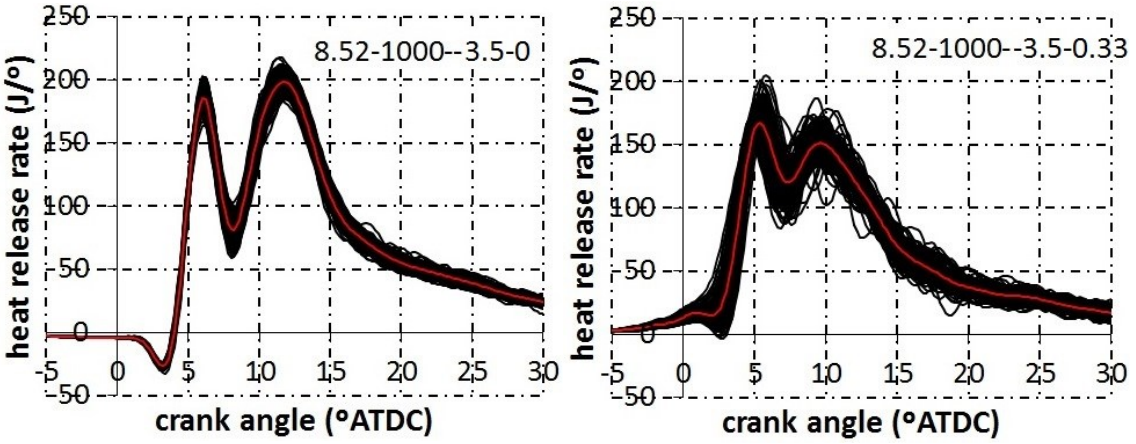

(g) (h)

Figure 34 continued

Interesting phenomena are shown by the average heat release rate profiles in Figure 34. With increasing gasoline fraction, the heat release rate peaks decrease at low load, and at medium load the first peaks representing premixed burning increase, while the second peaks representing diffusion burning decrease or even nearly vanish. Moreover, SOC in both 5.65-1124--9.4-0.5 and 8.52-1000--3.5-0.33 are more advanced than the other tests at the medium and high loads, respectively. SOC in 8.52-1000--3.5-0.33 is even earlier than SOI, indicating low to intermediate temperature heat release of the gasoline. The above phenomena probably infer that relatively less gasoline is burned in the premixed process at low load, while relatively more gasoline is burned in the premixed process at medium and high loads. The increase in premixed burning at medium and high loads might be an important reason for faster increase in the COVs of MHRR, MPRR, and PP shown in Figure 36, and also their higher values, compared with low load. As postulated in [87], premixed burning progresses much faster than diffusion burning, so small variations in the amounts of ignitable mixture "ready" at ignition can have a much larger effect on overall variations. These variations will propagate throughout the combustion process - creating larger variations in diffusion burning which would otherwise have been more consistent. This postulation also applies to this study. The gasoline is introduced into the cylinder through manifold injection, so most likely its amount is less

stable cycle-to-cycle than the amount of direct injected diesel fuel. The combustion initiation of gasoline may or may not be more "sensitive" than diesel fuel, to changes in pressure, temperature, and equivalence ratio. Regardless, in either case less stable fuel amount most likely plays an important role in higher combustion variation in dual-fuel operation.

The parameters mentioned in the last paragraph of Section 6.2 except SOI will be analyzed to get more quantitative information. Initially the sample Pearson correlation coefficients (called "correlation coefficients" for brevity) of 10 pairs of parameters are calculated using Equation (6.9): MHRR & SOI-CA10, MHRR & PP, MHRR & IMEPg, SOI-CA10 & CA10-CA50, SOI-CA10 & CA50, CA10-CA50 & IMEPg, CA50 & LPP, PP & MPRR, LPP & LMPRR, PP & IMEPg. No absolute value of correlation coefficient is consistently larger than 0.6 for any pair of parameters, meaning these parameters are not strongly linearly correlated in all the tests [90]. Consequently, all 9 parameters must be studied. It is also worth checking the COV of which parameter(s) is the optimal measure for evaluating CV, as done in [91], but this is beyond the scope of this paper.

The correlation coefficients between some parameters in a cylinder in a cycle and the same parameters in another cylinder in the next cycle were calculated also using Equation (6.9), to check whether the combustion in a cylinder in a cycle influences the combustion in the other cylinders in the next cycle. Four cylinders generate 12 pairs: cylinder 1 & cylinder 2, 1 & 3 … 4 & 3, including 4 pairs in firing order: 1 & 3, 3 & 4, 4 & 2, 2 & 1. The correlation coefficients, however, are fairly small for all the pairs. So the communications between the cylinders are negligible in terms of combustion. Persson, et al. came to the same conclusion when a cross-correlation for CA50 between different cylinders for an increased time separation in cycles is conducted [92].

$$r = \frac{\sum_{i=1}^{n}(X_i - \bar{X})(Y_i - \bar{Y})}{\sqrt{\sum_{i=1}^{n}(X_i - \bar{X})^2}\sqrt{\sum_{i=1}^{n}(Y_i - \bar{Y})^2}} \tag{6.9}$$

Where, r: correlation coefficient; n: number of cycles; X, Y: values of two parameters in a cycle; $\bar{X}$, $\bar{Y}$: values of two parameters averaged among all the cycles.

The PP values at high load are plotted against cycle # as an example of the CV of these parameters (Figure 35). The values continuously vary around the average values. Shahbakhti and Koch [83] studied the CV of HCCI combustion at over 430 operating points on two single-cylinder engines for five different blends of primary reference fuel. Three distinct patterns of CV of SOC, PP, and IMEP are observed: normal, periodic, and with weak/misfired ignitions. According to their standards, the cyclic variabilities studied here all belong to normal CV, inferring that the CV of the single-fuel and dual-fuel combustion in this study are less serious than HCCI combustion (for example).

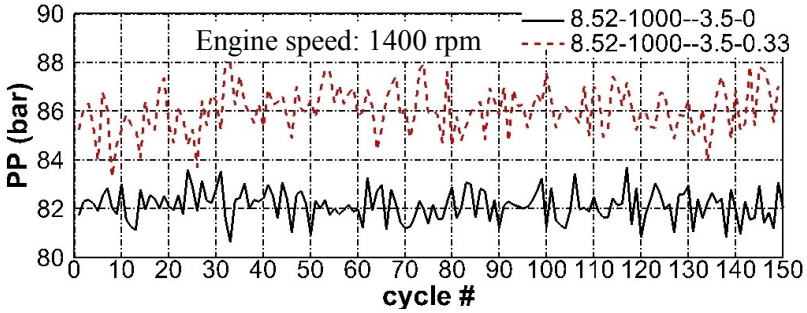

Figure 35 *PP values at high load as function of cycle #*

The CV of MHRR, SOI-CA10, CA10-CA50, PP, MPRR, and IMEPg are represented by their COVs, while the CV of CA50, LPP, and LMPRR are represented by their standard deviations (σ), with larger values indicating greater CV. Similar to the practice in [77], σ is used instead of COV for crank angle locations because location is not absolute and its "relative change" is meaningless.

As shown in Figure 36 (a), the COVs of MHRR and MPRR with highest gasoline fractions at medium and high load, and most COVs of CA10-CA50 at low and medium loads, are larger than 5%. Such test points are circled in Figure 36 (a). All the other COVs are lower than 5%. Most COVs increase consistently with increasing gasoline fraction. These facts indicate that the CV of MHRR, SOI-CA10, CA10-CA50, PP, MPRR, and IMEPg in dual-fuel tests is more serious than that in single-fuel tests. On the

other hand, the COVs of parameters do not show consistent trend with increasing load. The COVs of PP, MPRR, and MHRR are the smallest at low load.

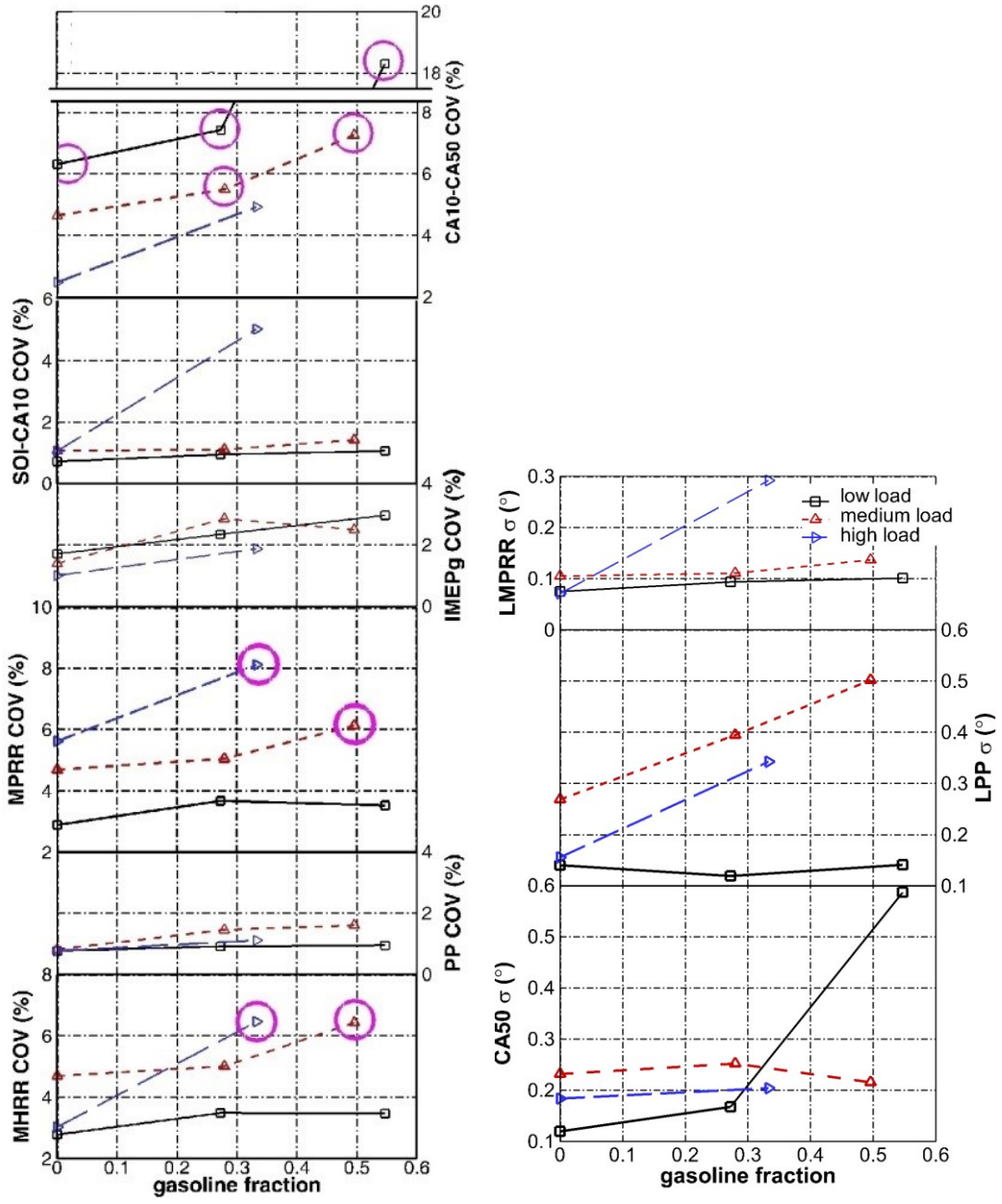

Figure 36 *(a) COVs of MHRR, PP, MPRR, IMEPg, SOI-CA10, and CA10-CA50, (b) standard deviations of CA50, LPP, and LMPRR, as functions of gasoline fraction at all three loads at 1400 rpm*

Figure 36 (b) shows that all the σ are smaller than 0.6º, meaning the crank angle locations vary within a narrow range, considering the crank angle resolution is 0.2º. With increasing gasoline fraction, the increase of CA50 σ at low load is about 0.5º, while all the other changes are smaller than 0.23º. The values of CA50 σ and CA10-CA50 COV with highest gasoline fraction at low load indicate the combustion phasing at low load is more seriously affected by dual-fuel operation than at medium and high loads.

6.5 CV in terms of determinism

The CV, although appearing to be stochastic through observing the "noisy" points shown in Figure 35, should be checked for determinism. Four techniques are used: probability density function (PDF), autocorrelation coefficient, return map, and symbol sequence statistics method. PDF reflects how the values of parameters distribute in all the cycles, and the latter three indicate the interactions of parameters in a cycle and the same parameters in the next cycle(s).

The calculation of PDFs and autocorrelation coefficients of the parameters follows the methods in [93, 94]. PDFs are calculated using Equations (6.10) through (6.15). The values of a parameter in all the cycles form a data series. The average value is subtracted from each value to create a new and normalized data series with Equation (6.10), then the PDF of the data series can be estimated by Equation (6.14). Gaussian PDF with the same average value (i.e. zero) and standard deviation as those of the data series is calculated with Equation (6.15). PDFs and the corresponding Gaussian PDFs of PP at high load are shown in Figure 37 as an example. If the parameter values follow Gaussian distribution, then the cause of parameter fluctuation is random (stochastic) and the value in a certain cycle does not depend on the value in any other cycle. The PDF curves deviate from the Gaussian PDF curves to some extent, so there should be deterministic component in the test data. The y intercepts of Gaussian PDF curves are smaller in 8.52-1000--3.5-0.33 than in 8.52-1000--3.5-0, indicating larger σ and CV in dual-fuel operation than in single-fuel operation.

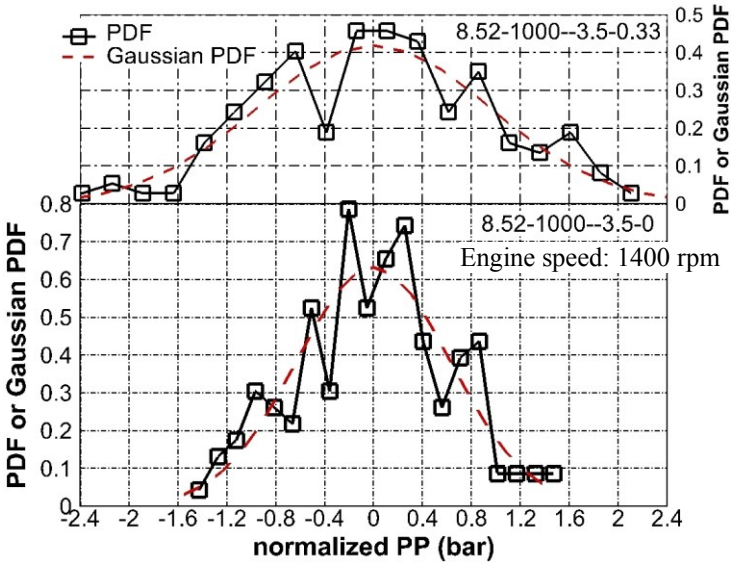

Figure 37 *PDF and the corresponding Gaussian PDF of PP at high load as function of normalized PP*

$$x_i = u_i - \bar{u} \quad (i = 1, 2 \ldots N) \tag{6.10}$$

$$w = (x_{\max} - x_{\min})/n \tag{6.11}$$

$$x_1 = x_{\min} + w/2 \tag{6.12}$$

$$x_j = x_{j-1} + w, \; j=2 \ \ldots \ n+1 \tag{6.13}$$

$$p(x)=Nx/(NW) \tag{6.14}$$

$$p_{ns}(x) = \frac{1}{\sigma\sqrt{2\pi}} e^{-\frac{1}{2}(\frac{x}{\sigma})^2} \tag{6.15}$$

Where, x_i, x_{min}, x_{max}: normalized value of a parameter in a cycle, and its minimum and maximum values among all the cycles; N: number of cycles; w: a narrow interval centered at x; n: number of intervals on x-axis. An integer no less than 1. Taken as 20 in this study; x_1, x_j: abscissa values of p in Figure 37; p: PDF; N_x: number of values within $x \pm w/2$; p_{ns}: Gaussian PDF; σ: standard deviation.

Autocorrelation coefficient is a quantitative way to show the interaction of a parameter in a cycle and that in the next rth cycle (r is lag number). For a data series x_i, the estimated autocorrelation coefficient $\hat{R}_r$ at the lag number r is defined by Equation

(6.16) and (6.17). The normalized value $\hat{R}_r / \hat{R}_0$ within ±1 is used to eliminate the influence of absolute values of $\hat{R}_r$. The closer the absolute value of $\hat{R}_r / \hat{R}_0$ is to 1, the more correlated the data values are with the next *r*th data values. The normalized autocorrelation coefficients were calculated with *r* up to 55 for the parameters. The values for PP at medium load are shown in Figure 38 as an example. There are several phenomena worth noting, observed from Figure 38 (and are consistent with normalized autocorrelation coefficients of other parameters not shown). First, most of the values are within ±0.2, meaning there is no strong linear correlation between the parameter in a cycle and that in the next *r*th cycle. Second, gasoline fraction seems not to influence the autocorrelation, because the values in dual-fuel operation are not significantly different from those in single-fuel operation. Third, the correlations at high load are generally slightly smaller than those at low and medium loads. Perhaps one of the reasons is that the combustion at high load is more robust, and less susceptible to the influence of previous cycles. The values of PP in 5.65-1124--9.4-0.27 are an exception to the above conclusions. The curve shows obvious regularity. Most values are within ±0.4. The peaks and valleys appear roughly in every sixth cycle, and are equidistant. The reason has yet to be studied.

$$\hat{R}_r = \frac{1}{N-r}\sum_{i=1}^{N-r} x_i x_{i+r} \text{ , } r=0,\ 2\ \ldots\ m.\ m \le N\text{-}1 \tag{6.16}$$

$$\hat{R}_0 = \frac{1}{N}\sum_{i=1}^{N} x_i^{\,2} = \overline{x^2} \tag{6.17}$$

Where, $\hat{R}_r$: autocorrelation coefficient; *N*: number of cycles; *r*: lag number; $\overline{x^2}$: average value of x^2 among all the cycles.

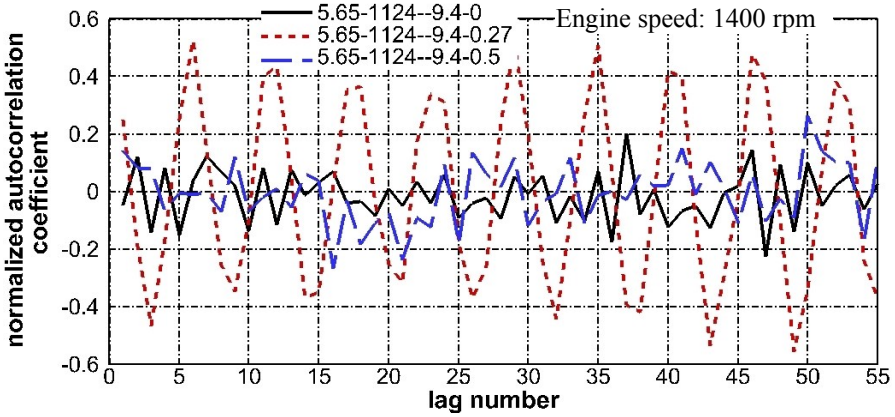

Figure 38 *Normalized autocorrelation coefficients of PP at medium load as function of lag number*

Return map is a graphic way to show the interaction between a parameter in a cycle and that in the next *r*th cycle [95, 96, 97]. The construction of quantile return maps is described in [95]. For a data set containing *N* values of a parameter, the smallest value is replaced with 1/*N*, the next smallest with 2/*N*, etc. This conversion is continued until the largest value is replaced with *N*/*N*, or 1. Neither the rank order nor the sequence of the data is changed, and the values are evenly distributed between 1/*N* and 1. Then the data series is converted into pairs of data in the form of (*x*, *y*), pairing each value of the first *N*-*r* cycles with the last *N*-*r* cycles. Finally a return map is plotted using the *N*-*r* pairs of data. An uncorrelated data series is shown as points with even density in the return map, while correlations appear as areas of points with higher and lower densities [98].

The quantile return maps of the parameters studied are calculated for *r* up to 15. The top and left three plots of Figure 39 shows example return maps of PP at medium load for *r* up to 3. The points are not distributed evenly in the whole areas, especially with *r* of 3, with the upper right and lower left corners having fewer points, which are similar to the return maps with *r* of 9 and 15 (not shown), while the opposite two corners have fewer points in the return maps with *r* of 6 and 12 (not shown). This phenomenon is consistent with what is shown by autocorrelation coefficients. These quantile return maps do not look as "nice" as those from [95] (one example is shown as the lower right

plot in Figure 39 for comparison), perhaps because there is more significant determinism and values from 3000 consecutive cycles are used to draw the return maps, while only 150 consecutive cycles are used here.

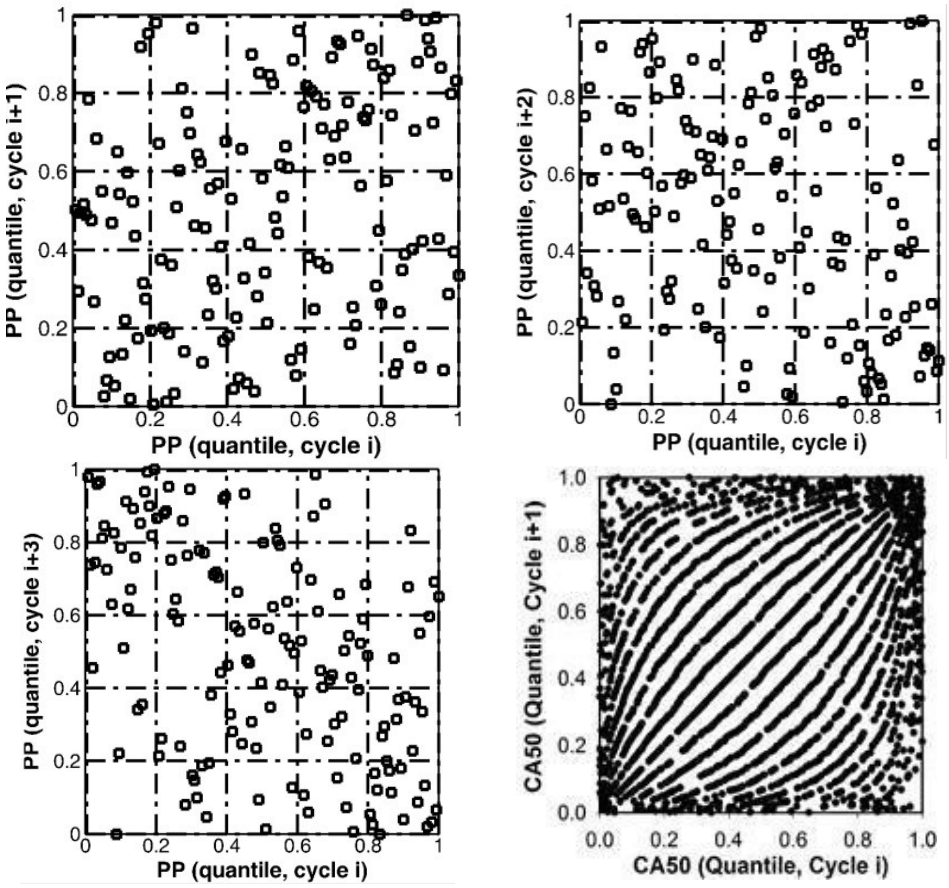

Figure 39 *Quantile return maps. First 3 are the maps of PP for lag number up to 3 in 5.65-1124--9.4-0.27 at 1400 rpm. Last one is the map for a certain A/F ratio from [95]*

The autocorrelation coefficients and return maps can only show the interaction of any two cycles, while symbol sequence statistics method can show the interaction of any number of consecutive cycles. Details of this method are described in [99, 100]. Binary or octal partitions are studied in [95, 99, 100]. Binary, quaternary, senary and octal

partitions are studied here, with sequence set size (n) of 2, 4, 6, and 8 respectively. The sequence lengths (L) for each partition are 2 - 8, 2 - 5, 2 - 4, and 2 – 3, respectively.

The symbol sequence histogram of IMEPg in 5.65-1124--9.4-0.27 is shown in Figure 40 as an example, with binary partition and various sequence lengths up to 5. The frequency is calculated through dividing the occurring count of each sequence by the total number of sequences. The latter is (N-L+1), where N is the number of cycles. The baseline frequency is n^{-L}, represented by the horizontal lines. The frequency above this line indicates the determinism in the data points. The sequences having largest frequencies for a certain L are repeated most times in all the cycles and are dominant sequences.

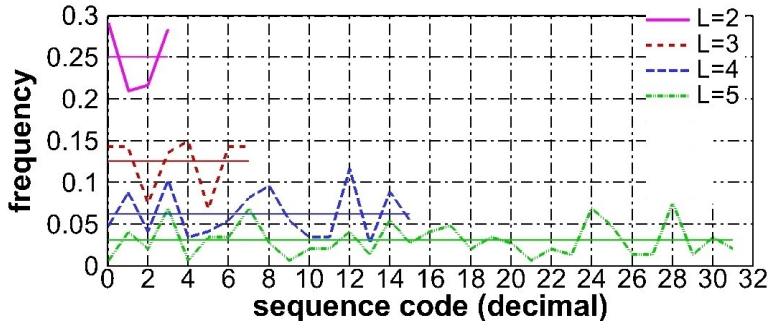

Figure 40 *Symbol sequence histogram of IMEPg in 5.65-1124--9.4-0.27 at 1400 rpm with binary partition and various sequence lengths*

The frequencies of parameter sequences in all the tests were calculated, for various partitions and sequence lengths. The dominant sequences of IMEPg are listed in Table 29 as an example. The sequences shown in red, bold and italicized fonts will be explained in the paragraph above Figure 41. Multiple sequences are included in some classifications as these sequences have the same frequencies. The sequences are expressed in binary, quaternary, senary and octal numbers for n of 2, 4, 6, and 8 respectively. Figure 40 and Table 29 are used as an example for the readers to better understand the significance of the sequences. In Figure 40, the points with sequence codes of 0, 4, 12, and 28 are the highest in each curve representing L=2 through 5, with

binary partition in 5.65-1124--9.4-0.27. These decimal numbers correspond to the binary numbers of 00, 100, 1100, and 11100 respectively, shown in the row of "5.65-1124--9.4-0.27" in Table 29 .

Table 29 *The dominant sequences of IMEPg in all the tests, for various partitions and sequence lengths*

n / test \ L	2						4		6	8
	2	3	4	5	6	7	2	3	2	2
1.88-827--8-0	10	010	0100	01001	*000100*		12	*020*	*31*	*01*
				10100	*001010*		20	*033*		*50*
					010010		33	*120*		*66*
					010100			*121*		*77*
					111111			*200*		
								322		
1.88-827--8-0.27	01	101	1101	*01101*			30	*313*	*14*	*14*
	10								*35*	*47*
										54
1.88-827--8-0.5	00	000	0001	00001	011110	*0011110*	02	*012*	*03*	*77*
						0111100	33	*022*	*14*	
						1111000		*101*	*45*	
								333		
5.65-1124--9.4-0	00	111	0010	00010	*000010*		30	*323*	*01*	*56*
					100001				*13*	
5.65-1124--9.4-0.27	00	100	1100	*11100*			33	*122*	*55*	*30*
5.65-1124--9.4-0.5	00	000	0111	00111	*001110*		10	*123*	*04*	*44*
								230	*21*	*57*
								303	*33*	*71*
									35	
									44	
8.52-1000--3.5-0	01	101	0101	01011	*101011*		03	*003*	*31*	*06*
	10						11	*112*		
							12	*213*		
							31	*311*		
8.52-1000--3.5-0.33	00	000	0000	00000	*000000*		32	*231*	*11*	*57*
								323		

The cycles are ranked in terms of IMEPg (or power). In the case of binary partition, half of the cycles with lower power are represented by 0, and half of the cycles with higher power are represented by 1. 1.88-827--8-0, 1.88-827--8-0.27, and 8.52-1000--3.5-0 show more oscillations between 0 and 1, while the other tests show more continuous 0

or 1. This means the prevalent feature of the cycles in the former tests is alternating higher and lower power, while that of the cycles in the latter tests is continuous higher power and then lower power, or vice versa. The cycles are classified more finely in terms of power in the cases of quaternary, senary, and octal partitions. For example, in the case of quaternary partition, the cycles falling into the first, second, third and fourth quarter range are represented by 0, 1, 2, and 3 respectively. The explanations of sequences are similar to those for the binary partition.

Much more obvious and regular alternating of high power and low power in consecutive cycles is observed by other researchers [83, 101]. A statement similar to the one given in [101] can be used to explain the alternating high power and low power in this study: late combustion phasing causes partial burn and low power, while partial burn also accumulates a lot of active radicals in the cylinder. Part of the radicals remains in the residual gas and will promote combustion in the following cycles and advance the combustion phasing, generating high power. High power cycles provide exhaust gas with lower temperature (or lower energy) to the turbocharger, so the intake air is compressed less, and finally the cylinder charge is compressed to lower pressure and temperature, resulting in late combustion phasing. Then the whole process repeats.

As mentioned in [95, 99, 100], modified Shannon entropy can be used to determine the optimal sequence length to be considered in a symbol sequence histogram, since the sequence length giving the lowest Shannon entropy indicates the greatest presence of determinism in the data. The relationship between modified Shannon entropy and sequence length for PP in all the tests with binary partition are shown in Figure 41 as an example. The curve shapes are similar for the other partitions. The optimal sequence lengths are 5 or 6 for binary partition, 3 for quaternary, and 2 for senary and octal. This applies to all the five parameters studied for modified Shannon entropy: IMEPg, IMEPn, PP, MPRR, and MHRR. The sequences of IMEPg with optimal sequence lengths are shown in red, bold and italicized fonts in Table 29 . This means in terms of the values of these parameters, consecutive 5 or 6 cycles is most deterministic if coarse partition (i.e. 2)

is considered, and 3 or 2 cycles if fine partitions (i.e. 4, 6, and 8) are considered. On the other hand, all the modified Shannon entropies are close to 1, larger than 0.92.

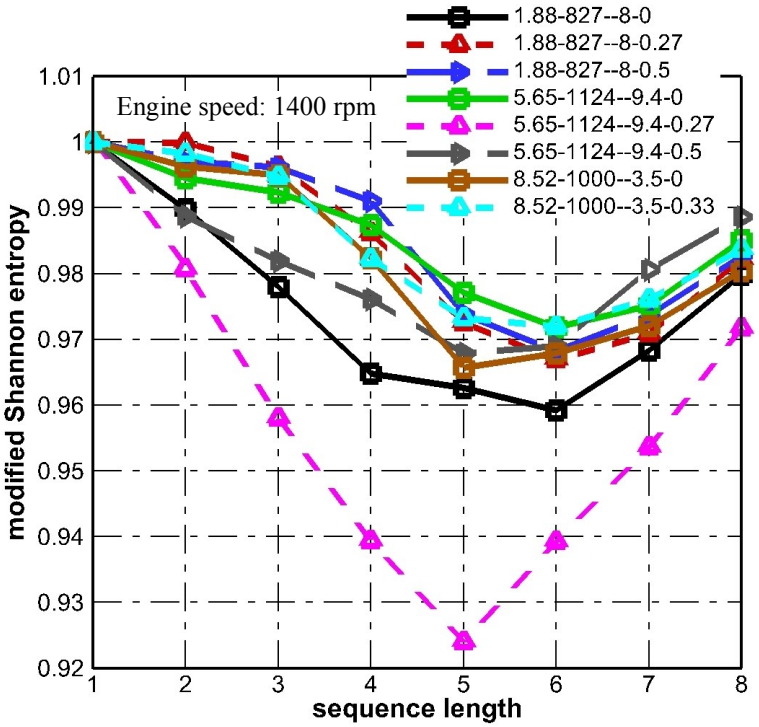

Figure 41 *Modified Shannon entropy as function of sequence length, for PP in all tests, with binary partition*

As to the influence of gasoline fraction on lowest modified Shannon entropy, IMEPg of all the tests are shown in Figure 42 as an example. In most tests at low and medium loads, the entropy first decreases and then increases with increasing gasoline fraction, meaning determinism is highest with medium gasoline fraction. There is no consistent trend at high load. As shown in Figure 41 and Figure 42, the lowest modified Shannon entropy in 5.65-1124--9.4-0.27 is less than those in most other tests, meaning its data has the largest determinism, which is shown more vividly in Figure 38.

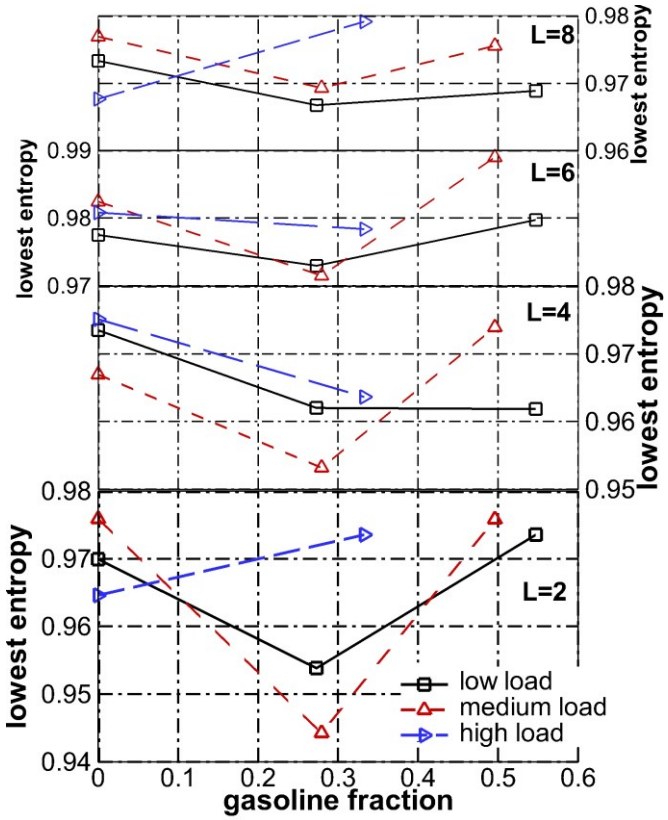

Figure 42 *Lowest modified Shannon entropy as function of gasoline fraction, for IMEPg in all the tests at 1400 rpm, with all the partitions*

6.6 Summary

Among the factors causing CV or influencing its magnitude, fuel spray penetration and CV of cylinder charging, overall A/F ratio, and fuel injection timing, tend to increase CV in dual-fuel operation. On the other hand, fuel type and fuel spray droplet size tend to increase CV in single-fuel operation.

Nine parameters were studied for analysis of CV in terms of magnitude: MHRR, SOI-CA10, CA10-CA50, CA50, PP, LPP, MPRR, LMPRR, and IMEPg. Their COV or σ are all basically going in the similar direction: increasing with increasing gasoline fraction. This means CVs of combustion timing, cylinder pressure, heat release, and indicated work, in terms of magnitude, are more serious in dual-fuel operation than in single-fuel

operation. Anyhow, the variations observed are smaller than those observed in HCCI type combustion systems in the literature.

Variations of gasoline amount and possibly gasoline low temperature heat release cause higher combustion variation in dual-fuel operation through affecting premixed burning.

Statistical methods show that most of the test data studied does not have strong determinism, and the influence of gasoline addition is small. Regardless, dominant sequences and optimal sequence lengths can be identified.

7. SUMMARY, CONCLUSIONS AND RECOMMENDATIONS FOR FUTURE STUDIES

7.1 Summary

Literature suggests that diesel/gasoline dual-fuel combustion as a combustion mode could yield very low NOx and PM emissions while maintaining good efficiency. It is promising in solving the problems of conventional LTC through better control of ignition and combustion.

The benefits of dual-fuel operation, and the potential of using gasoline fumigation to realize these benefits provide the major motivation to this research. This research is aimed at using gasoline fumigation in a medium-duty diesel engine to identify and quantify the influencing factors of diesel/gasoline dual-fuel LTC on engine efficiency and emissions. The factors include gasoline fraction, injection settings, rail pressure, intake pressure, and EGR level. This objective was realized through a series of experimental tests done at 1400 rpm and three loads (BMEP of 1.88, 5.65 and 8.52 bar, called low load, medium load, and high load respectively), including both diesel baseline tests and dual-fuel tests.

First, DOE and relevant statistical techniques were applied to tests, to identify the parameter settings for better engine performance. Twenty-three best models between 6 factors (intake pressure, rail pressure, SOI for diesel baseline tests, SOI for dual-fuel tests, EGR level, and gasoline fraction) and 5 targets (efficiency, NOx, smoke number, HC, and CO) were obtained through regression of test data. Confirmation tests were done based on best models. The observations are basically consistent with those from earlier tests: improved NOx and smoke emissions, but unimproved or deteriorated efficiency, HC and CO emissions. The optimization effort makes some achievements, but needs further improvement. The influence of each factor was analyzed. The measures to get better models were explained.

Second, parametric studies of gasoline fraction and injection timing were done to find their influence on efficiency and emissions. Efficiency generally decreases slightly by up

to 4% as gasoline fraction increases from 0 to 50%, more significantly at low load. Efficiency generally decreases slightly by up to 2.6% as injection timing is retarded from -15º ATDC to TDC, more significantly at low load. The causes were analyzed through energy balance. Generally, increasing gasoline fraction is beneficial for NOx and smoke emissions, but HC and CO emissions deteriorate especially at low load. An advance in injection timing, however, has the opposite influence. It is noted that at a certain load increasing gasoline fraction means decreasing diesel fraction, which also plays a role in the above phenomenon.

Finally, Individual cycle data were analyzed to study CV and its influence on dual-fuel efficiency and emissions. Fuel spray penetration and CV of cylinder charging, overall A/F ratio, and injection timing, tend to increase CV in dual-fuel operation. Fuel type and fuel spray droplet size tend to increase CV in single-fuel operation. The CV in dual-fuel operation is more serious than that in single-fuel operation, in terms of magnitude. Variations of gasoline amount and possibly gasoline low temperature heat release cause higher combustion variation in dual-fuel operation through affecting premixed burning. Most of the test data studied do not have strong determinism, and the influence of gasoline addition is small.

7.2 Conclusions

1. The important parameters influencing efficiency and emissions in dual-fuel operation are identified through regression of DOE-oriented test results: gasoline fraction, injection timing, rail pressure, intake pressure, and EGR level.
2. The significance of the above parameters is quantified: whether they have significant or insignificant, positive or negative influence on efficiency and emissions. This is indicated by the regression models shown in Table 26. The readers can use this table to investigate the influence of various parameters on engine efficiency and emissions in their similar dual-fuel research. For example, to improve efficiency in dual-fuel operation at medium load, intake pressure

needs to be decreased, injection timing advanced, EGR level and gasoline fraction increased, within their respective ranges shown in Table 15.

3. The parameter settings for better efficiency and emissions in diesel operation and dual-fuel operation at low load and medium load are obtained through regression and verified through tests. The specific values are shown in Table 25. The readers can use the parameter settings in this table to get better engine efficiency and emissions in their similar dual-fuel research. The engine can be viewed as a black box, producing corresponding output of engine efficiency and emissions with suitable input of parameter settings.
4. A guideline is provided to direct DOE-oriented development of dual-fuel engine research, which can identify the relationship among parameters and efficiency and emissions: define target → select parameters and levels → select design arrays → do tests → statistical analysis of results → find best models → optimization to find best parameter settings → confirmation tests.
5. A guideline is provided to apply CV analysis to the development of dual-fuel engine research in order to improve CV of combustion and performance: identify parameters to calculate for each cycle → acquire high-speed data from consecutive cycles in engine test → analyze sources of CV → analyze CV in terms of magnitude using "cyclic spread" of high-speed profiles and COV of parameters, and analyze CV in terms of determinism using probability density function, autocorrelation coefficient, return map, and symbol sequence statistics method.
6. A few gaps shown by the current state-of-the-art dual-fuel research are filled by this study. Dual-fuel operation is done with gasoline fumigation on a four-cylinder medium-duty diesel engine. Gasoline fumigation not only simplifies control strategy but also reduces hardware cost. Cylinder balancing is used to improve cylinder variation. DOE and relevant statistical techniques are used to aid the development. Cyclic variability was studied in dual-fuel operation and its influence on engine performance and efficiency.

7.3 Recommendations for future studies

1. Measures could be taken to improve gasoline evaporation and distribution, and to allow higher gasoline fraction. In the order of feasibility, the measures include: heating gasoline in the fuel line with electric heating tape or engine radiation heat; heating intake gas with an electric heater in the intake pipe; replacing the present injector (3 bar) with a high-pressure injector (at least dozens of bar). It could be a GDI injector but a suitable driving pump has yet to be found; replacing the present pump with a high-pressure pump, but this requires the plumbing which can resist high pressure; installing four port fuel injectors on each intake port. This involves significant work on cylinder head.
2. Engine performance at other loads and engine speeds, with more gasoline injection settings could be studied. The priority can be given to high load and double gasoline injection. They were planned but not studied. High load with high NOx and smoke emissions is expected to benefit from dual-fuel operation. Both single injection and double injections are studied widely in the literature, but only single injection was studied in this research.
3. Smoke number is based on the blackening of filter paper (reflectivity) and it may not accurately account for condensable organic hydrocarbons in the PM, which is an important PM mode with dual-fuel operation. Therefore PM emissions could be measured with the mini diluter in the lab to develop an understanding of the constituent species in PM.
4. To solve the problems about building regression models mentioned in Section 6.2: increasing the number of test runs; relating the models more closely to special knowledge of engine performance; using more DOE techniques and functions of statistics software. The aim is to build better models which can better predict engine performance with specified parameters, and can provide better engine test conditions.
5. To use DOE and statistical techniques in the research other than dual-fuel research, especially when many factors and multiple targets are involved.

6. To find some ways to analyze other sources of CV not studied now (Table 28), to get a better understanding of CV in dual-fuel operation. To use the conclusions to explain the time-averaged engine performance.

REFERENCES

[1] Bessonette, P., Schleyer, C., Duffy, K., Hardy, W., and Liechty, M.P., 2007, "Effects of Fuel Property Changes on Heavy-Duty HCCI Combustion". SAE Paper No. 2007-01-0191.

[2] De Ojeda, W., Bulicz, T., Han, X., Zheng, M., and Cornforth, F., 2011, "Impact of Fuel Properties on Diesel Low Temperature Combustion". SAE paper No. 2011-01-0329.

[3] Kalghatgi, G., Risberg, P., and Ångström, H., 2007, "Partially Pre-Mixed Auto-Ignition of Gasoline to Attain Low Smoke and Low NOx at High Load in a Compression Ignition Engine and Comparison with a Diesel Fuel". SAE paper No. 2007-01-0006.

[4] Kokjohn, S. L., Hanson, R.M., Splitter, D.A., and Reitz, R.D., 2009, "Experiments and Modeling of Dual-Fuel HCCI and PCCI Combustion Using In-Cylinder Fuel Blending". SAE paper No. 2009-01-2647.

[5] Zhong, S., Wyszynski, M.L., Megaritis, A., Yap, D., and Xu, H., 2005, "Experimental Investigation into HCCI Combustion Using Gasoline and Diesel Blended Fuels". SAE paper No. 2005-01-3733.

[6] Xu, H., Fu, H., Williams, H., and Shilling, I., 2002, "Modelling Study of Combustion and Gas Exchange in a HCCI (CAI) Engine". SAE paper No. 2002-01-0114.

[7] Xu, H., Williams, A., Fu, H., Wallace, S., Richardson, S., and Richardson, M., 2003, "Operating Characteristics of a Homogeneous Charge Compression Ignition Engine with Cam Profile Switching – Simulation Study". SAE paper No. 2003-01-1859.

[8] Xu, H., Rudolph, S., Liu, Z., Wallace, S., and Richardson, S., 2004, "An Investigation into the Operating Mode Transitions of a Homogeneous Charge Compression Ignition Engine Using EGR Trapping". SAE paper No. 2004-01-1911.

[9] Yap, D., Megaritis, A., Wyszynski, M.L., and Xu, H., 2004, "Residual Gas Trapping for Natural Gas HCCI". SAE paper No. 2004-01-1973.

[10] Yap, D., Megaritis, A., and Wyszynski, M.L., 2005, "An Experimental Study of Bioethanol HCCI". Combustion Science and Technology, 177:11, pp. 2039-2068, DOI: 10.1080/00102200500239911.

[11] Curran, S., Prikhodko, V., Cho, K., Sluder, C., and Parks, J., et al., 2010, "In-Cylinder Fuel Blending of Diesel/Gasoline for Improved Efficiency and Lowest Possible Emissions on a Multi-Cylinder Light-Duty Diesel Engine". SAE paper No. 2010-01-2206.

[12] Dempsey, A.B. and Reitz, R.D., 2011, "Computational Optimization of Reactivity Controlled Compression Ignition in a Heavy-Duty Engine with Ultra Low Compression Ratio". SAE paper No. 2011-24-0015.

[13] Leermakers, C.A.J., Somers, L.M.T., and Johansson, B.H., 2012, "Combustion Phasing Controllability with Dual Fuel Injection Timings". SAE paper No. 2012-01-1575.

[14] Splitter D., 2012, "High Efficiency RCCI Combustion". PhD. Thesis, University of Wisconsin-Madison, 2012, 320 pages; AAT 3542004, available through ProQuest http://disexpress.umi.com/.

[15] Heywood, J., 1988, "Chapter 10. Combustion in Compression-Ignition Engines" in "Internal Combustion Engine Fundamentals". 1988. McGraw-Hill, Inc. New York. ISBN 0-07-028637-X, 1988.

[16] Heywood, J., 1988, "Chapter 9. Combustion in Spark-Ignition Engines" in "Internal Combustion Engine Fundamentals". 1988. McGraw-Hill, Inc. New York. ISBN 0-07-028637-X, 1988.

[17] Curran, S., Cho, K., Briggs, T.E., and Wagner, R.M., 2011, "Drive Cycle Efficiency and Emissions Estimates for Reactivity Controlled Compression Ignition in a Multi-Cylinder Light-Duty Diesel Engine". Proceedings of the 2011 Internal Combustion Engine Division Fall Technical Conference, Morgantown, West Virginia USA, October 2-5, 2011. ICEF2011-60227.

[18] Lee, C., Lee, K., and Kim, D., 2003, "Experimental and Numerical Study on the Combustion Characteristics of Partially Premixed Charge Compression Ignition Engine with Dual Fuel". Fuel, 82 (2003), pp. 553–560.

[19] Jiang, H., Wang, J., and Shuai, S. J., 2005, "Visualization and Performance Analysis of Gasoline Homogeneous Charge Induced Ignition by Diesel". SAE paper No. 2005-01-0136.

[20] Hanson, R.M., Kokjohn, S.L., Splitter, D.A., and Reitz, R.D., 2010, "An Experimental Investigation of Fuel Reactivity Controlled PCCI Combustion in a Heavy-Duty Engine". SAE paper No. 2010-01-0864.

[21] Duffour, F., Ternel, C., and Pagot, A., 2011, "IFP Energies Nouvelles Approach for Dual Fuel Diesel-Gasoline Engines". SAE paper No. 2011-24-0065.

[22] Yang, B., Li, S., Zheng, Z., Yao, M., and Cheng, W., 2012, "A Comparative Study on Different Dual-Fuel Combustion Modes Fuelled with Gasoline and Diesel". SAE paper No. 2012-01-0694.

[23] Pohlkamp, K. and Reitz, R., 2012, "Reactivity Controlled Compression Ignition (RCCI) in a Single-Cylinder Air-Cooled HSDI Diesel Engine". SAE paper No. 2012-32-0074.

[24] Yoshida, K., Shoji, H, and Tanaka, H., 1998, "Study on Combustion and Exhaust Gas Emission Characteristics of Lean Gasoline-Air Mixture Ignited by Diesel Fuel Direct Injection". SAE paper No. 982482.

[25] Dunbeck, P.B. and Reitz, R.D., 2010, "An Experimental Study of Dual Fueling with Gasoline Port Injection in a Single-Cylinder, Air-Cooled HSDI Diesel Generator". SAE paper No. 2010-01-0869.

[26] Kokjohn, S., Hanson, R.M., Splitter, D.A., Kaddatz, J., and Reitz, R.D., 2011, "Fuel Reactivity Controlled Compression Ignition (RCCI) Combustion in Light- and Heavy-Duty Engines". SAE paper No. 2011-01-0357.

[27] Leermakers, C.A.J., Van den Berge, B., Luijten, C.C.M., Somers, L.M.T., de Goey, L.P.H., and Albrecht, B.A., 2011, "Gasoline-Diesel Dual Fuel: Effect of Injection Timing and Fuel Balance". SAE paper No. 2011-01-2437.

[28] Kouremenos, D. A., Rakopoulos, C. D., and Kotsiopoulos, P., 1990, "Comparative Performance and Emission Studies for Vaporized Diesel Fuel and Gasoline as Supplements in Swirl-Chamber Diesel Engines". Energy, Vol. 15, No. 12, pp. 1153-1160, 1990.

[29] De Ojeda, W., Zhang, Y., Xie, K., Han, X., Wang, M., and Zheng, M., 2012, "Exhaust Hydrocarbon Speciation from a Single-Cylinder Compression Ignition Engine Operating with In-Cylinder Blending of Gasoline and Diesel Fuels". SAE paper No. 2012-01-0683.

[30] Splitter, D., Hanson, R., Kokjohn, S., Wissink, M., and Reitz, R., 2011, "Injection Effects in Low Load RCCI Dual-Fuel Combustion". SAE paper No. 2011-24-0047.

[31] Zhang, Y., De Ojeda, W., and Wickman, D., 2012, "Computational Study of Combustion Optimization in a Heavy-Duty Diesel Engine Using In-Cylinder Blending of Gasoline and Diesel Fuels". SAE paper No. 2012-01-1977.

[32] Han, X., Xie, K., Zheng, M., De Ojeda, W., 2012, "Ignition Control of Gasoline-Diesel Dual Fuel Combustion". SAE paper No. 2012-01-1972.

[33] Alperstein, M., Swim, W. B., and Schweitzer, P., H., 1957, "Fumigation Kills Smoke -- Improves Diesel". 1957, presented at the SAE National Diesel Engine Meetings, Cleveland, Nov. 6, 1957.

[34] Hanson, R. M., Curran, S., and Wagner, R., 2012, "Piston Bowl Optimization for RCCI Combustion in a Light-Duty Multi-Cylinder Engine". SAE paper No. 2012-01-0380.

[35] Hanson, R.M., Kokjohn, S.L., Splitter, D.A., and Reitz, R.D., 2011, "Fuel Effects on Reactivity Controlled Compression Ignition (RCCI) Combustion at Low Load". SAE paper No. 2011-01-0361.

[36] Splitter, D., Hanson, R., Kokjohn, S., and Reitz, R., 2011, "Reactivity Controlled Compression Ignition (RCCI) Heavy-Duty Engine Operation at Medium-and

High-Loads with Conventional and Alternative Fuels". SAE paper No. 2011-01-0363.

[37] Durgun, O. and Sahin, Z., 2009, "Theoretical Investigation of Heat Balance in Direct Injection (DI) Diesel Engines for Neat Diesel Fuel and Gasoline Fumigation". Energy Conversion and Management, 50 (2009), pp. 43–51.

[38] Sahin Z., Durgun, O., and Bayram, C., 2008, "Experimental Investigation of Gasoline Fumigation in a Single Cylinder Direct Injection (DI) Diesel Engine". Energy, 33 (2008), pp. 1298–1310.

[39] Sahin, Z., Durgun, O., and Bayram, C., 2012, "Experimental Investigation of Gasoline Fumigation in a Turbocharged IDI Diesel Engine". Fuel, 95 (2012), pp. 113–121.

[40] Wang Y., Xie, H., Su, W., and Gao, H., 2002, "Investigation of Diesel/Gasoline Duel Fuel Quasi-Homogenous Charge Compression Ignition Combustion Process and Its Capacity of Reducing the Engine Emission". Journal of Combustion Science and Technology, Vol. 8 (2002) No. 6. (in Chinese)

[41] Kim, D., Kim, M., and Lee, C., 2004, "Effect of Premixed Gasoline Fuel on the Combustion Characteristics of Compression Ignition Engine". Energy & Fuels, 2004, 18, pp. 1213-1219.

[42] Alger, T., Hanhe, S., Roberts, C. E., and Ryan, T. W., 2005, "The Heavy Duty Gasoline Engine – A Multi-Cylinder Study of a High Efficiency, Low Emission Technology". SAE paper No. 2005-01-1135.

[43] Prikhodko, V.Y., Curran, S.J., Barone, T.L., Lewis, S.A., Storey, J.M., 2010, "Emission Characteristics of a Diesel Engine Operating with In-Cylinder Gasoline and Diesel Fuel Blending". SAE paper No. 2010-01-2266.

[44] Heywood, J., 1988, "Chapter 11. Pollutant Formation and Control" in "Internal Combustion Engine Fundamentals". 1988. McGraw-Hill, Inc. New York. ISBN 0-07-028637-X, 1988.

[45] Tree, D.R. and Svensson, K.I., 2007, "Soot Processes in Compression Ignition Engines". Progress in Energy and Combustion Science, 33 (2007), pp. 272–309.

[46] Kim, D., Kim, M., and Lee, C., 2005, "Combustion and Emission Characteristics of Partial Homogeneous Charge Compression Ignition Engine". Combustion Science and Technology, 177: pp. 107~125, 2005.

[47] Himabindu, M. and Mahalakshmi, N. V., 2007, "Experimental Studies on Dual Fuel Homogeneous Charge Diesel Combustion Engines to Improve Emission Characteristics". SAE paper No. 2007-01-4065.

[48] Kotani, D., 1998, "Study on Combustion Characteristics of Lean Mixture Ignited by Diesel Fuel Injection". JSAE Review, 19 (1998), pp. 311~317.

[49] Fang, W., Huang, B., Kittelson, D.B., and Northrop, W.F., 2012, "Dual-Fuel Diesel Engine Combustion with Hydrogen, Gasoline and Ethanol as Fumigants: Effect of Diesel Injection Timing". ICEF2012-92142.

[50] Gao, D., Yu, C., Yu, W., Wang, J., and Wang, Z., et al., 2013, "Research on Gasoline Homogeneous Charge Induced Ignition (HCII) by Diesel in a Light-Duty Engine". SAE paper No. 2013-01-1666.

[51] Dwivedi, U., Carpenter, C.D., Guerry, E.S., Polk, A.C., Krishnan, S.R., and Srinivasan, K.K., 2013, "Performance and Emissions Characteristics of Diesel-Ignited Gasoline Dual Fuel Combustion in a Single Cylinder Research Engine". ICEF2013-19108.

[52] Choi, D., Jung, H., Chi, Y., and Joo, S., 2013, "Diesel-Gasoline Dual Fuel Powered Combustion System based on Diesel Compression Ignition Triggered Ignition Control". SAE paper No. 2013-01-1718.

[53] Curran, S.J., Hanson, R.M., and Wagner, R.M., 2012, "Reactivity Controlled Compression Ignition Combustion on a Multi-Cylinder Light-Duty Diesel Engine". International Journal of Engine Research. 2012 13(3), pp. 216–225. DOI: 10.1177/1468087412442324.

[54] Ma, S., Chen, G., Zheng, Z., and Yao, M., 2013, "Study on High Load of HPCC Fuelled with Diesel/gasoline Dual Fuel at Different Engine Speeds". Transactions of CSICE. Vol.31 (2013) No.4. pp. 289-295. (in Chinese)

[55] Huang, M., 2001, "Investigating the Influence of Operating Parameters on Smoke Emission and Engine Noise in a 6105QB DI Diesel Engine". Master Thesis. Guangxi University. 2001. (in Chinese)

[56] Deng, Y., 2013, "Experimental and Simulation Studies of the Mixture of Biodiesel and F-T Diesel on a Diesel Engine". Master Thesis. Taiyuan University of Science and Technology. 2013. (in Chinese)

[57] Gothekar, S.A., Vora, K.C., Mutha, G.R., Walke, N.H., and Marathe, N.V., 2007, "Design of Experiments: A Systems Approach to Engine Optimization for Lower Emissions". SAE paper No. 2007-26-012.

[58] Montgomery, D.T., 2000, "An Investigation into Optimisation of Heavy-Duty Diesel Engine Operating Parameters when Using Multiple Injections and EGR". Doctoral dissertation. University of Wisconsin-Madison. 2000.

[59] Sales, L.C.M., Sodré, J.R., Huebner, R., Maia, C.B., 2007, "Distribution of the Fuel Flow in a Cold Start System Using an Electronic Fuel Injector". SAE paper No. 2007-01-2706.

[60] Bach, F., Hampe, C., Wagner, U., Spicher, U., Sauer C., 2012, "Low Temperature Gasoline Combustion with Diesel Micro-Pilot Injection in a Six-Cylinder Heavy Duty Engine". Proceedings of the ASME 2012 Internal Combustion Engine

Division Fall Technical Conference (ICEF 2012), September 23-26, 2012, Vancouver, BC, Canada. ICEF2012-92127.

[61] Lancaster, D.R., Krieger, R.B., and Lienesch, J.H., 1975, "Measurement and Analysis of Engine Pressure Data". SAE Paper No. 750026.

[62] Heywood, J., 1988, "Chapter 4. Properties of Working Fluids" in "Internal Combustion Engine Fundamentals", 1988. McGraw-Hill, Inc. New York. ISBN 0-07-028637-X, 1988.

[63] Heywood, J., 1988, "Chapter 6. Gas Exchange Processes" in "Internal Combustion Engine Fundamentals", 1988. McGraw-Hill, Inc. New York. ISBN 0-07-028637-X, 1988.

[64] Foster, D., 1985, "An Overview of Zero-Dimensional Thermodynamic Models for IC Engine Data Analysis," SAE International Fall Fuels and Lubricants Meeting and Exhibition, Tulsa, Oklahoma.

[65] Depcik, C., Jacobs, T., Hagena, J., and Assanis, D., 2007, "Instructional Use of a Single-Zone, Premixed Charge, Spark-Ignition Engine Heat Release Simulation," International Journal of Mechanical Engineering Education, 35(1), pp. 1-31.

[66] Chase, M.W., Jr., 1998, "Journal of Physical and Chemical Reference Data, Monograph No. 9, NIST-JANAF Thermochemical Tables, Fourth Edition", National Institute of Standards and Technology, Gaithersburg, Maryland 20899-0001, 1998.

[67] Bittle, J. A., Younger, J. K., and Jacobs, T. J., 2010, "Biodiesel Effects on Influencing Parameters of Brake Fuel Conversion Efficiency in a Medium Duty Diesel Engine". Journal of Engineering for Gas Turbines and Power, Vol. 132, 2010.

[68] Hohenberg, G., 1979, "Advanced Approaches for Heat Transfer Calculations", SAE Paper No. 790825.

[69] Fox, R.W., Pritchard, P.J., and McDonald, A.T., 2009, Introduction to Fluid Mechanics. John Wiley & Sons, Inc., Hoboken, New Jersey, pp. 699.

[70] Annamalai, K. and Puri, I., 2007, Combustion Science and Engineering. Taylor and Francis, Orlando, Florida, pp. 988.

[71] Yamamoto, M., Yoneya, S., Matsuguchi, T., and Kumagai, Y., 2002, "Optimization of Heavy Duty Diesel Engine Parameters for Low Exhaust Emissions Using the Design of Experiments". SAE paper No. 2002-01-1148.

[72] Liu, W., 2005, Design of Experiments. Tsinghua University Press, Beijing. ISBN 978-7-302-10141-3. (in Chinese)

[73] "Minitab help" in Minitab 17 software. Minitab Inc. Quality Plaza, 1829 Pine Hall Rd, State College PA 16801-3210, USA.

[74] Heywood, J., 1988, “Chapter 12. Engine Heat Transfer” in “Internal Combustion Engine Fundamentals”, 1988. McGraw-Hill, Inc. New York. ISBN 0-07-028637-X, 1988.

[75] Heywood, J., 1988, “Chapter 13. Engine Friction and Lubrication” in “Internal Combustion Engine Fundamentals”, 1988. McGraw-Hill, Inc. New York. ISBN 0-07-028637-X, 1988.

[76] Hendricks, T. and Ghandhi, J., 2012, “Estimation of Surface Heat Flux in IC Engines Using Temperature Measurements: Processing Code Effects”. SAE paper No. 2012-01-1208.

[77] Ozdor, N., Dulger, M., and Sher, E., 1996, “An Experimental Study of the Cyclic Variability in Spark Ignition Engines”. SAE paper No. 960611.

[78] Selim, M.Y.E., 2005, “Effect of Engine Parameters and Gaseous Fuel Type on the Cyclic Variability of Dual Fuel Engines”. Fuel 84 (2005), pp. 961–971.

[79] Sun, L., Liu, Y., Zhou, L., and Zeng, K., 2013, “Experimental Investigation of Cycle-by-Cycle Variations in a Natural Gas / Diesel Dual Fuel Engine with EGR”. SAE paper No. 2013-01-0853.

[80] Krishnan, S.R., Srinivasan, K.K., Singh, S., Bell1, S.R., and Midkiff, K.C., et al., 2004, “Strategies for Reduced NOx Emissions in Pilot-Ignited Natural Gas Engines”, ASME Journal of Engineering for Gas Turbines and Power, Vol 126: pp. 665-671, 2004. doi: 10.1115/1.1760530.

[81] Srinivasan, K. K., Krishnan, S.R., Singh, S., Midkiff, K.C., Bell, S.R., 2006, “The Advanced Injection Low Pilot Ignited Natural Gas Engine: A Combustion Analysis”, ASME Journal of Engineering for Gas Turbines and Power, Vol 128: pp. 213-218, 2006. doi: 10.1243/09544070JAUTO104.

[82] Ozdor, N., Dulger, M., and Sher, E., 1994, “Cyclic Variability in Spark Ignition Engines - A Literature Survey”. SAE paper No. 940987.

[83] Shahbakhti, M. and Koch, C.R., 2008, “Characterizing the Cyclic Variability of Ignition Timing in a Homogeneous Charge Compression Ignition Engine Fuelled with N-Heptane/Isooctane Blend Fuels”. International Journal of Engine Research, 9.

[84] Enaux B., Granet, V., Vermorel, O., Lacour, C., and Pera, C., 2011, “LES Study of Cycle-to-Cycle Variations in a Spark Ignition Engine”. Proceedings of the Combustion Institute, 33 (2011) pp. 3115–3122.

[85] Aghdam, E.A., Burluka, A. A., Hattrell, T., Liu K., and Sheppard, C.G.W., et al., 2007, “Study of Cyclic variability in an SI Engine Using Quasi-Dimensional Combustion Model”. SAE paper No. 2007-01-0939.

[86] Beck, K.W., Sarikoc, F., Spicher, U., Van den Hoevel, H., and Duerrwaechter, M., et al., 2010, “Experimental Investigations of Two-Stroke SI Combustion with

Simultaneous Cycle-Based Fuel Consumption Measurements". SAE paper No. 2010-32-0061.

[87] Bittle, J. A., Knight, B., and Jacobs, T. J., 2010, "Biodiesel Effects on Cycle-to-Cycle Variability of Combustion Characteristics in a Common-Rail Medium-Duty Diesel Engine". SAE paper No. 2010-01-0867.

[88] Naber, J.D. and Siebers D.L., 1996, "Effects of Gas Density and Vaporization on Penetration and Dispersion of Diesel Sprays". SAE paper No. 960034.

[89] Gimenez, B., Tinaut, F., Melgar, A., and Payri, R., 2004, "Effects of the Operating Variables and Atomization Parameters on Diesel Spray Characteristics by Means of a Transient Evaporative Spray Atomization Model". SAE paper No. 2004-01-2013.

[90] Koopmans, L., Backlund, O., and Denbratt, I., 2002, "Cycle to Cycle Variations: Their Influence on Cycle Resolved Gas Temperature and Unburned Hydrocarbons from a Camless Gasoline Compression Ignition Engine". SAE paper No. 2002-01-0110.

[91] Chanchaona, S., McFeaters, J.S., and Raine, R.R., 1990, "Effects of High Compression Ratio and Combustion Chamber Shape on Cycle-to-Cycle Variability". SAE paper No. 900385.

[92] Persson, H., Pfeiffer, R., Hultqvist, A., Johansson, B., Ström, H., 2005, "Cylinder-to-Cylinder and Cycle-to-Cycle Variations at HCCI Operation with Trapped Residuals". SAE paper No. 2005-01-0130.

[93] Kouremenos, D.A., Rakopoulos, C.D., and Kotsos, K.G., 1992, "A Stochastic Experimental Investigation of the Cyclic Pressure Variation in a DI Single-Cylinder Diesel Engine". International Journal of Energy Research, 16 pp. 865-877.

[94] Rakopolous, D.C., Rakopoulos, C.D., Giakoumis, E.G., Papagiannakis, R.G., and Kyritsis, D.C., 2008, "Experimental-Stochastic Investigation of the Combustion Cyclic Variability in HSDI Diesel Engine Using Ethanol–Diesel Fuel Blends". Fuel, 87 (2008) pp. 1478–1491.

[95] Agarwal, A.K., 2011, "Experimental Investigation on Intake Air Temperature and Air-Fuel Ratio Dependence of Random and Deterministic Cyclic Variability in a HCCI engine". SAE paper No. 2011-01-1183.

[96] Wagner, R.M., Drallmeier, J.A., and Daw, C.S., 1998 "Prior-Cycle Effects in Lean Spark Ignition Combustion - Fuel/Air Charge Considerations". SAE paper No. 981047.

[97] Wagner, R.M., Daw, C.S., and Green, J.B., 2001, "Characterizing Lean Spark Ignition Combustion Instability in Terms of a Low-Order Map". Second Joint Meeting of the US Sections of the Combustion Institute, Oakland, California, USA, March 25-28, 2001.

[98] Scholl, D. and Russ, S., 1999, "Air-Fuel Ratio Dependence of Random and Deterministic Cyclic Variability in a Spark-Ignited Engine". SAE paper No. 1999-01-3513.

[99] Finney C.E.A., Green, J. B., and Daw, C.S., 1998, "Symbolic Time-Series Analysis of Engine Combustion Measurements". SAE paper No. 980624.

[100] Green, J.B., Daw, C.S., Armfield, J.S., Finney, C.E.A., Wagner, R.M., et al., 1999, "Time Irreversibility and Comparison of Cyclic-Variability Models". SAE paper No. 1999-01-0221.

[101] Shi, C., Nagai, K., and Iida, N., 2009, "Analysis of the Combustion Dispersion Mechanism in HCCI Engine". SAE paper No. 2009-32-0086.